UNIVERSITÀ DEGLI STUDI DI PADOVA

UNIVERSITA' DEGLI STUDI DI PADOVA

Dipartimento di Ingegneria Industriale DII

Corso di Laurea Magistrale in Ingegneria Energetica

Hydrogen valley: study about hydrogen production and end-use in an industrial location in Northern Italy

Relatore: Prof.ssa Anna Stoppato

Laureanda: Arianna Carli

Anno Accademico 2022/2023

Data 04/07/23

Contents

Abstract

In this thesis, a possible future hydrogen valley near Villadossola is discussed. After a general overview on green hydrogen compared with other fuels and other varieties of hydrogen, classified according to the production process, we investigate its possible distribution chain, future cost forecasts and how legislation may intervene. The operativity of the existing hydroelectric power plants under auction for a total size of 8MW base load, and the design of the future 6MW peak photovoltaic park are also analyzed. Concerning the latter an analytical and design discussion is proposed. Electrolyzers for a size of 8MW will be connected both to the hydroelectric power plants and to the photovoltaic park. Their existing types, and those of storage systems, will be classified in order to adopt the best solution according to the needs. Finally, the possible end users of hydrogen will be divided into three main areas: hydrogen for industries, for transportation and process hydrogen for chemical industry.

Introduction

Due to the market repercussions of recent geopolitical developments, the increasing difficulty of extracting non-renewable sources, and the growing restrictions on their usage, it is becoming increasingly important to explore alternatives for energy supply. Among various opportunities, hydrogen represents a valid substitute. The reasons are multiple. Firstly, its combustion does not produce CO_2 emissions. Additionally, currently, it is not subject to the same taxation regime as conventional fuels unless used in endothermic engines. Among the major advantages it offers is the possibility of storage, allowing energy to be stored in a chemical form with negligible deterioration compared to the obsolescence of, for example, batteries. Moreover, hydrogen can be produced without emissions itself.

Currently, the sector that absorbs the vast majority of hydrogen production is the chemical industry, which consumes approximately 1 Mt of hydrogen per year. From this order of magnitude of consumption, which we emphasize is solely related to the chemical industry, we understand the importance of replacing this hydrogen, currently produced from non-renewable sources, with green or blue hydrogen, or other types analyzed in detail later on.

Another possible application of hydrogen is as a fuel in boilers for heating water, for which models already exist that can use mixtures of conventional natural gas and hydrogen up to 100% of the latter. Furthermore, the thesis also evaluates the possibility of using hydrogen in metallurgical industrial processes, particularly in preheating furnaces for billets.

Below is a detailed summary of all the chapters in the thesis:

- An investigation was conducted on the existing hydroelectric watercourse to comprehend the characteristics of the plants, their connections, and production. The hydroelectric plants participating in the watercourse consist of seasonal reservoirs and regulating basins. They utilize Pelton and Francis turbines that operate at low flow rates and high heads. The entire watercourse has the capacity to reach a peak power of 35.7 MW and ensures an 8 MW baseload. Additionally, it was observed that the average daily production follows the

typical M-curve pattern, with peaks corresponding to periods of high demand. This factor influenced the selection of operational hours for the electrolysis plant.

- The project of the photovoltaic system was carried out starting from the knowledge of the dimensions and characteristics of a disused industrial area on which there used to be a steel mill. Following the choice of components and sizing, a 6 MW peak photovoltaic system was obtained with an estimated production of $E_{Grid} = 7.52\ GWh/y$ and an equivalent number of hours of $h_{pv} = 1252.7\ h/y$.

- To choose the electrolysers to install, a study of the literature was initially conducted to identify the maturity of the technology, the materials used, the wear of the components operating in a variable way, investment costs and plant simplicity. Afterwards, various technical sheets of electrolysers on the market were compared. Despite the cost due to the noble metals present in PEM electrolysers, these have reduced dimensions due to the simplicity of the plant, high yields and high operating ranges. The 6 MW ($h_e = 1252.7\ h/y$) photovoltaic plant and 8 $MW_{baseload}$ hydroelectric watercourse provide enough energy to power a 7.5 MW electrolysis plant, that works 7000 h/y consisting of three 2.5 MW PEM electrolysers. Considering the government incentive provided, the levelized cost of hydrogen (LCOH) was calculated, in order to have a price base to guarantee; then an investment analysis was carried out for photovoltaics and electrolysers. From these analyses it emerges that the investment in photovoltaics can be recovered efficiently by selling around 40 €/MWh with the government incentive. Even the investment in electrolysers is recovered efficiently if the LCOH is used as the base price and an adequate margin of 0.3 €/kg is attributed. However, the unknown factor of the hydroelectric plant remains; this is not part of the incentives because it already exists but supplies for a large part of the energy. Weighing the price of energy on the operating hours of renewable energy production, an energy cost for hydrogen production of 75 €/MWh was chosen, corresponding to a sale price of $P_{H_2} = 5.17$ €/kg, $P_{H_2} = 0.44$ €/Sm^3.

- The cost-effectiveness in substituting green hydrogen in industrial processes depends on the type of process, the proximity of the production plant with the utilization plant, and the market value of CO_2 and natural gas (including transportation, taxes and general charges for the period). By fixing a value of green hydrogen for which the investment is fully recoverable, threshold values were found for the cost of natural gas and market value of CO_2 above which there is real convenience in substitution.

In the transportation sector, the total cost of ownership (TCO) of diesel rigid trucks was compared with that of fuel cell rigid trucks. For these, the different components of TCO were analyzed, assuming incentives in an early stage of research and development consisting of: a government aid in investment, a road toll differentiated by vehicle, and a carbon tax. Under these conditions it was found that hydrogen trucks purchased at this stage are cost-effective compared to diesel trucks if the cost of hydrogen is $< 6€/kg$.
Hydrogen can be adopted as a raw material in the field of industrial chemistry. In this sector, the replacement of gray hydrogen with green hydrogen was analyzed taking into account the process of producing gray hydrogen from natural gas and the given value of green hydrogen. It was found that the replacement in the chemical industry is convenient even for lower natural gas costs than those for which it is convenient to replace green hydrogen in the process industry.

Chapter 1

Renewable hydrogen

In the development of the various renewable sources, increasingly massive every year, hydrogen will play a very important role as energy vector allowing the accumulation of renewable energy in the form of clean chemical energy. This will make it possible to completely decarbonise many processes and to increase the EGC (Equivalent Guaranteed Capacity) of the electricity grid. EGC corresponds to the renewable power capable of maintaining the same LOLE (Loss Of Load Expectation) of the grid, thus guaranteeing the same number of hours of outage with intermittent power. This ensuries greater coverage of demand even in the presence of intermittent power, e.g. renewable power. Currently, there is skepticism regarding the convenience of hydrogen due to the multiple transformations that must take place to obtain this molecule. In order: from renewable electricity, through electrolysers, to hydrogen, with an efficiency of around $60 - 80\%$ (according to [36]), and then, through a combustion reaction, or a fuel cell with an efficiency around 60%, without neglecting storage and accumulation. All these processes cause different energy losses. On the contrary, batteries have decidedly higher yields with lower accumulation capacities, and fossil resources simply need to be extracted.

Although today there is this discrepancy, research on batteries has been much more funded than that on electrolysers. Consequently for electrolysers and fuel cells a great improvement is expected over time in the next 10 years which could bring this technology to be more competitive. Today there is funding given by the government to encourage the development and generation of green hydrogen such as the PNRR (Piano Nazionale di Ripresa e Resilienza). These funds are essential to guarantee the first functioning hydrogen valleys.

Investing in hydrogen, rather than usual non-renweable resources, such as oil, natural gas, lithium for batteries, etc., would help to reduce global conflicts triggered

by the inhomogeneity of resources worldwide. There are indeed ongoing researches trying to develop electrolysers without rare earth, which are likely to be the cause of future conflicts.

1.1 The potential of hydrogen

As described in [5], hydrogen from renewable sources today has high costs. However, it is believed that the reduction of investment costs on renewable energies, such as solar and wind energy, and the advancement of electrolysers may make this technology cheaper than other hydrogen production methods in the near future. For example, alkaline electrolysers (ALK) in recent years (from 2014 to 2019) have reduced their costs by 40% in Europe, and in Asian countries it reached 80%. Consequently, future prospects assuming an increase in sales volumes and a constant reduction in costs, a production cost of around $0.67 \div 1.52$ €$/kg$ of hydrogen from renewable sources could be reached in 2050 (taken as conversion factor dollars to euros 1\$ = 0.95€). Given the calorific value of hydrogen ($LHV_{H_2} = 33.33\ kWh/kg$), this is equivalent to an energy cost between

$$C_{en,1} = \frac{0.67}{33.33} \times 10^3 \simeq 20\ \frac{€}{MWh};\quad \&\quad C_{en,2} = \frac{1.52}{33.33} \times 10^3 \simeq 45\ \frac{€}{MWh}; \tag{1.1}$$

which reconverted into €$/Sm^3$ of natural gas (through $LHV_{NG} = 9.8\ kWh/Sm^3$) would correspond to a price of:

$$C_{NG,1} = \frac{0.67}{33.33} \times 9.8 \simeq 0.2\ \frac{€}{Sm^3};\quad \&\quad C_{NG,2} = \frac{1.52}{33.33} \times 9.8 \simeq 0.4\ \frac{€}{Sm^3}. \tag{1.2}$$

This energy price is competitive when compared with the market price of natural gas over the last years as we can see in the graph shown in Figure 1.1. We note that the price of natural gas can vary on the basis of various conditions affecting supply and demand, for example due to government policies or conflicts or variations in the price of oil, or more or less rigid winters. We can observe a decrease in prices in 2020 due to the COVID-19 pandemic followed by a recovery in demand with a consequent price increase in 2021, going towards a further price increase in 2022 due to the Russian conflict against Ukraine. In this complicated geopolitical context we can experience the volatility of gas prices and how much renewable hydrogen could do to reduce this leverage held by the countries that possess resources. Furthermore, even if the costs of hydrogen will be similar (or a little more inconvenient) there will be the guarantee of an almost constant price of green hydrogen.

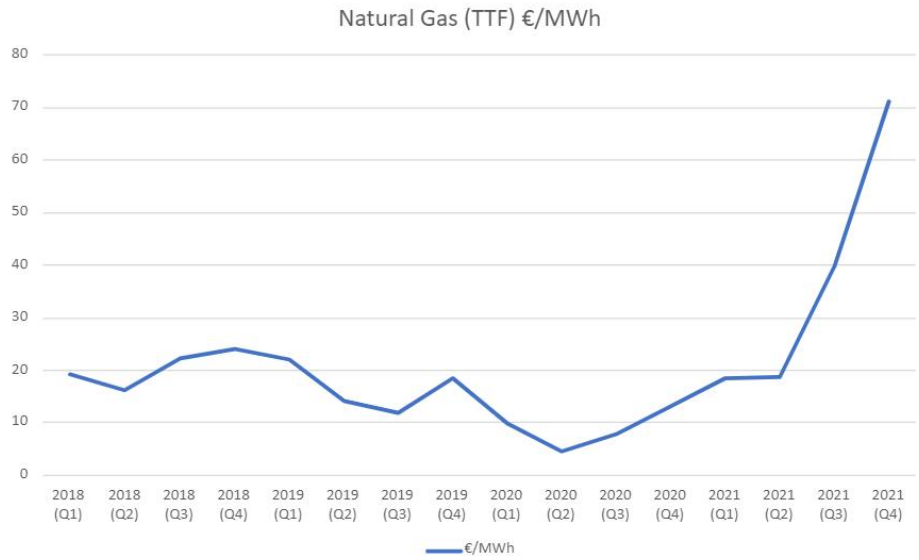

Figure 1.1: Natural gas prices from 2018 to 2021 in €/MWh according to TTF (Title Transfer Facility) from IEA.

1.1.1 Hydrogen types

Hydrogen is already used today in various processes, such as the production of ammonia and methanol, and its production has increased over time. However, the current production of hydrogen is almost entirely derived from fossil fuels as it is cheaper ($0.95 - 2.85$ €/kg).
Hydrogen is distinguished into different categories according to the type of process by which it is obtained as described in [31]:

- **Green hydrogen:** when hydrogen is produced by electrolysers, which completely utilise electricity from renewable sources;
- **Grey hydrogen:** hydrogen produced from fossil sources, mostly coal or natural gas, which is produced without the use of CO_2 removal systems;
- **Blue hydrogen:** through the combination of grey hydrogen and carbon capture and storage (CCS), to avoid most of the greenhouse gas emissions of the process;
- **Turquoise hydrogen:** hydrogen, through the pyrolysis of a fossil fuel, where the byproduct is solid carbon;

- **Yellow hydrogen:** where hydrogen is produced by electrolysis using the electricity produced by a nuclear plant.

In the short term, green hydrogen may be more difficult to develop in large quantities, as its production would draw on a large amount of renewable electricity. For this reason, in the transition from fossil fuels to green hydrogen, there will be a short transition period for blue hydrogen, which will allow a more gradual penetration of green hydrogen into the market.

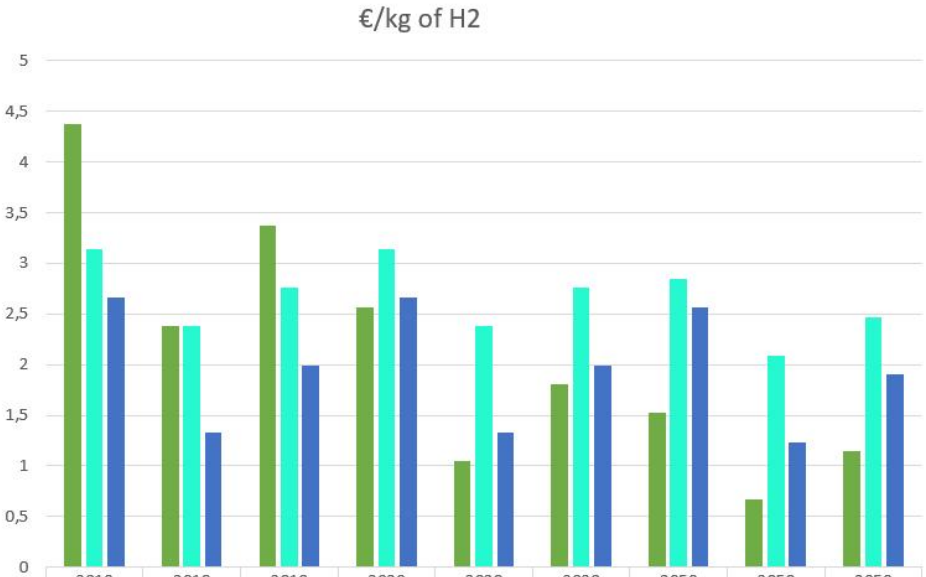

	2019 Cmax	2019 Cmin	2019 Cav	2030 Cmax	2030 Cmin	2030 Cav	2050 Cmax	2050 Cmin	2050 Cav
H2 green	4,37	2,375	3,3725	2,565	1,045	1,805	1,52	0,665	1,14
H2 coal CCS	3,135	2,375	2,755	3,135	2,375	2,755	2,85	2,09	2,47
H2 NG CCS	2,66	1,33	1,995	2,66	1,33	1,995	2,565	1,235	1,9

Figure 1.2: Cost forecasts of green hydrogen, hydrogen from coal with CCS and from natural gas with CCS, in €/kg.

In fact, as we can see from the graph in Figure1.2, whose data have been taken from [5], there is an interchangeability in the temporal evolution of the cost of the two technologies for producing hydrogen. We pass from blue hydrogen to green hydrogen, for which forecasts indicate greater convenience in 2050 of green hydrogen, with a tie in 2030. However, these forecasts are possible only assuming that large-scale investments will be made in the coming years for large productions of green hydrogen. We can therefore now understand the importance of the role of incentives

and funds allocated by governments to solicit investments in this sense, making this resource more convenient in view of a sustainable future.

1.1.2 Storage methods and costs

We can group storage techniques into three macro-categories, based on the state in which hydrogen is stored: gaseous, liquid and solid.
Possible storage methods in the gaseous state:

- Salt caves;
- Exhausted gas fields;
- Pressurized containers;
- Rock caverns;

If natural depleted deposits or salt caves are available, there is the possibility of having large underground storable volumes suitable for containing hydrogen. In these cases the storage costs are very low, as nature has already created the main structure in which to store and storage times can be longer (months, seasons). In addition, since the accumulation is underground, there is almost no surface obstruction. However, in the absence of these natural structures, it is necessary to resort to pressurized containers which have a greater surface area and contain smaller volumes.
Possible liquid storage methods:

- Liquid hydrogen;
- Ammonia;
- LOHCs (liquid organic hydrogen carrier);

As we can see from the flow diagram in Figure1.3, hydrogen in ambient conditions is in gaseous form, consequently if we want to bring it into liquid form we must both compress and cool it. This is expensive, in fact this type of storage is used for small quantities and for a short time. For this reason, for larger volumes and longer periods, it is possible to think of chemically binding this molecule, as for example by forming ammonia or through organic liquids for which liquid state is obtained in ambient conditions or by compression.

Possible solid state storage method:

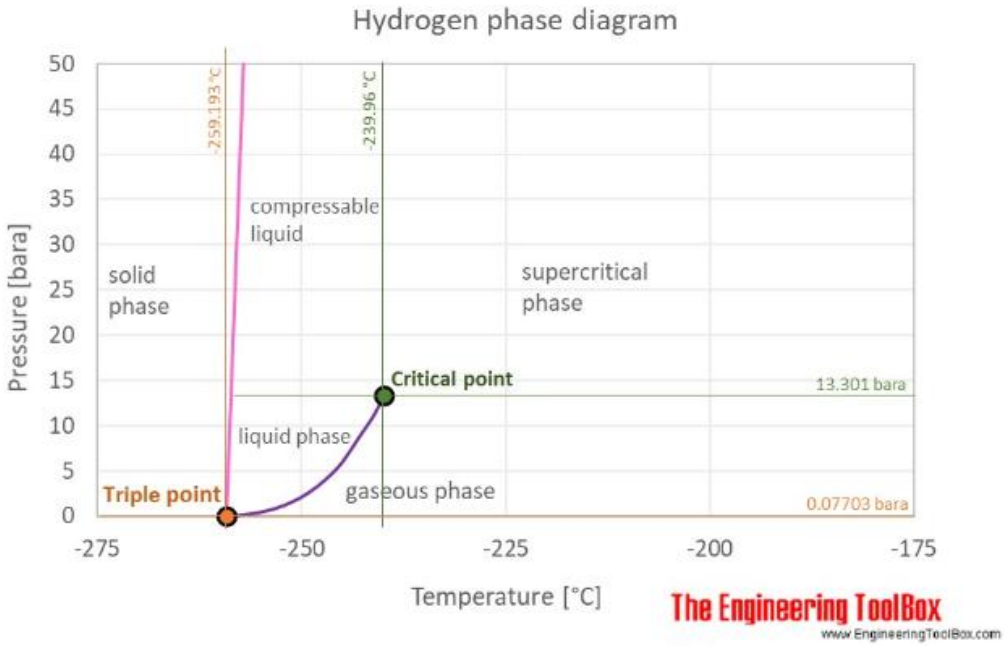

Figure 1.3: Phase T,P diagram of hydrogen.

- Metal hydrides;

Solid storage systems exploit the crystalline chemical structures of metal hydrides in which interstitial sites are generated where the dissociated hydrogen molecules bind. In this way we can accumulate a lot of hydrogen in small volumes, and since the bonds are weak enough, we do not spend so much energy to create and break them. These properties are ideal and the research looks promising for the creation of hydrogen storage systems, but as explained in [23] they are still in the testing phase and therefore data on marketed prototypes are not yet available.

The Table1.1 shows the current and forecast leveled costs of storage (LCOS) according to [5], taking into account future prospects for technological evolution.

1.1.3 Transport methods and costs

The specific volume under standard conditions of natural gas and hydrogen, respectively, is:

- $v_{gn} = 1.41\ Sm^3/kg$;

	LCOS [€/kg] (ref)	LCOS [€/kg](future)	Geografical aveilability
Salt caves	0.22	0.11	Lim.
Exhausted gas fields	1.81	1.02	Lim.
Rock caverns	0.68	0.22	Lim.
Pressurized container	0.18	0.16	Not lim.
Liquid hydrogen	4.34	0.90	Not lim.
Ammonia	2.69	0.83	Not lim.
LOHCs	4.28	1.77	Not lim.
Metal hydrides	Not ev.	Not ev.	Not lim.

Table 1.1: Possible levelized costs of storage (LCOS).

- $v_{H_2} = 12.65\ Sm^3/kg$.

This means that to transport $1kg$ of hydrogen under standard conditions we have a volume that is about nine times higher than the one occupied by $1kg$ of natural gas. As previously mentioned, this is problematic for storage if we do not have large natural stocks available, as it forces us to compress or compress, and possibly cool, the gas or bind it with other elements, and therefore lose energy. However, it must be considered that transportation is also a particular type of storage and this is already used for natural gas. To date, the Italian natural gas distribution network is thought to be able to host a 2% volume of hydrogen.

If we compare the flow speed ($\bar{w}$) of the two gases at the same regime (therefore the same Re number), diameter of the pipeline and standard conditions, we obtain that speed is affected solely by the characteristics of the fluid. In particular, it depends on the relationship between dynamic viscosity of the fluid and density.

- $\mu_{gn} = 11.2 \times 10^{-6}\ Pa\ s$, $\mu_{H_2} = 9 \times 10^{-6}\ Pa\ s$;
- $\rho_{gn} = 0.71\ \frac{kg}{Sm^3}$, $\rho_{H_2} = 0.08\ \frac{kg}{Sm^3}$;

$$Re = \frac{\rho \bar{w} D}{\mu}; \tag{1.3}$$

$$\bar{w}_{gn} = \left(\frac{Re}{D}\right) \cdot \frac{\mu_{gn}}{\rho_{gn}} = \left(\frac{Re}{D}\right) \cdot \frac{11.2 \times 10^{-6}}{0.71} = \left(\frac{Re}{D}\right) \cdot 1.58 \times 10^{-5}\ \frac{m}{s}; \tag{1.4}$$

$$\bar{w}_{H_2} = \left(\frac{Re}{D}\right) \cdot \frac{\mu_{H_2}}{\rho_{H_2}} = \left(\frac{Re}{D}\right) \cdot \frac{9 \times 10^{-6}}{0.08} = \left(\frac{Re}{D}\right) \cdot 1.13 \times 10^{-4}\ \frac{m}{s}. \tag{1.5}$$

We note that hydrogen under standard conditions flows ten times faster than natural gas. Since the dynamic viscosity and density depend on temperature and pressure, for higher pressures in the pipelines transporting natural gas, hydrogen alone would flow about three times faster than natural gas (same calculations performed using the gas properties provided by the MiniRefProp (at 3 $bar, T = 25°C$) which confirms what was said in [5]). For this reason, the difference in density does not affect the quantities of gas transported so much and therefore it is still potentially convenient. The fact remains that the natural gas distribution network will have to be radically modified and re-adapted to host hydrogen. This will involve large investments in order to be able to comply with all the safety rules already imposed today for natural gas. Contrary to the extraction of natural gas which is strongly localized, the production of green hydrogen should not necessarily have to be so. Consequently this new gas will travel shorter routes not necessarily having to cross countries and continents as currently happens with gas pipelines. For this aspect there could be a great convenience, given that today the cost of transporting natural gas is 30% of the total cost in the bill. The Table 1.2 shows the costs related to the transport of hydrogen. Most of them are known, as today there are already methods of transport used by chemical industries that employ hydrogen. Data taken from [5] where compression and motion associated with storage were also taken into account.

$[t/d] \setminus km$	$1 - 10\ km$	$10 - 10^2\ km$	$10^2 - 10^3\ km$	$10^3 - 10^4\ km$
	Transmission pipelines (compr. H_2**)[€**$/kg$**]**			
$10^2 - 10^3\ [t/d]$	0.05	$0.05 - 0.1$	$0.1 - 0.55$	$0.55 - 2.85$
	Distribution pipelines (compr. H_2**) [€**$/kg$**]**			
$10 - 10^2\ [t/d]$	$0.05 - 0.06$	$0.06 - 0.21$	$0.21 - 1.73$	< 2.85
	Trucks (compr. H_2 **or LOHCs if** $> 10^2$ **km) [€**$/kg$**]**			
$1 - 10\ [t/d]$	$0.62 - 0.72$	$0.65 - 1.64$	$0.91 - 3.68$	$3.68 - 6.37$

Table 1.2: Comparison of H2 transport costs in €$/kg$ based on the type of distribution, on the distance in km and the quantity transported per day (t/day).

1.1.4 European backbone project

The EHB (European Hydrogen Backbone) project is illustrated in [39] following a detailed analysis of the future demand for hydrogen in the various industrial sectors. This project aims at the gradual creation of an infrastructure dedicated to the distribution of hydrogen, to increase the resilience of the European energy system, according to the plan drawn up by the European commission RepowerEU. This structure is technically feasible and will create a huge benefit in terms of hydrogen transport, storage and distribution costs in the future.
Analysis conducted by EHB found that a hydrogen pipeline can carry 65 TWh/y of energy in the form of hydrogen.
In the plan drawn up by REpowerEU, the target is 10 Mt (330 TWh/y), this will require five major, large-scale corridors that will spread across Europe, connecting every member country.
In this paragraph we now list the cost components for the construction of these pipelines.
Capex:

- pipeline capex;
- compressor capex;

Variable opex:

- compressor power;

Fixed opex:

- pipeline $O\&M$ (% of Capex);
- compressor $O\&M$ (% of Capex);

The table in the Figure 1.4, taken from [39], shows the operating costs in $M€/km$, associated with the construction of gas pipelines for the transport of hydrogen. Under simplified hypotheses, scenarios of low, medium, high cost and three types of diameter pipelines in inches $(20, 36, 48)$ were analysed, considering pipelines of small, medium and large dimensions. The offshore plants values are those of the onshore plants multiplied by 1.7. The costs associated with compression and the related fixed (for compression and piping) and variable operating costs are also reported, in the three electricity cost scenarios $(40, 60, 80\ €/MWh)$.

Cost parameter		Low	Medium	High	Unit
Pipeline Capex, new	Small	1.4	1.5	1.8	M€/km
	Medium	2.0	2.2	2.7	
	Large	2.5	2.8	3.4	
	Offshore Medium	3.4	3.7	4.6	
	Offshore Large	4.3	4.8	5.8	
Pipeline Capex, repurposed[27]	Small	0.2	0.3	0.5	
	Medium	0.2	0.4	0.5	
	Large	0.3	0.5	0.6	
	Offshore Medium	0.3	0.4	0.5	
	Offshore Large	0.4	0.5	0.6	
Compressor station Capex		2.2	3.4	6.7	$M€/MW_e$
Electricity price		40	60	80	€/MWh
Pipeline operating & maintenance costs		0.8	0.9	1.0	€/year as % of Capex
Compressor operating & maintenance costs		1.7	1.7	1.7	
Weighted average cost of capital		5.0			%
Depreciation period pipelines		40			Years
Depreciation period compressors		25			

Figure 1.4: Values used to estimate the total investment, operating and maintenance costs for the construction of a hydrogen pipeline (under simplified assumptions).

1.1.5 Marginal cost of abatement using hydrogen

In general, when we are in market conditions with perfect competition, the optimal quantity of goods produced by a firm is the one for which there is market equilibrium, namely when the price equals the marginal cost of production (cost of obtaining an incremental unit of good). However, when we consider industrial activities, associated with these there is always an environmental damage function. The environmental damage is a quantity that is taken into account from a social point of view, but if there were no systems that oblige companies to take it into account, this quantity would not be quantified by market forces. Consequently, if we want to maximize the social benefit, the quantity produced under market equilibrium is not that optimal from the social point of view. There are several tools to bring the

production of companies to a socially optimal production:

- Environmental Standard, where regulations limit emissions and sanction those who do not comply with the standard;
- Environmental taxes, where the value of the tax is commensurate with the damage;
- Subsidies for depollution, where a negotiation takes place between social partners to bring production to the optimum from a social point of view;
- Tradable permits, through the issue of certificates that are purchasable on the market.

In the event that the cleanup is imposed by standards, we will have that different companies will have different cleanup costs and therefore this does not allow us to obtain the result imposed at the minimum cost. If instead a tax is introduced, firms will tend to clean up as long as their marginal cost of cleaning up is lower than the value of the tax, after which they will prefer to pay the tax. This approach is good as long as the correct value is associated with the tax. In fact if this is too low, a partial reduction of pollution is obtained, while if it is too high, there may be economic damage to companies. A good solution is that of tradable permits, where emissions are limited, but these can be negotiated on the ETS (Emission Treading System) market, for large CO_2 emitters. In this way the same results as the other methods are obtained but with a lower overall cost, since companies with lower costs tend to clean up more than required and sell the difference to those who instead have higher costs and therefore can afford to clean up less. The plot in Figure1.5 shows the trend of the CO_2 market over the last ten years.
As we can observe from the graph in the Figure1.5, the price associated with the emissions of CO_2 on the market today, expressed in $€/tCO_2$, is around 100 $€/tCO_2$, we can also observe an increase in the price in recent years due to the annual and progressive reduction of emission quotas by the state (2.2 $\%/y$), which uses a cap and trade system.
Therefore, we have a market in which we can trade carbon permits regulated by the GSE (Electrical Services Manager) which organizes and manages white, green certificates and emission quotas exchange and the state which, through regulation, increasingly limits emissions over the years.

In this context, every energy producer must guarantee that a certain fraction of the produced electricity comes from renewable resources. Hence, whose who do not produce electricyt from renweable resources are obliged to buy the market equivalent

Figure 1.5: Market trend of tradable carbon permits in €/tCO_2, in recent years, from [18].

in carbon credits. Vice versa, those who produce green energy, upon request to the GSE (Gestore del Sistema Elettrico), obtain the issue of green certificates which can be sold on the market. On the other hand, those who are not producers (apart from cogeneration) can invest in increased efficiency and therefore obtain the release of white certificates again from the GSE, and sell the excess on the market or through bilateral contracts. In general, as has been said, there is an emission limit that the state grants. This limit is fixed through a certain number of emission allowances for each plant; any surplus of quotas can be kept for a certain term or sold directly, while any deficit can be compensated through market purchases.

The use of hydrogen can create the ideal condition for reducing emissions in those sectors where the abatement of CO_2 is very difficult. Consequently, if by 2050 it were possible to have a green hydrogen price of around 0.95 €/kg, the marginal cost of abatement in many of these hard-to-abate sectors would become lower than the market value of carbon cerdits, and therefore investments in decarbonisation would be interesting.
As we can see from the graph in the Figure1.6, the marginal costs of reducing the CO_2 of some of these sectors have been reported, such as the steel mill, the cement industry, the transport industry and so on, with values of 50 €/tCO_2 for steel

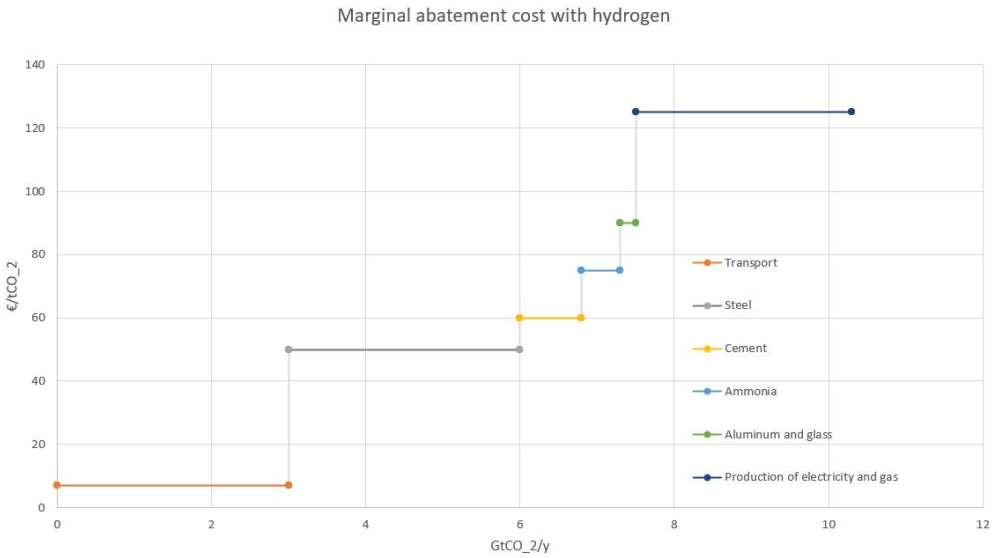

Figure 1.6: Marginal abatement cost in sectors that are difficult to abate, using hydrogen at 0.95 €/kg in the perspective of 2050, [5].

for instance. In reality, these values should be compared with the market values envisaged in the future, which, however, based on increasingly strict restrictions and possible less and less economic interventions, will likely induce an upwards trend of cause the price of the shares.

1.2 National hydrogen strategy

In 2015, the first formal commitment agreements were made by the EU (European Union) in the fight against climate change. Through the Paris Agreement (COP 21) and the Sustainable Development Goals (Agenda 2030) a limit has been set on the increase in global temperature. Subsequently, the first decarbonisation plans were created and therefore of these objectives were implemented. We mentioned the Clean Energy Package (2016) established by the EU, which requires a reduction in emissions of 40% of CO_2 by 2030 with reference to 1990 emissions, and subsequently the European Green Deal (2019) which sets the 'zero emissions target for 2050. For these, each member country must draw up its own plan in accordance with European directives. In Italy, the PNIEC (Integrated National Plan for Energy and Climate) and the National Energy Strategy were established in 2019 and 2017 respectively. The PNIEC describes the role of hydrogen in achieving the objectives set by the EU in sectors of difficult decarbonisation and in the management of grid overgeneration from renewable sources.
We are now going to explain the role of hydrogen within the government plans at Italian and European level in the decarbonisation plans for 2030 and 2050, adapted from [15].

For 2030 the following objectives are set:

1. 2% of the final energy demand made up of H_2;
2. reduction of CO_2 emissions by 8 Mton;
3. Installation of 5 GW of electrolyser capacity to produce H_2;
4. investments of 10 billion euros for hydrogen generation alone, half of which will be provided by European funds;
5. increase in GDP (27bn);
6. creation of many temporary (200k) and permanent (10k) jobs;

While for 2050:

1. Hydrogen growth in energy mix from today less than 2% to $13 - 14\%$;
2. Installation of 500 GW of electrolyser capacity to produce H_2;
3. Penetration of hydrogen up to 20% in final energy consumption.

1.2.1 Organization of production, transport and storage

Where the demand for green hydrogen will concentrate, it will generate favorable conditions for the formation of the first hydrogen valleys in certain geographical areas. In this way, the demand will meet the supply provided by these. Therefore the points where these valleys will form will have to be strategic, such as near crucial road and railway interconnections and near industrial districts. Unfortunately, it is often difficult to identify similar areas that are also good from the point of view of renewable producibility. For instance, for wind power, the presence of obstacles, or for photovoltaics the difficulty of occupying large areas near industrial districts. It is therefore necessary to identify the configuration with the lowest cost of production and transport and create clear regulations, so that those who make investments are facilitated and not left in uncertainty. Three possible production/transport models have been identified:

1. **Total production on site:** in this way the transport cost is minimized as it is produced directly where it is consumed;

2. **On-site production with transport of electricity:** the renewable electricity produced is transported via grid from the place of production to the point of consumption where the electrolysers then transform it into hydrogen;

3. **Centralized production with hydrogen transport:** the renewable electricity produced is used directly on site to produce hydrogen and this, via the gas network or heavy transport, is transported to the users.

The first alternative turns out to be the most standard and the one most corresponding to the concept of hydogen valley. But as mentioned earlier, not all situations lend themselves to having power generation in the vicinity of hydrogen production. It is thus a good alternative, but it is not versatile for every situation.
To date, due to the lack of a hydrogen distribution network (less than 2 % is mixed into the natural gas network in the near future) the third alternative is the most expensive, but in a longer-term and global view of the system as a whole, it will guarantee benefits that exceed the costs.
In fact, today it is possible to exploit the second alternative, that is to take advantage of the electricity grid to transfer the renewable energy produced, with a final refund, paid by the state, as compensation for the general charges related to the electrical system. In this way it could also be possible to achieve a better and more efficient management of the accumulations and exploit the economies of scale in the purchase of electrolysers.
This was made possible thanks to the resolution issued on November 8, 2022 by

ARERA (Regulatory Authority for Energy, Networks and the Environment) [13] and the decree of the Minister of Ecological Transition of September 21, 2022 [28]. These laws define the conditions for accessing the concessions on the consumption of renewable energy in electrolysis plants for the production of green hydrogen.
Access to the concessions is granted to public and private entities that consume renewable electricity for the production of green hydrogen provided that the hydrogen is:

a) produced by reducing greenhouse gas emissions by 73.4% in the life cycle, compared to the reference fossil fuel 94 gCO_{2eq}/MJ, or involving emissions lower than 3 tCO_{2eq}/tH_2;

b) the electricity used for the production of green hydrogen is covered by guarantees of renewable origin (issued by the GSE), pursuant to article 46 of Legislative Decree 199/21;

c) calculation and verification of the reduction requirement emissions according to current ISO standards;

d) if the connection to the electrolysis system is direct then the emission factor must have a zero value.

If these guidelines are respected, the company is exempt from paying the variable part, expressed in $c€/kWh$, of the general charges related to the electrical system. General system charges are a share that corresponds to approximately $20 - 30\%$ of the total cost of energy, based on the type of user and to the period. This type of incentive is recognized on a final balance basis reimbursement of the charges paid, and it can be combined with others related to plants for the production of green hydrogen.
The general system charges consist of, [19]:

- A_{SOS}, general charges relating to the support of energy from renewable sources and cogeneration;

- A_{RIM}, remaining general charges, as incentives dedicated to the production of energy from non-biodegradable waste (that does not fall under the renewable section), nuclear safety, territorial compensation measures, system research support, promotion of energy efficiency and so on;

These two groupings, in turn, have a trinomial form in the case of non-domestic users:

1. power share expressed in $c€/kWy$;
2. fixed share expressed in $c€/pp$ per withdrawal point;
3. variable share expressed in $c€/kWh$;

With regard to these three items, the exemption from payment only concerns the last one, which corresponds to the variable amount in $c€/kWh$ for the two cases A_{SOS} and A_{RIM}.

From the D.L. 30 April 2022, [12], the hydrogen produced under the conditions described above does not fall within the energy products (article 21 of the consolidated text, Legislative Decree 26 October 1995, n. 504), and therefore is not subject to excise duty unless directly used in heat engines as a fuel.
In this regulatory framework, the concessions provided by the state are clear, nevertheless, in the withdrawal of green energy from the electrical grid with guarantees of origin, there are many other non-negligible cost items. For example, the tax regime for green energy with a guarantee of origin is the same as for non-renewable energy. Consequently, green hydrogen, once generated, does not undergo double taxation since taxes are already paid on electricity taken from the network. Furthermore, the adequacy of a tax in such circumstances should be assessed, since as previously noticed, the tax is the value attributed to all those activities that cause environmental damage, which must be taken into account from a social point of view. However, if the mentioned activity does not cause damage but on the contrary intervenes by avoiding emissions, this should be taken into account when deciding the value to be taxed, otherwise an economic damage may be incurred. In fact, these initiatives should be evaluated very carefully, since even in a scenario in which hydrogen is self-produced without going through the electricity grid, the cost of energy is always the largest cost item. Consequently, relocating the electrolysers could still be not very convenient, despite the first concessions provided by the state.

1.2.2 Demand for hydrogen in different sectors

Green hydrogen turns out to be a safe and reliable fuel from a geopolitical point of view and in the future (2050) it will play an essential role in the decarbonisation of those so-called "hard-to-abate" sectors (energy-intensive or heavy transport/aviation). In the short term (2030) it will become progressively competitive in some sectors, such as those in which non-green hydrogen is already used as a raw material (chemical industry and petroleum refining). Furthermore, through state grants, green hydrogen will contribute to decarbonising the sectors of heavy transport, non-electrified railways, in industry and its blending in a certain percentage by

volume (2%) in the natural gas grid will stimulate its market.

Long-haul heavy transport sector

According to the European Environment Agency (EEA), emissions from the transport sector account for around a quarter of the overall CO_2 emissions across the EU. For the light transport sector, from 2035 the sale of new petrol and diesel cars will be banned in the European Union. Therefore, all cars, vans and light-duty vehicles sold in the EU will have to produce zero CO_2 emissions. This industry appears to be moving towards battery electric vehicles, which have a lower total cost of ownership (TCO) than hydrogen or green fuel alternatives.

For trucks and lorries, the EU aims to reduce CO_2 emissions by 30% by 2030, with reference to the values issued in 2019, for all new heavy vehicles sold (with an intermediate goal in 2025 of a reduction of 15%). In addition, by 2025 manufacturers will have to ensure that at least 2% of the market share is made up of low or zero-emission vehicles. Respecting these targets should achieve an emission reduction of approximately 25% in the road transport sector (trucks and lorries). Information taken from [6] and [15]. In the long-distance heavy transport sector, the industry is moving towards the use of hydrogen, biofuels and biomethane. In this sector, in fact, refueling times must be short and good mileage must be guaranteed. For this reason, the electric alternative is currently inconvenient in terms of autonomy, long refueling times and high weight of the batteries. The TCO of fuel cell trucks is not yet competitive, but instead has higher mileage and shorter refueling times; for this reason, if the cost of vehicles and hydrogen will decrease over the next ten years, also TCO will become competitive. Switzerland has strongly encouraged heavy hydrogen mobility, in fact it has already created a network of refueling stations for hydrogen vehicles. In this context it could be interesting to expand this network also at the Italian level. Therefore starting from northern Italy covering the Italian nerve centers bordering on Switzerland, such as for example the E62 which connects Italy (starting from Genoa), Switzerland and France, the E35 passing near Milan and the A22 Modena-Brenner which connects with Austria.

Rail transport

In Italy about a third of the rail transport network is not electrified and is therefore mobilized by diesel trains, which contribute to national CO_2 emissions.

From [15], it is estimated that in the next ten years, fuel cell trains will also become competitive with diesel trains. Already today there are fuel cell trains in operation, as in Germany. In other European countries there are plans to completely replace the fleets of diesel trains, as will happen in the United Kingdom and France

in the next twenty years. In Italy, given the now high age of many diesel trains, which will have to be replaced in the coming years, it is estimated that by 2030, half of the diesel trains that travel on non-electrifiable routes will be replaced with fuel cell trains.
The first lines in Italy where the conversion will be more convenient are those with the greatest crowds, such as in Piemonte, Sardinia and Sicily. As regards the infrastructures dedicated to refueling, it will be useful to identify strategic points where both trucks and hydrogen trains will be able to refuel.

Chemical industry
In the chemical industry, hydrogen is already used as a feedstock, such as in ammonia production processes (for making fertilizers and other ammonia-based chemicals), methanol and petroleum refining. However, gray hydrogen is used today in these processes, i.e. hydrogen created with natural gas using SMRs (Steam Methane Reformers), without the adoption of CO_2 capture systems, therefore with an emissions production of about $7 - 9\ kg_{CO_2}/kg_{H_2}$, as described in [15].

The current production of gray hydrogen has been estimated approximately $1\ Mt_{H_2}/y$, for a corresponding production of emissions of $3.5 - 4.5\ Mt_{CO_2}/y$ and a penetration on end uses of 1%. Therefore, the use of green hydrogen in this sector has been evaluated as one of the most promising to be developed by [15] in order to reduce emissions.
The already existing projects in this sense are based on the simple replacement of the production methodology of the raw material used through electrolysers or using already existing systems but with the capture of CO_2 (CCS), thus blue hydrogen. It has been estimated that the transition from gray hydrogen to green (or blue) will take place in the next few years and therefore by 2030 the projects that have now started will be fully operational, covering almost all production with green hydrogen or using CO_2 removal systems.

Hydrogen blending
Blending green hydrogen into the natural gas grid, which today hosts tens billions cubic meters of natural gas emitting approximately 160 Mt_{CO_2}, could significantly contribute to the decarbonisation and evolution of the natural gas grid to a hydrogen network. Furthermore, the phenomenon of overgeneration from renewable sources, such as for solar energy, can be exploited to produce hydrogen at a lower cost and therefore make it more competitive.

In Italy the technical limit is still under discussion. In particular, one has to ensure first the acceptable volumetric percentage of hydrogen in today's natural gas network, and second any needed changes both to the network and to the regulatory

framework regarding risk and safety. It is thought that by 2030, our network will be able to host up to 2% by volume of hydrogen. Moreover, many boiler manufacturers are retrofitting their models to accommodate up to 100% of hydrogen.
Another sector with high potential is the primary steel industry, for which hydrogen represents the only alternative to fossil-derived fuels, to produce pre-reduced DRI (Direct Reduced Iron), with zero CO_2 emissions.

Chapter 2

Hydroelectric power plants

In the past the hydropower plant was split from the steel mill that was originally connected in self-consumption, and the latter has been decommissioned. The reason was the transition to the free market, this made it more convenient to sell hydropower directly to the grid. As of today, the land in which the steel mill stood is being reclaimed and planned for a future photovoltaic park that in conjunction with hydroelectric power plants will provide electricity to electrolyzers for hydrogen production.

2.1 Hydroelectric watercourse system

In general we can distinguish two types of hydroelectric systems based on their different disposition with respect to the river,[21]:

a. run of river systems;

b. systems with seasonal reservoir and regulating basins.

In the case studied, hydroelectric plants are seasonal reservoir and regulating basins, using Pelton and Francis turbines, more suitable for larger heads and smaller flow rates.
Hydroelectric plants can be classified according to the duration of the available reserve as reservoir, basin, and run-of-river. The storage time of the reserve is defined as the time required to supply the storage itself with a volume of water equal to the useful capacity, with the average annual flow rate of the watercourses that flow into it (excluding any type of pumping).
For a seasonal reservoir we need a storage duration $n \geq 400\ h$, in this way if for instance in winter we have more water coming from the river, we can accumulate this

and use it in a different season. For a regulation basin, weekly or daily, the storage duration needs to be $2 < n < 400\ h$, this allows a daily or weekly regulation based on the trend of the energy price and therefore of the demand. For $n \leq 2\ h$ we have run-of-river systems, which are instead operational when there is water flowing into the river. In our case, as described below, the Larecchio dam is a sisonal reservoir and the Agrasina and Cipata dams are daily modulation basins.
Since they are not run-of-river power plants, a minimum vital flow (MVF, in italian DMV) of waterways must be guaranteed by law.
MVF $\stackrel{\text{def}}{=}$ is the instantaneous flow rate to be determined in each homogeneous section of the watercourse which must guarantee protection of the physical characteristics of the watercourse, chemical-physical characteristics of the waters as well as the maintenance of the biocoenoses typical of the local natural conditions. According to the definition provided by [32] (Po River Basin District Authority), which is responsible for all the tributaries of the Po River.
So MVF is the minimum flow that must be released on the stream for environmental reasons of flora and fauna and for civilian reasons. We therefore list the main needs required for the evaluation of the MVF:

- protection of the balance of aquatic ecosystems;
- protection of the landscape and therefore of the "naturalness" of the river;
- protection of water use;
- respect for the chemical-physical quality of the water.

MVF calculation can be performed by:

- calculation by experimental equations;
- theoretical calculation;
- the flow duration curve;
- fixed percentage of the average flow rate;
- hybrid methods;
- relating the size of the basin to the minimum flow rate.

In Italy, the regulation for the award of concessions defines the calculation methodology at the regional level. Therefore the calculation methodology can vary according

to the region to which the river stretch belongs or according to the main river to which the river is affluent. In our case, the calculation methodology refers to that drawn up by the Po River Basin Authority, which uses the following formula:

$$MVF = k * q_{meda} * S * M * Z * A * T \times 10^{-3} = MVF_{idro}(M * Z * A * T) \ \frac{m^3}{s} \tag{2.1}$$

$$k = -2 \times 10^{-3} * S + 0.14; \quad if \quad S < 1000 \ km^2; \tag{2.2}$$

Where:

- k: is an experimental parameter determined for single hydrographic areas;
- q_{meda}: average annual specific flow per unit of basin area ($l/(s \ km^2)$);
- S: area of the natural basin subtended by the section of the catchment area (km^2);
- M: morphological parameter;
- Z: the largest of (N,F,Q), where N is the naturalness coefficient, F is the water use coefficient and Q is a parameter that considers the quality of the river water;
- A: parameter relating to the interaction between surface water and groundwater;
- T: flow modulation time;

River	S	k	Q_{meda}	MVF_{idro}	$(M * Z * A * T)$	MVF
	km^2	$--$	m^3/s	m^3/s	$--$	m^3/s
Isorno	71.3	0.139	2.53	0.351	0.856	0.3
Melezzo	56.2	0.139	1.96	0.272	0.882	0.24
Fenecchio	16.0	0.140	0.55	0.077	0.781	0.06
Nocca	11.1	0.140	0.43	0.060	0.832	0.05

Table 2.1: MVF values of streams and rivers of our interest, values taken from the technical annex [14], $Q_{meda} = q_{meda} * S * 10^{-3}$ in (m^3/s);

In the Table2.1, the MVF values of some of the main streams and rivers used by the hydroelectric watercourse system are reported; these values have been taken from the technical annex of the Piedmont region [14].
Based on the flow rates used by hydroelectric plants, a classification can be made:

1. low flowrate $Q < 10\ m^3/s$;
2. meduim flowrate $10 < Q < 100\ m^3/s$;
3. large flowrate $100 < Q < 1000\ m^3/s$;
4. very large flowrate $Q > 1000\ m^3/s$.

In our case these are plants that work at low flow rates, therefore at $Q < 10\ m^3/s$. Based on the installed nominal power P_n, the hydroelectric plant is classified according to the following categories:

i. micro plants: $P_n < 0.1\ MW$;
ii. mini plants: $0.1 < P_n < 1\ MW$;
iii. small plants: $1 < P_n < 10\ MW$;
iv. large plants: $P_n > 10\ MW$.

In this case we can say that the plants installed in the hydroelectric watercourse system all correspond to the category of small plants apart from the Montecrestese plant which belongs to the category of mini plant. Furthermore, hydroelectric plants can also be classified according to the available head (H), in the following categories:

a) low head for $H < 50\ m$;
b) medium head for $50 < H < 250\ m$;
c) high head $250 < H < 1000\ m$;
d) very high head $H > 1000\ m$.

In our case, the plants in the hydroelectric watercourse system fall into the high-head-jump category (around $400\ m$).

2.1.1 Hydroelectric plants present

Agrasina plant,[26]
Plant located in Montecrestese (VB), at an altitude of 1365 m above sea level. It draws from the waters of the Larecchio dam (seasonal reservoir at 1853 m above sea level) and from the Isorno torrent. Plant built between 1951 and 1953 uses a Pelton turbine and two Frencis turbines for a total power of 5.1 MW and an average annual production of 7500 MWh/y (jump between $400 - 450$ m).

Cipata plant
Plant located in Montecrestese (VB), an altitude of 960 m above sea level. Withdrawals from the waters of the Agrasina dam (daily tank at 1365 m) from the Isorno torrent. The plant built between 1950 and 1953 uses two Pelton turbines for a total power of 10.6 MW and an average annual production of 31600 MWh/y (jump of about 400 m).

Nuova Ceretti plant
Plant located in Montecrestese (VB), an altitude of 480 m above sea level. Withdraw from the waters of the Cipata dam (daily tank at 960 m). The plant built in 1927 and renovated between 1995 and 1998. It uses a Pelton turbine for a total power of 10.5 MW and an average annual production of 40300 MWh/y (jump of about 450 m).

Pontetto plant
Plant located in Montecrestese (VB), an altitude of 360 m above sea level. It draws from the waters of the Avonso lake (daily reservoir at 680 m above sea level) and from the Isorno stream and its tributaries (Rio Nocca and Gillino). The plant was built between 1925 and 1926. It uses two Pelton and two Francis turbines for a total power of 8.8 MW and an average annual production of 20500 MWh/y (jump of around 320 m).

Montecrestese plant
Plant located in Montecrestese (VB), an altitude of 300 m above sea level. It draws from the waters of the Isorno stream. The plant was built between 1940 and 1946. It uses two Francis turbines for a total power of 0.7 MW and an average annual production of 4100 MWh/y.

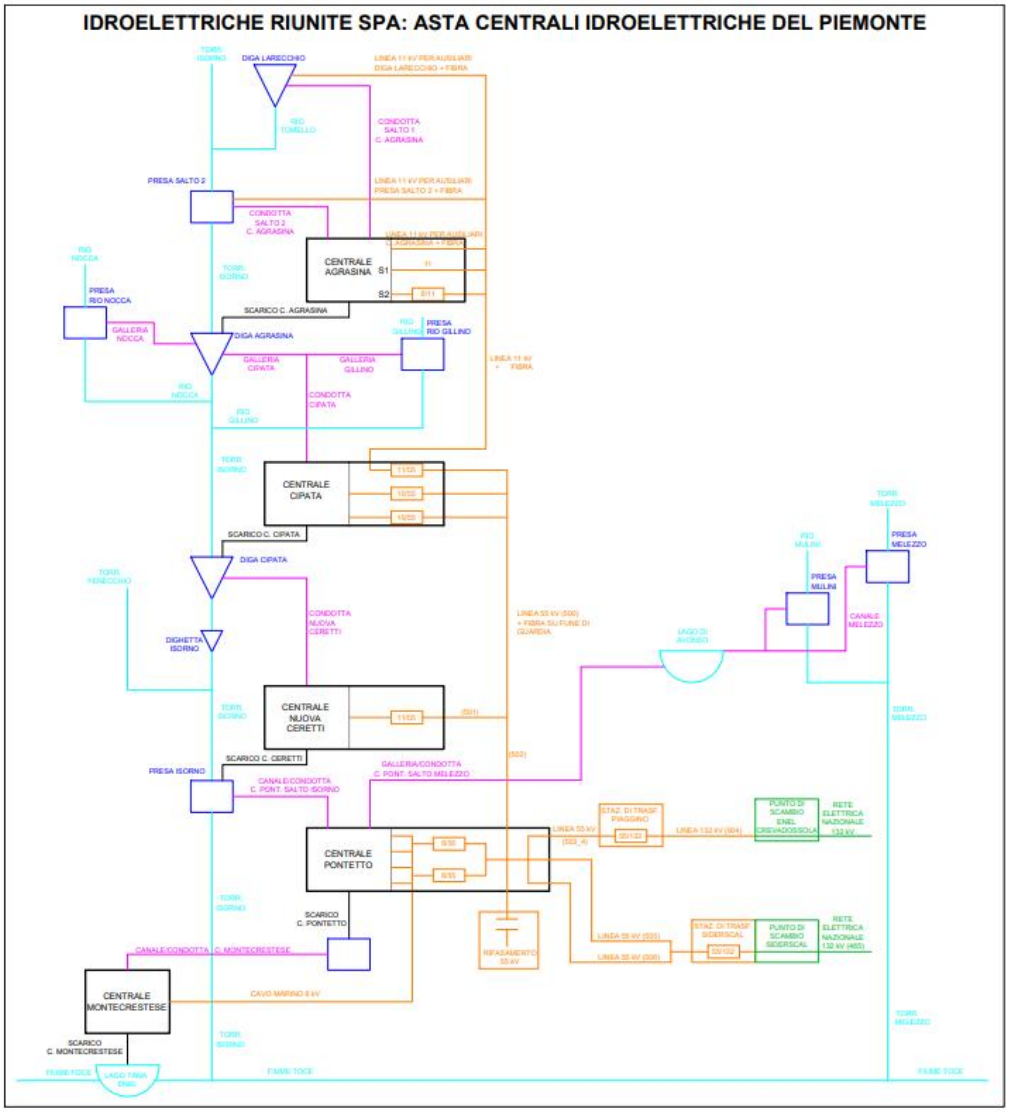

Figure 2.1: Block diagram of reservoir hydropower plants in watercourse. lines in light blue: natural streams and rivers; lines in orange: power connections; fuchsia lines: jump lines, pipelines, tunnels and penstocks; squares in blue: intake works; blue triangles: dams; light blue semicircles: natural lakes (Edited by Giacomo Magoni).

2.1.2 Water line diagram

The block diagram depicted in Figure2.1 begins with the Isorno Stream (light blue line) which is the main stream passing through the Isorno Valley. The Larecchio dam, at an elevation of about 1853 meters above sea level, which is the largest of those listed and for which we have the largest accumulation. Water reaches the Algrasina power plant via two jumps:

- Jump 1: Takes water from Larecchio Dam;
- Jump 2: Takes water from both the Larecchio Dam outlet and the Isorno Stream.

Downstream of the Algrasina power plant, the water that has been turbined is discharged to the Agrasina dam. The Agrasina dam in addition to receiving water from the Isorno stream also receives water from the rio Nocca and rio Gillino which are two tributaries of the Isorno River which in fact reconnect below the Agrasina dam. A tunnel starts from the Agrasina dam and later in a penstock until it reaches the Cipata power plant. Discharge water from the Cippata power plant, together with water from the Isorno stream reach the Cipata dam.
Agrasina and Cippata dams are daily modulation basin, since the water level in these can range from 100% to 0% in a day, these are also called modulation basins.
The jump connected to the Nuova Ceretti power plant starts from the Cippata dam, the discharge of which is connected to the intake of the Isorno torrent (therefore discharging directly into the main river), the waters of the Isorno torrent and the Fenecchio tributary arrive at the intake. Through the canal/duct C. Pontetto jump Isorno (Figure2.1) the water reaches the Pontetto power plant. Two jumps reach the Pontetto power station:

- Jump 1: canal/duct to Pontetto power plant from Isorno jump;
- Jump 2: tunnel/duct to Pontetto power plant from Melezzo jump (which starts from Avonso Lake).

At the outlet of the Pontetto power plant we have the intake connected by canal/duct to the Montecrestese power plant, this power plant in turn discharges to Lake Tana into which the Toce River passes and to which the Isorno stream flows. The Toce River flows through the towns of Villadossola, Domodossola and Valdossola.

2.1.3 Electrical connections

The electrical connections, represented by the orange lines in Figure2.1, these serve:

- auxiliary services;
- The motion of dam sluice gates;
- the lines carrying the energy produced by the power plants in which the squared transformation ratios are represented.

As we can see in Figure2.1 starting from the Agrasina power plant we have that it starts a 11 kV line used for auxiliaries and a first 6/11 kV transformer whose output is connected to the same 11 line. At the Cippata power plant the voltage is further raised by means of a first 11/55 kV transformer and the energy produced by the Cippata power plant is subjected to a 10/55 kV transformation whose output is connected to the same main line now at 55 kV (which is the line that will reach Villadossola also called the 55 Line). At the Nuova Ceretti power plant we have another 11/55 kV transformer connected to the same main line and sending to the Pontetto power plant we have a 6 kV connection to the Montecrestese power plant and through two 6/55 transformers connect to the 55 kV main line. At the Pontetto power plant there is the Piaggino transformer station owned by Idroelettriche Riunite which raises the voltage from 55 to 132 kV, finally this is sent to the Enel exchange point in Crevadossola (green color) and then fed into the national power grid operated by Terna. Or it can be sent at 55 kV to the Villadossola station, where the voltage is raised to 132 kV at the Siderscal transformer station and transferred at the Siderscal exchange point to the national power grid. As we can see, the line coming to Villadossola is a double 55 kV line, while the line coming to Piaggino is a single line. Between Pontetto and Villadossola we have a distance of about 15 km. This hydroelectric plant as a whole generates a capacity of $8MW_{baseload}$.

2.2 Management and sale of hydropower

Hydroelctric watercourse system optimization is done based on the previous day's electricity price, i.e., based on what is called the day-ahead market, where the sale of energy is carried out by an external result-guarantee operator. Energy must be produced at the instant it is demanded to maintain grid stability (50 Hz). A forecast curve is constructed based on measurements and estimates made by TERNA the previous day for the next day. Normally, the energy price has an M-shaped profile as can be seen from the graph in Figure2.2 taken from the GME (Gestore Mercati

Energetici) website, [20] taken on a typical day. The hourly purchase price curve has this pattern because in the middle hours of the day there is usually a drop in price due to the presence of solar renewable energy from photovoltaics, while there are usually price peaks in the morning between 8 and 10 and in the evening between 18 and 21, which are the time slots when the overlap between civilian and industrial demand occurs and thus the electricity turns out to have price peaks. At night there is less consumption (thus less demand) and consequently the price goes down.

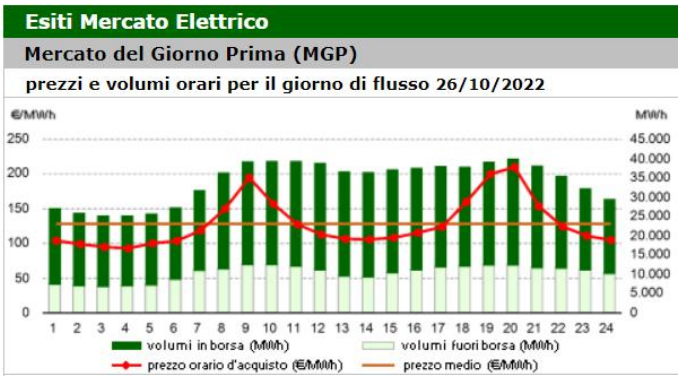

Figure 2.2: Hourly power purchase price trend.

Demand coverage is the responsibility of the transmission system operator (TSO), which is responsible on an instant-by-instant determination of which plants need to be in production and which are not needed to cover demand (in Italy this is TERNA). The TSO has the goal of covering demand by minimizing the cost function, which in the case of a competitive market corresponds to minimizing purchase prices (marginal cost equal to price in a perfect competition market).
Based on the ordering of plants according to the marginal cost of production, the order of merit to production can be constructed. Starting with the plants that have lower variable cost of production to go up as the demand for energy goes up, so the value of energy on the grid is a function of the marginal cost of generation of the plants.

2.2.1 The optimum condition

Consider that we have to supply a certain load P_u by using n plants of power P_i, assume that the supplied power is not upper bound.

We write the hourly cost function (objective function to be minimized) as:

$$C_T = \sum_{i=1}^{n} C_i(P_i) \quad \left[\frac{€}{h}\right] ; \tag{2.3}$$

we write the constraint function as:

$$\Psi = P_u - \sum_{i=1}^{n} P_i = 0; \tag{2.4}$$

we then write the Lagrangian function $L(P, \lambda)$:

$$L(P, \lambda) = \sum_{i=1}^{n} C_i(P_i) + \lambda \left(P_u - \sum_{i=1}^{n} P_i \right) ; \tag{2.5}$$

we now look for the constrained minimum critical points, then derive the Lagrangian function with respect to the power P_i and with respect to λ and set equal to zero:

$$\begin{cases} \frac{\partial L(P,\lambda)}{\partial P_i} = \frac{\partial}{\partial P_i} \left[\sum_{i=1}^{n} C_i(P_i) + \lambda \left(P_u - \sum_{i=1}^{n} P_i \right) \right] = 0 \; ; \quad i = 1, .., n; \\ \frac{\partial L(P,\lambda)}{\partial \lambda} = P_u - \sum_{i=1}^{n} P_i = 0 \; ; \end{cases} \tag{2.6}$$

$$\begin{cases} \frac{dC_i}{dP_i} - \lambda = 0 \quad i = 1, .., n \\ P_u - \sum_{i=1}^{n} P_i = 0 \end{cases} \tag{2.7}$$

$$\frac{dC_1}{dP_1} = \cdots = \frac{dC_n}{dP_n} = \lambda \tag{2.8}$$

we can thus observe that the value of energy on the grid is given by the marginal cost of the plants called upon to produce it. The last plant called to produce is the marginal plant representing the value of energy (λ).

2.2.2 Basin hydroelectric production optimization

These plants have very low variable cost (only the cost of raising and lowering the inlet gates) and do not work throughout the day like flowing water plants (for which

they work as long as water is flowing and there is no flooding).
For basin plants, we have the option of working for a certain number of hours per day depending on the basins ($3 \div 12$ h/day). Consequently, it is convenient to have the basin plants work during the hours when the market value of energy is highest and thus we monetize the water in the basin as the lost cost of equivalent production in thermoelectric generation. To identify the exact hours of operation, we rely on estimated demand curves as we can see in Figure 2.3 (load duration curve (LDC) from TERNA). Therefore, in general we tend to push the production of reservoir hydro plants toward the peak period, but not too much because otherwise the corresponding power between the ordinates does not enclose an area equal to all the energy we can produce. We would then have a plant that works too much during peak periods, therefore we cannot generate all the energy that we can with the power available.

Figure 2.3: Load duration curve (LDC) from TERNA 2021 website [38].

If hydropower ($P_{H_j}^{max}$) is always insufficient ($\forall\ t \in [0, T]$) to cover the total power required (P_{u_j}), in this case thermoelectric power generation (P_{S_j}) is used throughout the time horizon, we must then optimize the time trend of the corresponding power.

Hypothesis: Total power of hydropower plants in no period j of T is sufficient to feed the load: $\rightarrow P_{H_j}^{max} < P_{u_j}; \quad j = 1, ..., n_T$.

Objective: Minimize the total production cost $C(P_s)$.
Constraints:

$$\sum_{j=1}^{n_T} \Delta t_j \ \dot{q_j} = q_{tot}; \tag{2.9}$$

$$P_{u_j} - P_{H_j} - P_{S_j} = 0; \quad j = 1, ..., n_T. \tag{2.10}$$

Where $\dot{q_j}$ is the flow rate of water used by the hydropower in the j-th time period and q_{tot} is the total amount of water available.
We write the Lagrangian function subject to the constraints on flow rate and power with the respective Lagrange multipliers γ and λ_j:

$$L = \sum_{j=1}^{n_T} \Delta t_j \ C_j(P_{S_j}) + \sum_{j=1}^{n_T} \lambda_j \left(P_{u_j} - P_{H_j} - P_{S_j}\right) + \gamma \left(\sum_{j=1}^{n_T} \Delta t_j \ \dot{q_j} - q_{tot}\right) \tag{2.11}$$

$$\begin{cases} \frac{\partial L}{\partial P_{S_j}} = \Delta t_j \frac{dC_j(P_{S_j})}{dP_{S_j}} - \lambda_j = 0 \quad j = 1, .., n_T; \\ \\ \frac{\partial L}{\partial P_{H_j}} = -\lambda_j + \gamma \ \Delta t_j \frac{d\dot{q_j}}{dP_{H_j}} = 0 \quad j = 1, .., n_T; \\ \\ \frac{\partial L}{\partial \lambda_j} = P_{u_j} - P_{H_j} - P_{S_j} = 0 \quad j = 1, .., n_T; \\ \\ \frac{\partial L}{\partial \gamma} = \sum_{j=1}^{n_T} \Delta t_j \ \dot{q_j} - q_{tot} = 0 \quad j = 1, .., n_T; \end{cases} \tag{2.12}$$

$$\Delta t_j \frac{dC_j(P_{S_j})}{dP_{S_j}} = \Delta t_j \gamma \frac{d\dot{q_j}}{dP_{H_j}} \Rightarrow \gamma = \frac{\frac{dC_j(P_{S_j})}{dP_{S_j}}}{\frac{d\dot{q_j}}{dP_{H_j}}} \tag{2.13}$$

Where γ is the pseudo shadow price of water, it provides information on when to use the water reserve. The shadow price represents by how much the cost increases for a change in constraint that makes it more stringent. In this way, we can assign a value to the water flowing through our system and then determine based on the accumulation in which part of the load duration curve to place our production, maximizing the price but still staying in a range of production below the peak and thus guaranteeing all the energy that can be produced.

2.2.3 Number of equivalent hours

A general formula to express the nominal power P_N produced by a hydroelectric plant can be expressed by the following relationship:

$$P_N = \eta(\rho g)QH = \frac{E_{tot}}{H_e}; \tag{2.14}$$

where η is the efficiency of the hydraulic turbine (in our case Pelton or Francis), $(\rho\ g)$ is the specific gravity of the liquid, Q is the volumetric flow rate and H is the head.
Since these plants are already existing and operational, we know their average annual energy production E_{tot}, consequently we can calculate the number of equivalent hours H_e for which the system works at nominal power. The number of equivalent hours can be defined as:

$$H_e = \frac{\textbf{Energy Produced}}{\textbf{Nominal Power}} = \frac{\int_0^{h_y} P_i(t)dt}{P_N} = \frac{E_{tot}}{P_N} = 2913.2\ \frac{h}{y}; \tag{2.15}$$

where h_y are the hours in a year ($h_y = 8760\ h/y$).
Furthermore, we can calculate the capacity factor C_f.
C_f is the ratio between the real energy produced over a period of time and the energy that would have been produced if the plant had operated at nominal power P_N for the same period. We write the C_f formula for the time period of one year ($h_y = 8760 h/y$):

$$C_f = \frac{\int_0^{h_y} P_i(t)dt}{P_N * h_y} = \frac{E_{tot}}{E_N} = 0.33. \tag{2.16}$$

	Agrasina	Cipata	Nuova C.	Pontetto	Montecrestese	Tot
E_{tot}(MWh/y)	7500	31600	40300	20500	4100	104000
P_N (MW)	5.1	10.6	10.5	8.8	0.7	35.7
H_e (h/y)	1470.6	2981.1	3838.1	2329.5	5857.1	2913.2
C_f	0.17	0.34	0.44	0.27	0.67	0.33

Table 2.2: Values of annual average energy produced E_{tot}, nominal power P_N, equivalent number of hours per year H_e, and capacity factor C_f of individual plants and of the entire hydroelectric watercourse, values taken from [26].

The Table2.2 shows the average annual electricity production values E_{tot}, the installed power P_N, the equivalent hours H_e and the capacity factor C_f for the individual plants and for the entire hydroelectric watercourse system.

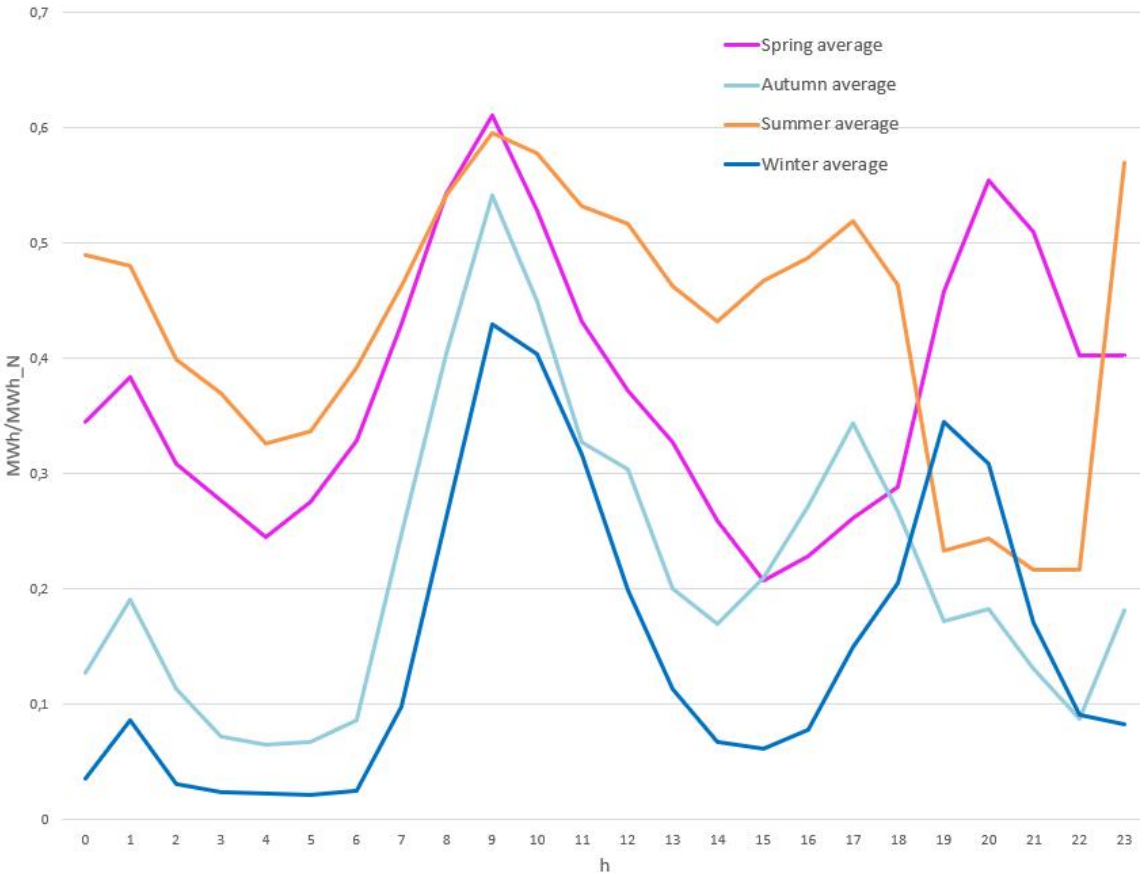

Figure 2.4: Average daily production normalized to nominal production for each season in 2021.

The graph in Figure2.4 shows the seasonal average hourly production values, normalized with respect to the hourly production at nominal power P_N. So to find this graph an hourly average was taken for each month of the year. The months were then grouped by seasons and then the seasonal hourly average was performed. The measured values were then normalized with respect to the hourly production at nominal power. The plotted values obtained correspond to the capacity factor for each hour of the day, but expressed with respect to the average energy actually produced for each hour in each season. As we can see, the curves representing the capacity factor for the different seasons have fairly similar trends, with peaks corresponding to the hours of peak demand for electricity on the grid. We can therefore observe that hydroelectric production follows the price and under the constraints described in the previous paragraph (of limited flow and always insufficient power),

production is optimised. Furthermore, since the hydroelectric watercourse can not only exploit daily reservoirs, it can also draw on a seasonal reserve, it is possible to work throughout the year by adequately distributing the reserves and based on the electricity market trend during the year.

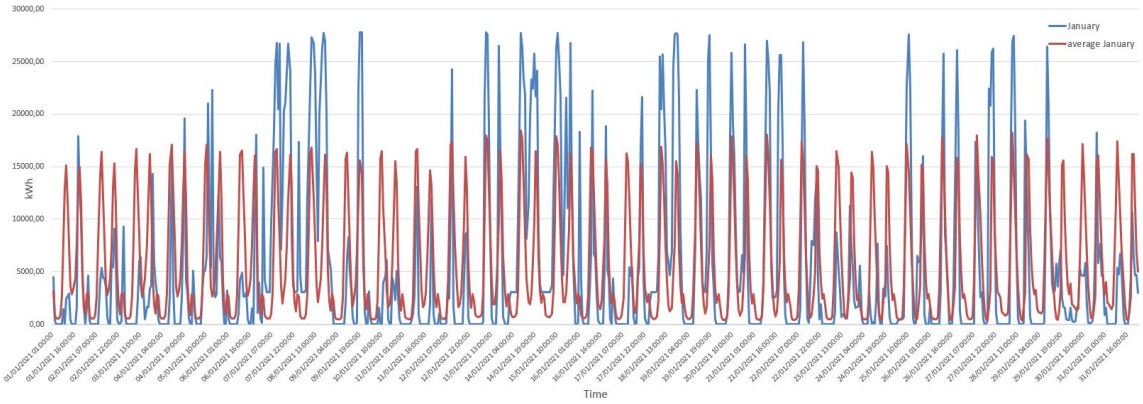

Figure 2.5: Daily production in Jenuary 2021 in blue in comparison with the January average monthly production in red.

In the plot in the Figure2.5 we can observe the production of January compared to the monthly average of that month.

Chapter 3

Photovoltaic system

3.0.1 Reclamation, filling and investment phases PNRR

In participating in the National Recovery and Resilience Plan (in Italian PNRR, Piano Nazionale Ripresa e Resilienza), two manifestations of interest were submitted:

1. candidacy as a brownfield site;
2. expression of interest in investing in hydrogen.

This subsection shows the operational steps required for project development.

Brownfield site remediation
At the site where the Villadossola steel mill stood, now being dismantled with future redevelopment project and photovoltaic park, three main points where remediation needs to be carried out have been noted. Two of these consist of metal pollution and one of transformer oil, the underlying aquifer is not affected. Site remediation involves the removal of the contaminated soil, this will be disposed of and depending on the dangerousness of the waste will change in cost per quintal of disposal.
Subsequently, monitoring and verification by ARPA (Agenzia Regionale per la Protezione Ambientale) will take place, through coring.

Site filling and redevelopment
Once the reclamation has been completed and recognized by the regional agency, the filling and redevelopment phase can begin.
The backfill material has already been selected for this stage, based on its proximity, quality and cost.
The choice was made to use waste marble quarry material, which will have zero material and transportation cost, minus the cost of processing the last layer deposited.

3.1 Photovoltaic park installation and design

The brownfield area covers about 90000 m^2, almost all of which has been earmarked for the installation of a 6 MW_{peak} photovoltaic system. The following boundary clearances have been kept for this land:

- 30 m from the railway (east side);
- 20 m from Sempione Street (west/south-west side), to avoid shading due to the difference in height of 7 m;
- 50 m from the middle of Ovesca creek (north side).

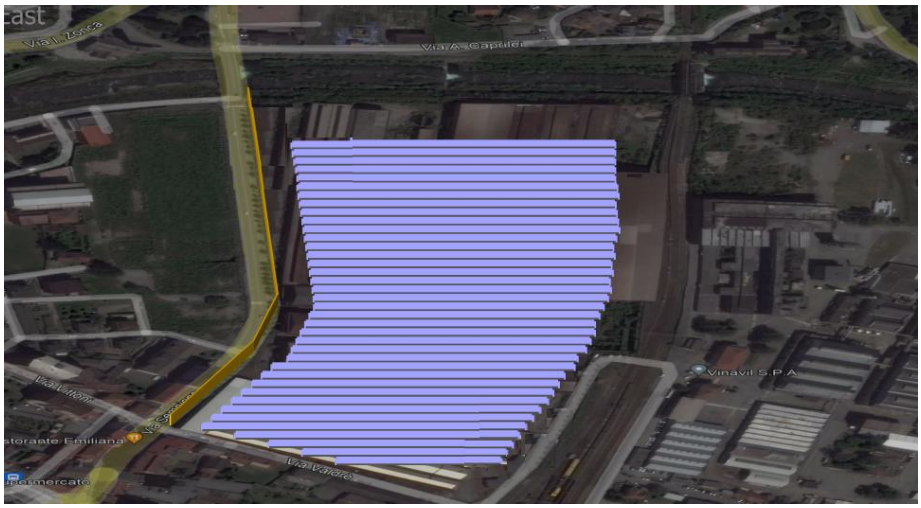

Figure 3.1: photovoltaic park preview

In this way, a useful area for the installation of the photovoltaic park of approximately $A_{useful} = 61600\ m^2$ was identified as shown in Figure3.1 .
The design calculation of this plant was performed using the following design program: PVsyst. In this paper we report the idea of the operations that are performed for sizing.
The data sheet in [35] for the solar module summarized in Table3.2 and the data sheet in [34] for the inverter were used, summarized in Table4.4.
The temperatures $T_{env,min}$ and $T_{env,max}$, were taken from [10] and location and altitude data from [40]. Environmental, location, irradiation, and land geometric data are summarized in Table3.1.

Environmental input Data:		
Latitude φ	N	46.07°
Longitude ψ	E	8.26°
$T_{env,min}$	$[°C]$	-8
$T_{env,max}$	$[°C]$	30
β	-	30°
A_{useful}	$[m^2]$	61600
G	$[W/m^2]$	1000
H_{Inc}	$[kWh/m^2\ y]$	1577.4
H_{eff}	$[kWh/m^2\ y]$	1436.1
h_y	$[h/y]$	1200
δ_{ss}	-	23.45°
δ_{ws}	-	$-23.45°$
Altitude	$[m]$	274

Table 3.1: Site input environmental data.

Photovoltaic module input data:		
$P_{max,STC}$	$[W_p]$	600
NOCT	$[°C]$	45
h_{modul}	[m]	2.465
L_{modul}	[m]	1.134
W_{modul}	[m]	0.035
$V_{MP,STC}$	[V]	45.3
$V_{OC,STC}$	[V]	53.5
$I_{MP,STC}$	[A]	13.25
$I_{SC,STC}$	[A]	14.03
η_{modul}	-	0.2149
β (V)	$[\%/°C]$	-0.275
α (I)	$[\%/°C]$	0.045
γ (Pmp)	$[\%/°C]$	-0.35
FF	-	0.80

Table 3.2: PV input data, taken from [35]

Inverter input data:		
$P_{max,pv,array}$	$[W_p]$	185000
$\eta_{UE,inv}$	-	0.9869
$V_{MPPT,min}$	[V]	500
$V_{MPPT,max}$	[V]	1500
V_{MIV}	[V]	1500
$I_{MPPT,max}$	[A]	26
$I_{SC,MPPT,max}$	[A]	40
N. inverter input	-	18
N. MPPT input	-	9

Table 3.3: Inverter input data, taken from [34]

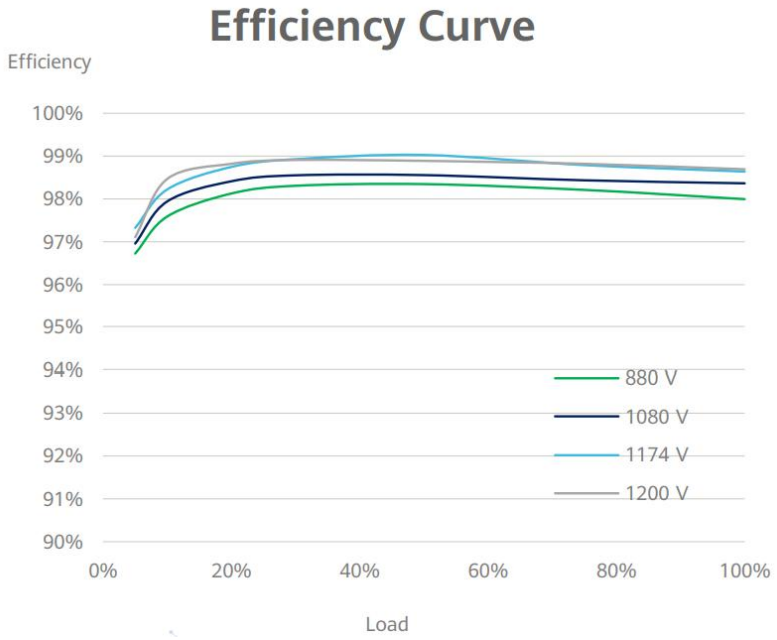

Figure 3.2: Plot of inverter efficiency ($\eta_{EU,inv}$) as load size changes, taken from catalog [34].

3.1.1 Calculation of maximum and minimum design temperatures

As first we calculate the maximum and minimum temperature of the photovoltaic cell, these cell temperatures occur, for an irradiated photovoltaic cell, when we have

the maximum and minimum ambient temperatures respectively ($T_{env,max}$, $T_{env,min}$):

$$T_{cell,max} = T_{env,max} + \frac{G}{0.8}(NOCT - 20°C) = 61.25°C \ ; \tag{3.1}$$

$$T_{cell,min} = T_{env,min} + \frac{G}{0.8}(NOCT - 20°C) = 23.25°C \ ; \tag{3.2}$$

3.1.2 Choice of tilt angle

In this case, an angle of inclination $\beta = 30°$ is chosen, while from the website given in [40], setting the latitude and longitude of the location where the photovoltaic system will be installed, setting the "optimize slope" option we get a $\beta \cong 40°$.
In general, the choice of tilt angle is acceptable if it falls in the range between $30° \leq \beta \leq 40°$, the range for which there is the greatest transposition factor, defined as the ratio of irradiation on the tilted plane to irradiation on the horizontal plane. This is calculated over the period of one year for different angles of inclination and azimuth (angle to the south).
The angle of inclination can also be calculated as:

$$\beta_{opt} = \varphi - 10° = 36°. \tag{3.3}$$

3.1.3 Design calculation of current voltage and power

Let us now calculate the limiting values of voltage current and power. When the ambient temperature is low ($T_{env,min}$), we have that the voltage at the point of maximum power ($V_{MP,max}$) results maximum (maximum among the possible voltage values at the MPP). This value is calculated under sunny conditions preceded by clouds, under these conditions during the passage of clouds the photovoltaic cell is not directly irradiated and therefore the temperature of the cell will tend to the temperature of the outside environment ($T_{env,min}$). Under these ambient conditions, the conditions of maximum voltage at the MPP (maximum power point) and maximum open circuit voltage are reached:

$$V_{MP,max} = V_{MP,STC}\left[1 + \frac{\beta}{100}(T_{env,min} - 25°)C\right] = 45.52 \ V; \tag{3.4}$$

a power spike is generated under these conditions:

$$P_{max} = P_{max,STC}\ \frac{G}{1kW/m^2}\left[1 + \frac{\gamma}{100}(T_{env,min} - 25°C)\right] = 669.3 \ W_p; \tag{3.5}$$

the analog occurs for the determination of $V_{OC,max}$:

$$V_{OC,max} = V_{OC,STC}\left[1 + \frac{\beta}{100}(T_{env,min} - 25°C)\right] = 58.36\ V. \tag{3.6}$$

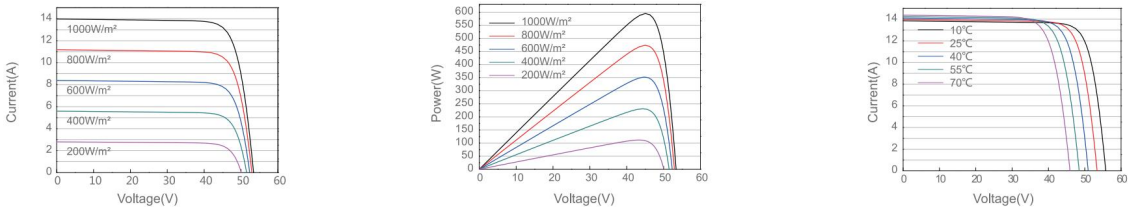

Figure 3.3: characteristic curves (I-V) with different values of irradiance G and temperature T and characteristic curve (P-V) with different values of irradiance G, taken from catalog in [35].

Temperature has an effect on the semiconductor in the passage of electrons from the conduction band to the valence band; the higher the temperature, the easier it is to promote electrons into the conduction band and thus the lower the voltage will be, as we can see in the graph (I-V) in Figure3.3. In fact, as temperature increases the difference between the Fermi level of the doped semiconductor and the Fermi level of the intrinsic semiconductor decreases. Through increasing temperature we are able to release more electrons, and the primary mechanism of electron promotion becomes silicon bond breaking and not promotion due to the presence of the dopant (the higher the temperature the more the semiconductor behaves like an intrinsic semiconductor). So when the ambient temperature is high ($T_{env,max}$), the cell is brought to the $T_{cell,max}$ for which we have that the voltage in the MPP working conditions results in minimum:

$$V_{MP,min} = V_{MP,STC}\left[1 + \frac{\beta}{100}(T_{cell,max} - 25°C)\right] = 40.78\ V; \tag{3.7}$$

vice versa for the current we reach the maximum conditions in the short circuit conditions when the temperature is high:

$$I_{SC,max} = I_{SC,STC}\ \frac{G}{1kW/m^2}\left[1 + \frac{\alpha}{100}(T_{cell,max} - 25°C)\right] = 14.26\ A. \tag{3.8}$$

3.1.4 Calculation of the number of modules in series and parallel

Now we calculate the maximum and minimum number of modules in series for each MPPT input of the inverter and under MIV (maximum input voltage) conditions. For these we take the integer part rounded down in the maximum condition and the integer part rounded up in the minimum condition:

$$N_{max,MPPT} = int\left(\frac{V_{MPPT,max}}{V_{MP,max}}\right) = 32 \ ; \tag{3.9}$$

$$N_{min,MPPT} = int\left(\frac{V_{MPPT,min}}{V_{MP,min}}\right) + 1 = 13 \ ; \tag{3.10}$$

$$N_{max,MIV} = int\left(\frac{V_{MIV}}{V_{OC,max}}\right) = 25 \ . \tag{3.11}$$

The range of modules in series is between:

$$N_{min} = N_{min,MPPT} = 13 \ ; \quad N_{max} = min\left(N_{max,MPPT}, N_{max,MIV}\right) = 25 \ ; \tag{3.12}$$

the average between N_{min} and N_{max}:

$$N_{M,series} = \frac{N_{min} + N_{max}}{2} = 19 \ . \tag{3.13}$$

Now we calculate in number of strings in parallel, in this case then we will have to refer to the maximum current supported by each MPPT input of the inverter $I_{MPPT,max}$ versus the maximum current for a single module under short circuit conditions $I_{SC,max}$, approximating by defect:

$$N_{M,parallel} = int\left(\frac{I_{MPPT,max}}{I_{SC,max}}\right) = 1 \ ; \tag{3.14}$$

We calculate in the number of total modules allowed by each inverter by the ratio of the maximum power that the inverter accepts from each panel array to the nominal power of the module, approximating by defect:

$$N_{M,inv} = int\left(\frac{P_{max,pv,array}}{P_{max}}\right) = 308 \ ; \tag{3.15}$$

3.1.5 Calculation of distance between modules, shading

To find the total number of inverters to be installed, we must first estimate how many panels can be installed in the useful area (A_{useful}), considering a panel tilt with respect to the horizontal plane of $\beta = 30°$ and a southern exposure. Under these conditions, we need to estimate the minimum distance to be interposed between each panel, so that on the day when the sun at zenith (noon in true solar time) is lowest in the year (winter solstice), it does not generate a shadow on the next panel. We calculate the solar altitude angle for the winter solstice α_{ws} under the conditions described, knowing that at noon the hour angle ω=0:

$$sin(\alpha_{ws}) = sin(\delta_{ws})sin(\varphi) + cos(\delta_{ws})cos(\varphi)cos(\omega) = sin(\delta_{ws})sin(\varphi) + cos(\delta_{ws})cos(\varphi) \tag{3.16}$$

through trigonometric relations we obtain:

$$sin(\alpha_{ws}) = cos(\varphi - \delta_{ws}) = sin(90° - \varphi + \delta_{ws}) \tag{3.17}$$

$$\alpha_{ws} = 90° - \varphi + \delta_{ws} = 20.48° \ . \tag{3.18}$$

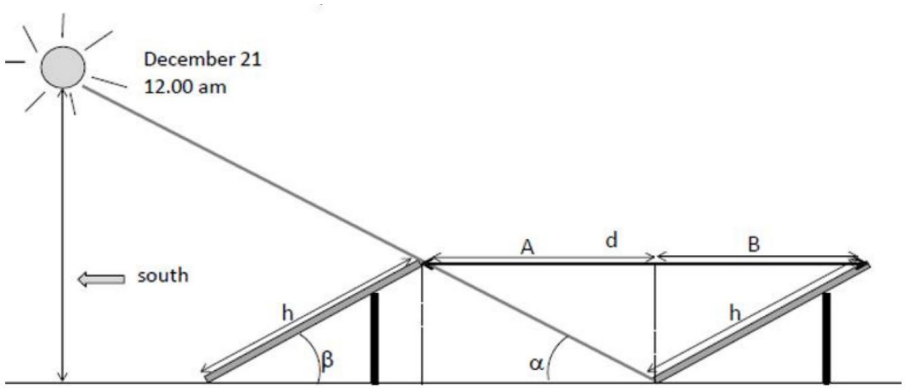

Figure 3.4: Illustrative drawing of module spacing to avoid shading between modules.

$$B = h\ cos(\beta) = 2.13\ m; \qquad l = h\ sin(\beta) = 1.23\ m; \tag{3.19}$$

$$A = \frac{l}{tan(\alpha)} = 3.3\ m; \qquad d = A + B = 5.43\ m. \tag{3.20}$$

Where B is the projection of the tilted module on the ground, l the tilted module height, A the distance between the end of one module and the beginning of the next, d the distance between the beginning of one module and the next, as shown in the Figure3.4.
Through the values found we calculate the area of the inclined module occupied on the ground $A_{tilt,M}$ and the area of the inclined module occupied on the ground including the distance between modules $A_{tilt,M+A}$ as follows:

$$A_{tilt,M} = B * L_{modul} = 2.42\ m^2; \qquad A_{tilt,M+A} = d * L_{modul} = 6.16\ m^2. \tag{3.21}$$

Note the useful area A_{useful}, we can then find the number of panels that can be installed as:

$$N_M = int\left(\frac{A_{useful}}{A_{tilt,M+A}}\right) = 10000; \tag{3.22}$$

and thus a total installed power of:

$$P = N_M * P_{max,STC} = 10000 \times 600 = 6000000\ W_p = 6\ MW_p. \tag{3.23}$$

We can now also calculate the number of inverters N_{inv} of the [34] type to be inserted as:

$$N_{inv} = int\left(\frac{N_M}{N_{M,inv}}\right) = 32. \tag{3.24}$$

3.1.6 Cartesian diagram

The Cartesian diagram in legal time shown in the Figure3.5 is useful for observing the effect of shading. In fact if we know the range of azimuth angle coverage (γ_s or AZ) due to the presence of nearby buildings and the value of solar height angle (α or HS), these values can be plotted in the abscissas and ordinates of the Cartesian diagram, respectively, and thanks to these we can identify the periods of the year and the hours when shading of our plant occurs. In addition, it is possible to calculate the contour of the horizon line for a given location. Since the photovoltaic plant is located in a hilly environment, it is necessary to take into account the different horizon and therefore the different hourly angles of sunrise and sunset, for which a reduction of about $2 - 3\%$ in radiation was considered.
In the Cartesian diagram in Figure3.5 we can see that the dashed black lines represent

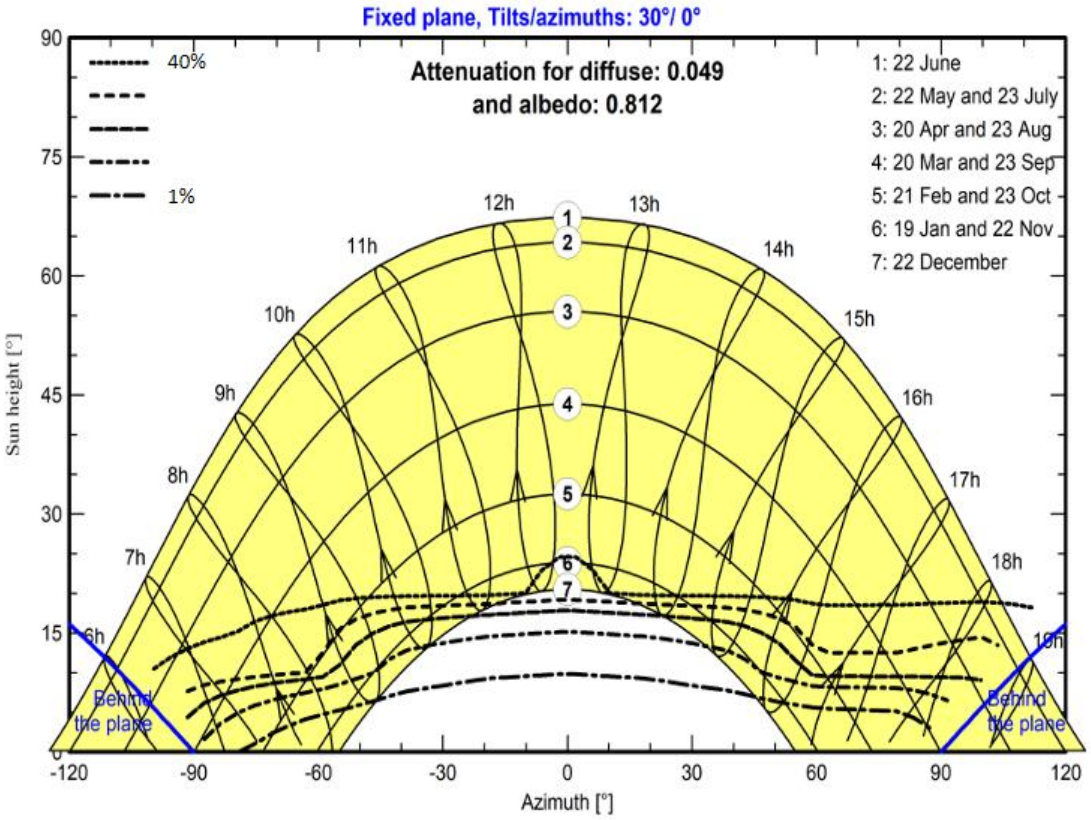

Figure 3.5: Cartesian diagram in legal time.

different scenarios from 1% to 40% of shading losses. These lines consider various cases because the projects for the buildings near the photovoltaic system have not yet been defined.
In this project, the presence of a difference in height of $h_w = 7\ m$ on the south-west side was taken into account and therefore a distance from the difference in height (Sempione Street) of $d_{s-w} = 20\ m$ was taken, obtained by:

$$d_{s-w} = \frac{h_w}{tg(20°)} = 19.23\ m \quad \rightarrow \quad d_{s-w} = 20\ m. \tag{3.25}$$

This does not affect the irradiance that much, changing the sunset time on the modules, as we can see in Figure3.6 , in the winter months from November to February between 15 and 15:30 in true solar time.

The Table3.4 shows the average daily values of global irradiance on the inclined plane of 30° for each month in the case of presence and absence of shadow due to

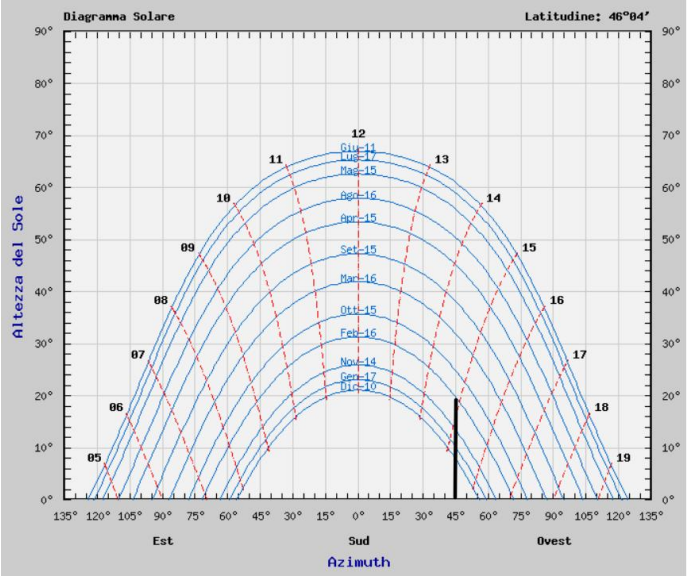

Figure 3.6: Cartesian diagram in true solar time (From ENEA website).

month	obstacle	$H_{inc,g,m}$	obstacle	$H_{inc,g,m}$	unit
Jan	absent	2.31	from $15h12'$ to ω_{ss}	2.07	kWh/m^2
Feb	absent	3.05	from $15h00'$ to ω_{ss}	2.64	kWh/m^2
Mar	absent	4.03	absent	4.03	kWh/m^2
Apr	absent	4.5	absent	4.5	kWh/m^2
May	absent	4.84	absent	4.84	kWh/m^2
Jun	absent	5.4	absent	5.4	kWh/m^2
Jul	absent	5.76	absent	5.76	kWh/m^2
Aug	absent	5.13	absent	5.13	kWh/m^2
Sep	absent	4.45	absent	4.45	kWh/m^2
Oct	absent	3.15	absent	3.15	kWh/m^2
Nov	absent	2.13	from $15h00'$ to ω_{ss}	1.94	kWh/m^2
Dec	absent	1.85	from $15h30'$ to ω_{ss}	1.75	kWh/m^2

Table 3.4: table of the average daily irradiance for each month in the presence and absence of an obstacle; (from ENEA website,[17]);

the difference in altitude of 7 m present southwest at a distance of 20 m from the photovoltaic system. By calculating the overall annual average irradiance in the two cases we obtain an overall reduction in the presence of an obstacle of 1.97%.

3.1.7 Balance of system efficiency and system producibility

Efficiency and losses:	
η_{modul}	0.2149
$\eta_{EU,inv} * \eta_e$	0.9838
L_c	0.1143
η_{BOS}	0.8857

Table 3.5: grouped efficiency and loss values;

Now that we know the characteristics of our system, we can calculate the energy produced annually E_{ideal} and the annual energy injected into grid E_{Grid}.
Known the annual value of effective incident irradiation ($H_{eff} = 1436.1 \ \frac{kWh}{m^2y}$) and the number of panels to be installed (N_M) we can identify the total panel area as:

$$A_{tot,M} = N_M * L_{modul} * h_{modul} = 27953 \ m^2; \tag{3.26}$$

$$E_{ideal} = H_{eff} * A_{tot,M} * \eta_{modul} = 8.63 \ GWh; \tag{3.27}$$

$$E_{Grid} = H_{eff} * A_{tot,M} * \eta_{modul} * (1 - L_c) * \eta_{UE,inv} * \eta_e = \tag{3.28}$$

$$= E_{ideal} * (1 - L_c) * \eta_{UE,inv} * \eta_e = 7.52 \ GWh$$

In the loss diagram shown in the Figure3.7, we can observe the contributions of each type of loss. These for simplicity have been grouped into three macro categories (reported in Table3.5) those concerning, the module efficiency (η_{modul}), the inverter efficiency multiplied by the various electrical losses ($\eta_{UE,inv} * \eta_e$), and L_c which takes into account optical, ohmic losses, temperature and cable losses.
The loss diagram Figure3.7 is useful as it allows us to consider the contribution of each type of loss and therefore to consider the system in real conditions and no longer in STD conditions, which in reality do not they almost never reach during the year.

So to calculate the annual production of the photovoltaic system we must consider the losses of the BOS system (Balance of system), through η_{BOS}, efficiency which in general contains the following various loss terms:

1. irradiance $< 1000 \ W/m^2$;

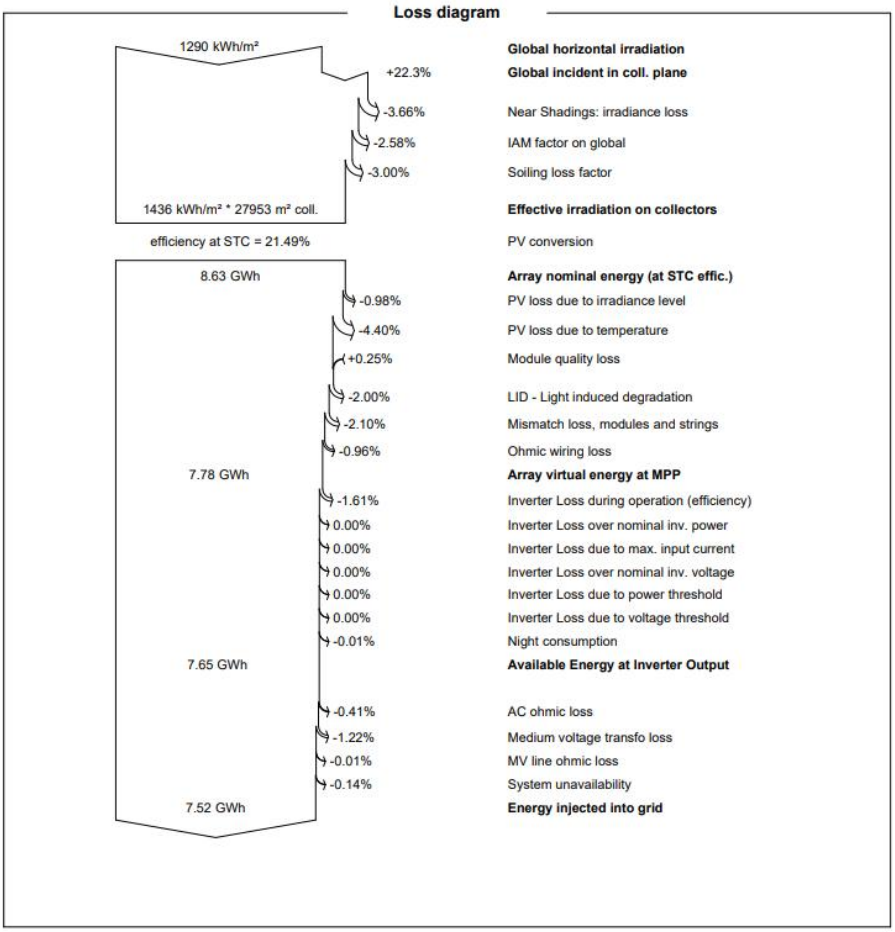

Figure 3.7: loss diagram, BOS (balance of system)

2. dirt on the modules;
3. temperature effect;
4. shadow;
5. losses due to the presence of the DC side cables due to the Joule effect;
6. defects in tracking the MPP in the chopper;
7. inverter losses
8. AC side losses.

The η_{BOS} efficiency does not replace the module efficiency under standard conditions (η_{modul}) but takes into account other losses that occur in all the rest of the system components.
It can therefore be rewritten as follows:

$$\eta_{BOS} = \eta_{EU,inv} * (1 - L_c) * \eta_e = 0.8857 \tag{3.29}$$

$$E_{Grid} = E_{ideal} * \eta_{BOS} = 7.52\ GWh \tag{3.30}$$

Month	H_{Hor}	$H_{d,Hor}$	T_{Amb}	H_{Inc}	H_{Eff}	E_{Array}	E_{Grid}	PR
	kWh/m^2	kWh/m^2	$°C$	kWh/m^2	kWh/m^2	GWh	GWh	–
January	53.7	18.31	5.45	104.7	91.4	0.521	0.494	0.786
February	66.9	28.77	5.35	104.0	94.9	0.539	0.522	0.836
March	119.3	45.29	9.89	157.7	146.5	0.811	0.785	0.830
April	106.5	58.89	13.19	116.6	106.7	0.585	0.566	0.809
May	150.5	76.72	17.87	153.7	140.9	0.758	0.734	0.796
June	157.9	71.39	22.50	155.6	142.9	0.753	0.728	0.780
July	205.8	78.72	26.82	207.9	191.9	0.995	0.964	0.773
August	156.8	67.79	26.49	170.7	157.5	0.817	0.791	0.772
September	112.9	48.39	20.80	137.5	127.1	0.674	0.652	0.790
October	70.8	35.60	13.58	99.9	91.5	0.505	0.488	0.814
November	37.4	20.40	11.79	58.9	52.4	0.292	0.280	0.792
December	51.3	15.73	5.88	110.1	92.4	0.529	0.512	0.775
Year	1289.9	566.01	15.02	1577.4	1436.1	7.779	7.518	0.794

Table 3.6: monthly irradiation table;

The Table3.6 shows the measured irradiation values grouped by month of the following quantities:

- H_{Hor}: Horizontal global irradiation;
- $H_{d,Hor}$: Horizontal diffuse irradiation;
- T_{Amb}: Ambient temperature;
- H_{Inc}: Global incident in the collector plane;
- H_{Eff}: Global effective, corrected for IAM and shading;
- E_{Array}: Effective energy at the array output;

- E_{Grid}: Energy injected into the grid;
- PR: Performance ratio.

3.1.8 Number of equivalent hours and PR

The number of equivalent hours H_e is defined as:

$$H_e = \frac{\textbf{Energy Produced}}{\textbf{Nominal Power}} = \frac{\int_0^{h_y} P_i(t)dt}{P_n} = \frac{E_{Grid,y}}{P_n} = 1252.7\ \frac{h}{y}; \tag{3.31}$$

($h_y = 8760\ h/y$). The number of equivalent hours is a very useful parameter when deciding on an investment, in fact this value allows us to compare renewable plants of different sizes and types and to compare them with each other. The most convenient choice will be the plant with the highest number of equivalent hours and the lowest investment cost. For instance, if we install a photovoltaic system with a power greater than the planned one, and therefore if we use a greater area, we will have greater losses due to shading and consequently a lower number of operating hours compared to the installed nominal power and a higher investment cost.

The PR (performance ratio) of a photovoltaic system is equal to the energy produced by the system (E_{Grid}), divided by the nominal power of the system (P_n) (Plant Nominal Power), multiplied by the irradiance in standard conditions ($1\ kW/m^2$) divided by the irradiation on the inclined plane of the modules (H_{Inc}):

$$PR = \frac{E_{Grid}}{P_n} * \frac{1\ kW/m^2}{H_{Inc}} = H_e * \frac{1\ kW/m^2}{H_{Inc}} = 0,794 \tag{3.32}$$

We can rewrite the PR formula as the product of the equivalent number of hours, i.e. the number of hours in which the photovoltaic system should work at its nominal power in order to produce the measured energy, by the inverse of the number of hours that would be necessary for the measured irradiation to affect the panels if the irradiance were equal to the standard irradiance of $1kW/m^2$. In the graph in Figure3.8 we can see the PR values for the different months.

R is the transposition factor, ie the ratio between global irradiation on the inclined incident plane (H_{Inc}) and the global irradiation on the horizontal plane (H_{Hor}):

$$R = \frac{H_{Inc}}{H_{Hor}} \tag{3.33}$$

This ratio is greater in the winter months, as the modules are inclined by 30°, consequently we have a greater incident irradiation on the inclined modules in the winter period than we would have on the module if it were horizontal.

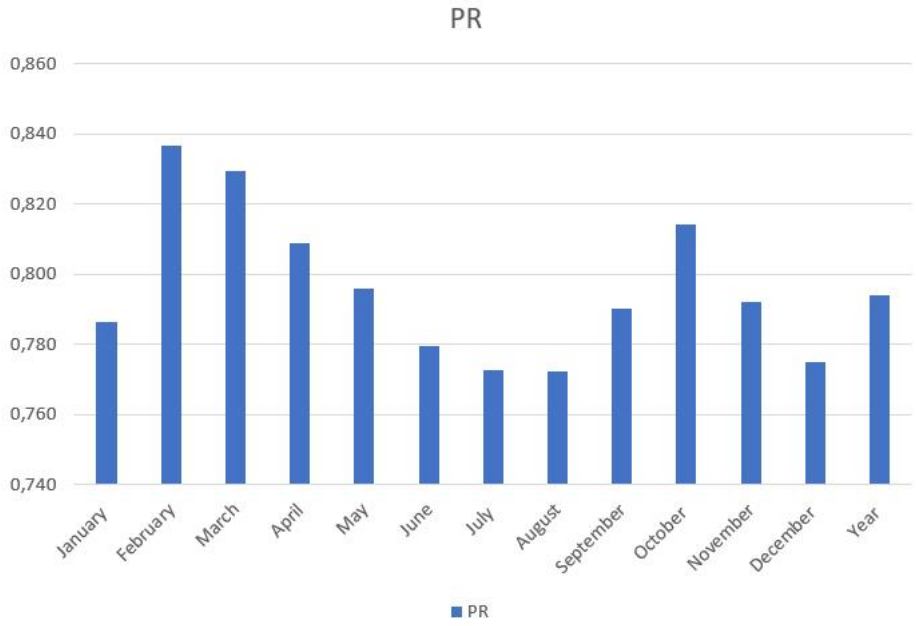

Figure 3.8: PR values in different months.

R_{Eff} is the ratio between effective and incident irradiation:

$$R_{Eff} = \frac{H_{Eff}}{H_{inc}} \tag{3.34}$$

It takes into account the losses due to shading of the photovoltaic system, the incidence angle modifier (IAM) and the soiling losses during the year. The annual percentage value of these losses amounts to about 9% but during the year this percentage varies, higher in the winter period when the sun is lower in the sky and we have more shade, lower in the summer period.

The capacity factor C_f is the ratio between the real energy produced in a period of time and the energy that would have been produced if the plant had operated at the nominal power P_N for the same period. In this case, the C_f expressed for each month has been reported in Table3.7 along with the other parameters listed above.

$$C_f = \frac{\int_0^{h_y} P_i(t)dt}{P_N * h_y} = \frac{E_{tot}}{E_N} = 0.143. \tag{3.35}$$

	R	R_{Eff}	H_e	PR	C_f
	$--$	$--$	h/y	$--$	$--$
January	1.95	0.87	82.3	0.786	0.111
February	1.55	0.91	87.0	0.837	0.129
March	1.32	0.93	130.8	0.830	0.176
April	1.09	0.92	94.3	0.809	0.131
May	1.02	0.92	122.3	0.796	0.164
June	0.99	0.92	121.3	0.780	0.169
July	1.01	0.92	160.7	0.773	0.216
August	1.09	0.92	131.8	0.772	0.177
September	1.22	0.92	108.7	0.790	0.151
October	1.41	0.92	81.3	0.814	0.109
November	1.57	0.89	46.7	0.792	0.065
December	2.15	0.84	85.3	0.775	0.115
Year	1.22	0.91	1252.7	0.794	0.143

Table 3.7: Monthly and annual values of the transposition factor R, R_{Eff}, equivalent hours H_e, performance rate PR and capacity factor C_f.

Chapter 4

Electrolyzers and Investment analysis

4.1 Elecrtolyzers

The basic electrolysis reaction requires energy in the form of electricity (E_{el}) and it consist in the simple splitting of a water molecule (H_2O) into hydrogen (H_2) and oxygen (O_2):

$$1H_2O + E_{el}(237.2\ kJ\ mol^{-1}) \rightarrow \text{Heat}(48.6\ kJ\ mol^{-1}) + 1H_2 + \frac{1}{2}O_2 \tag{4.1}$$

Thermal efficiency
In order to determine the thermal efficiency of an electrolyzer, it is essential to assess the relationship between the benefits derived from electrolysis, such as the production of hydrogen, and the effort expended in its production, which is represented by the energy consumed during the process. In PEM and ALK electrolysis water is supplied in the liquid state, while for SOE electrolysis it is supplied in the vapor state. Consequently, we must differentiate in terms of energy in order to define the performance of these processes.

- The higher heat value of hydrogen is ${\Delta H_R}^0 = HHV_{H_2} = 3.54\ kWh/Nm^3$
- The lower heat value of hydrogen is ${\Delta H_R}^0 = LHV_{H_2} = 3.00\ kWh/Nm^3$

When water is provided in a liquid state, the determination of the energy content of hydrogen requires a decision on whether to refer to the upper or lower calorific value. If we evaluate the thermal efficiency of the electrolyser within the overall conversion

chain then we can relate it to LHV_{H_2}, where $\dot{V}_{H_2}$ represents the volume flow rate of hydrogen, according to the following formula:

$$\eta_{LHV} = \frac{\dot{V}_{H_2} LHV_{H_2}}{P_{el}}. \tag{4.2}$$

If, on the other hand, the entire chain is not considered, the HHV_{H_2} is used for electrolysers that use water in the liquid state since it is necessary to take into account the reaction enthalpy used to pass from water in the liquid state to hydrogen in the gaseous state and consequently this corresponds to HHV_{H_2} under standard conditions:

$$\eta_{HHV} = \frac{\dot{V}_{H_2} HHV_{H_2}}{P_{el}}. \tag{4.3}$$

Cell efficiency

We can calculate the minimum energy to obtain the electrolysis reaction of water by calculating the Gibbs free energy (ΔG):

$$\Delta G = nFE_{rev}; \quad E_{rev} = \frac{\Delta G}{nF} = 1.23\ V; \tag{4.4}$$

Here, n represents the number of electrons involved, F is Faraday's constant (equal to 96500), and E_{rev} denotes the applied reversible voltage, which is equal to 1.23 V. However, this process is not ideal, in fact some entropy (ΔS) is generated and consequently the minimum real voltage required V_{TN} for the reaction to take place is equal to (4.5):

$$V_{TN} = \frac{\Delta G}{nF} + \frac{T\Delta S}{nF} = \frac{\Delta H}{nF} = 1.48\ V; \tag{4.5}$$

V_{TN} is also called thermo neutral voltage. We can therefore calculate the voltage efficiency as the ratio between the minimum required voltage V_{TN} at a certain temperature T compared to the actual voltage of the cell V_{cell} at the same temperature T and current i:

$$\eta_V = \frac{V_{TN}}{V_{cell}}. \tag{4.6}$$

We can also calculate the Faraday efficiency, denoted as η_i. This parameter is utilized to determine the actual number of electrons transported in the electric circuit between the two electrodes where the OER (Oxygen Evolution Reaction) and HER

(Hydrogen Evolution Reaction) reactions occur, in comparison to the ideal number of electrons that should be transported. The number of electrons transported is directly proportional to the number of hydrogen molecules produced, consequently this relationship can be expressed as the ratio between the volume flow of hydrogen actually produced $\dot{V}_{H_2}$ compared to the ideal volume flow $\dot{V}_{H_2,id}$:

$$\eta_i = \frac{\dot{V}_{H_2}}{\dot{V}_{H_2,id}}. \tag{4.7}$$

We can therefore calculate the efficiency of the cell η_{cell} as the product of the efficiencies:

$$\eta_{cell} = \eta_V * \eta_i. \tag{4.8}$$

4.1.1 Proton Exchange Membrane Elecrtolyzers PEMEL

The electrolysis process of water in a PEM (Proton Exchange Membrane) electrolyser (PEMEL) takes place following the two half-reactions (4.9) Oxygen Evolution Reaction (OER) and (4.10) Hydrogen Evolution Reaction (HER) whose union constitutes the global reaction (4.11). Liquid water molecule reaching the anode is oxidized into oxygen (released in gaseous state), two electrons and two hydrogen ions (two protons) are released at the anode. The electrons through the circuit that connects the anode to the cathode will move towards the cathode, while the protons reach the cathode by diffusion through a proton exchange membrane. At the cathode, the electrons combine with the protons, reducing and forming hydrogen in the gaseous state.

$$\text{Anode} \quad H_2O \longrightarrow 2H^+ + \frac{1}{2}O_2 + 2e^- \tag{4.9}$$

$$\text{Cathode} \quad 2H^+ + 2e^- \longrightarrow H_2 \tag{4.10}$$

$$\text{Global} \quad H_20 \longrightarrow H_2 + \frac{1}{2}O_2 \tag{4.11}$$

As mentioned in [36], this particular type of electrolyzer enables the production of high-purity hydrogen. This is achieved through the use of solid polysulfurized membranes, which exhibit excellent proton exchange capabilities with high conductivity

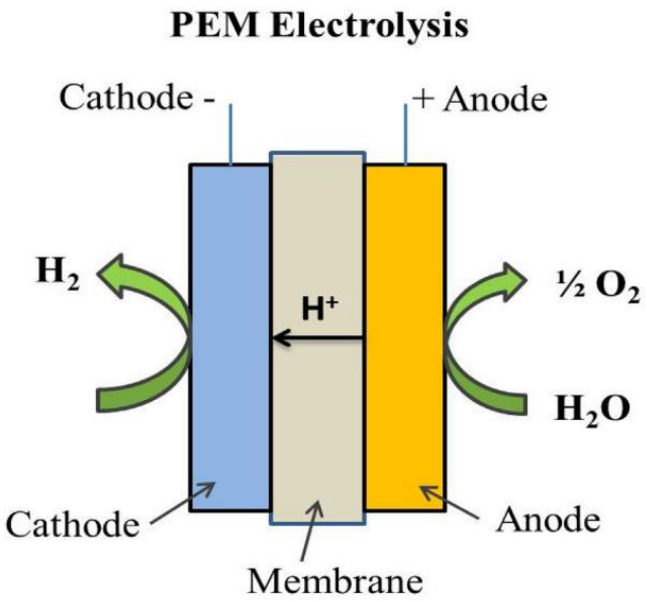

Figure 4.1: Pattern of operation of a PEM electrolyser, taken from [36]

and low permeability, especially in comparison to other gaseous products. PEM electrolysers work at high pressures and a low temperature range, between 20 and $80°C$ and pressure between 30 and 80 bar. This technology features a compact design, good behavior in operating in variable conditions such as when powered by renewable sources and a high current density ($\simeq 2\ A/cm^2$).
Regrettably, this technology is costlier compared to ALK alkaline electrolysers primarily because of the substantial utilization of noble metals like platinum (Pt) or palladium (Pd) at the cathode (HER). These noble metals are chosen for their exceptional resistance to corrosion and oxidation, which contribute to their higher cost. While on the anode side (OER) we have the presence of noble metals in the form of iridium oxide IrO_2 or ruthenium oxide RuO_2. To date, for the side (HER), an attempt is being made to develop electrolysers with palladium-based cathodes, which has electrocatalytic properties, that are very similar to platinum, and is much more abundant on earth at a lower cost than platinum. Furthermore, ongoing research is focused on the development of low-cost supported carbon catalysts for HER, utilizing materials that are abundant in nature. However, commercial prototypes using these catalysts have not yet been constructed.
Metal oxides are used as electrocatalysts in (OER) side, among the studied ones that have the greatest metallic conductivity are iridium oxide (IrO_2) and ruthenium oxide (RuO_2). Due to the acidic environment created by the proton exchange membrane,

IrO_2 exhibits lower corrosion compared to RuO_2. However, it also demonstrates lower performance compared to the latter. As a result, initial efforts were made to combine the desirable properties of these two electrocatalysts to achieve anodes that are both durable and efficient. However, the scarcity and consequent high cost of iridium have led researchers to explore alternatives. Presently, they are attempting to partially replace this element with non-noble metal oxides, specifically utilizing transition metals that are more abundant in nature and less expensive. The study reported in [36], concluded that mixed metal oxides help to improve the stability of materials by avoiding their corrosion, improving efficiency and cost. We can therefore conclude that this technology is undergoing various developments over time which will lead it to be competitive with other similar technologies. We now list the advantages and disadvantages attributed to PEM electrolysers.

Advantages

- rapid system response and good behavior in dynamic conditions (suitable for renewable sources);
- compact design;
- high current densities;
- high purity hydrogen (99.99%) and high production rate;
- high efficiency $(80 - 90\%)$.

Disadvantages

- use, even if in reduction, of noble materials;
- still high component costs;
- low durability due to acidic environment.

4.1.2 Alkaline electrolysers AEL

The electrolysis process of water in an ALK (ALKaline) electrolyser (AEL) takes place following the two semi-reactions in sequence HER in the cathode side (4.12) and OER in the anode side (4.13), which together form the global electrolysis reaction (4.14).

$$\text{Cathode} \quad 2H_2O + 2e^- \longrightarrow H_2 + 2OH^- \tag{4.12}$$

$$\text{Anode} \quad 2OH^- \longrightarrow H_2O + \frac{1}{2}O_2 + 2e^- \tag{4.13}$$

$$\text{Global} \quad H_2O \longrightarrow H_2 + \frac{1}{2}O_2 \tag{4.14}$$

As we anticipated, the alkaline electrolysis process takes place starting from the cathode where sodium hydroxide $NaOH$ or potassium hydroxide KOH is added to the water in a percentage by weight of around $20 - 40\%$ as described in [2]. These molecules act as electrolytes by increasing the conductivity of the mixture and forming a basic mixture therefore rich in OH^- groups in solution.
At the cathode, two water molecules are reduced by accepting two electrons and forming hydrogen released in the environment near the cathode and two hydroxyl groups OH^- which will diffuse towards the anode by concentration difference through a diaphragm, positioned in close proximity between the cathode and the anode. Once the two anions have reached the anode, they give up their electron to the anode, oxidizing into oxygen and water. In this process the oxidation electrons transferred to the anode are the same electrons which reduce the water in the initial phase of the process.
The electrodes are made of nickel-plated steel, which are coated with catalysts, OER side (Ni,Co,Fe, Ru/Ir-based), HER side (Ni,C,Pt-based). As reported in [2] this type of electrolyser allows to obtain hydrogen at a low investment cost but at a not too high purity and high maintenance costs of the electrodes which are subject to corrosion and therefore to frequent replacement. ALK electrolysers work at pressures between $3 - 30$ bar, generally lower than PEM electrolysers and always guarantee lower current densities with respect to these. The operating temperature range is low, between 50 and $80°C$, if the temperature is exceeded by $80°C$ there is an increase in efficiency but at the expense of the durability of the electrodes due to increased corrosion.
Alkaline electrolysers have undergone several developments in their design and the materials used in order to reduce costs and improve efficiency. Initially a unipolar design was used in which each cell contained two electrodes, the alkaline solution and a separator, and each cell could also be connected externally to the others. In recent times, there has been a shift from the conventional design, which was known for its large dimensions and weight, to a more advanced bipolar cell design. In this new design, cells are stacked together and divided by metal plates that function as both cathodes and anodes on opposite sides. This innovative design brings several benefits, including compactness and reduced weight of the electrolyzers, as well as improved resistance to higher pressures.
The current density is also affected by the design, so much that [2] shows an increase

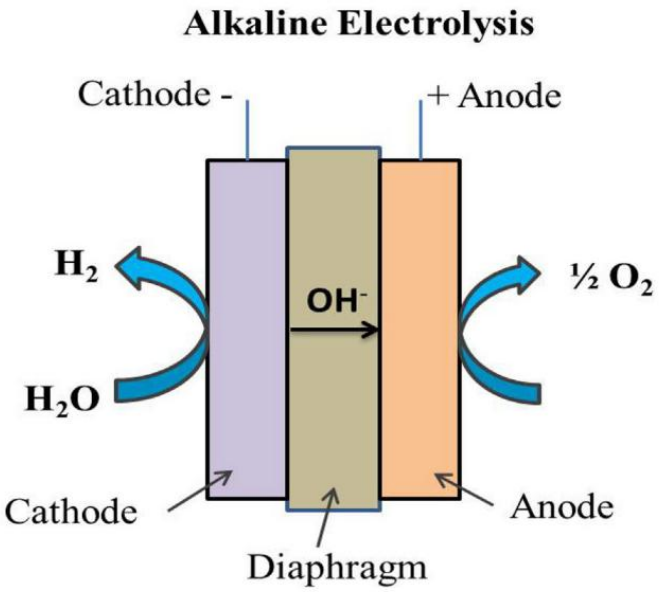

Figure 4.2: Pattern of operation of a AEL, taken from [36]

from 0.5 A/cm^2 to over 1 A/cm^2 for the latest and most efficient configurations. Nowadays the most innovative systems of alkaline electrolysers also use a new internal design, called zero gap, in order to further reduce the internal resistances. The zero gap design involves positioning the electrodes as close as possible to the separator to minimize resistances. Additionally, this design incorporates appropriately sized holes in the electrodes to facilitate the evacuation of gas bubbles that form on the catalyst's surface. The objective is to prevent the formation of excessively small bubbles that can stagnate and impede the reaction at specific points. As we can see from the graph in Figure4.3 where the zero gap technology is compared with the traditional technology, for the same current density the required voltage decreases.

Advantages

- efficiency between $70 - 80\%$;
- does not use noble materials as catalysts;
- stabilized and commercialized technology;
- low costs;

Disadvantages

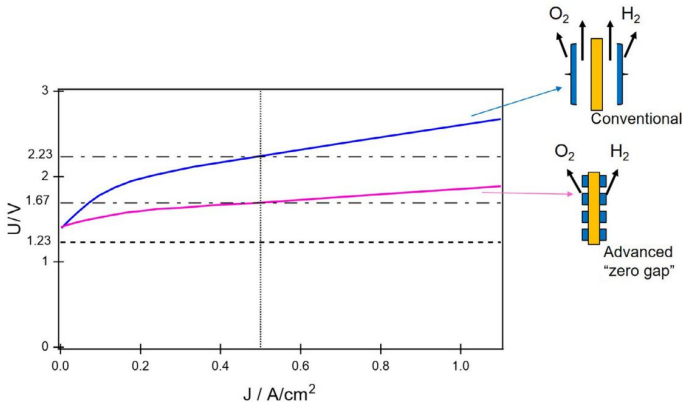

Figure 4.3: Improvements made by zero gap technology, from [2].

- does not work well in dynamic conditions;
- easy deterioration of the electrodes (especially if the operating temperatures are exceeded);
- low current density;
- low gas purity;
- low working pressure;

4.1.3 Anion Exchange Membrane electrolyzer AEMEL

Anion exchange membrane (AEM) electrolysers (AEMEL) are considered to be somewhere between alkaline electrolysers and PEMELs. In these electrolysers water is fed into the anode side and flows across the anion exchange membrane. Upon reaching the cathode, each water molecule is reduced by accepting an electron, leading to the production of hydrogen gas and two hydroxyl groups through the HER (Hydrogen Evolution Reaction)(4.15) half-reaction. The hydrogen escapes as a gas from the cathode side, while the hydroxyl groups diffuse across the anion exchange membrane to the anode. At the anode, the hydroxyl groups release their electrons, oxidizing according to the OER (4.16) half-reaction and therefore water and oxygen are formed.

$$Cathode \quad 2H_2O + 2e^- \longrightarrow H_2 + 2OH^- \tag{4.15}$$

$$Anode \;\; 2OH^- \longrightarrow \frac{1}{2}O_2 + H_2O + 2e^- \tag{4.16}$$

$$Global \;\; H_2O \longrightarrow H_2 + O_2 \tag{4.17}$$

This type of electrolyser works at a pressure of about 30 *bar* and a temperature

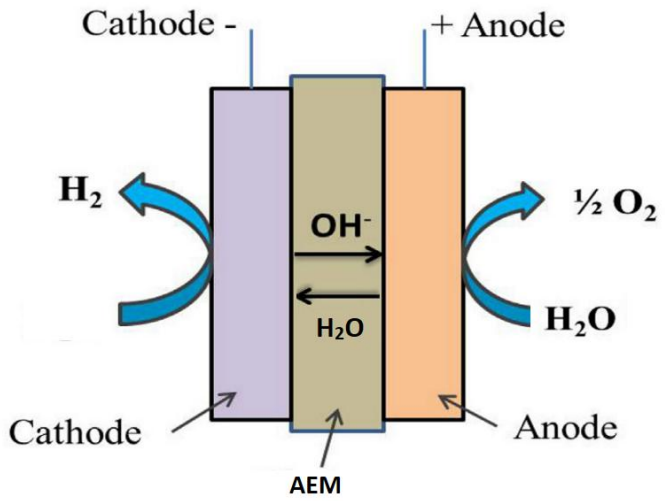

Figure 4.4: Pattern of operation of a AEMEL.

range between 50 and 70°C, [42]. Normally, cerium or lanthanum oxide $Ni/CeO_2 - La_2O_3/C$ or $Ni - Fe$ are used as catalysts on the OER side (anode), while on the HER side (cathode) Ni, $Ni - Mo$, $CuCoO_3$, so AEMELs don't use noble metals as catalysts like PEMs do. The purity of the hydrogen produced with AEM technology is similar to PEM electrolysers, therefore very high at 99.99%, as explained in [42]. The anion exchange membrane is made up of a main polymeric structure which gives solidity and resistance to the structure and makes it impermeable to other molecules, combined with functional groups which allow the transport of anions such as $-NH_3{}^+$. The presence of functional groups are essential to improve the conductivity of the hydroxyl groups OH^-, in fact these have a lower mobility than the hydrogen ions H^+. For this reason, many studies have focused on improving the ionic mobility through the functional groups, but it has been noted that by increasing it too much, the polymeric structure and therefore its physical characteristics are compromised. Today a compromise is being sought. AEM electrolysers use KOH potassium hydroxide as electrolyte but in a very low concentration (1 mol/l) compared to alkaline electrolysers, consequently the reaction environment is less basic

and therefore there are less degradation problems of the components due to corrosion.

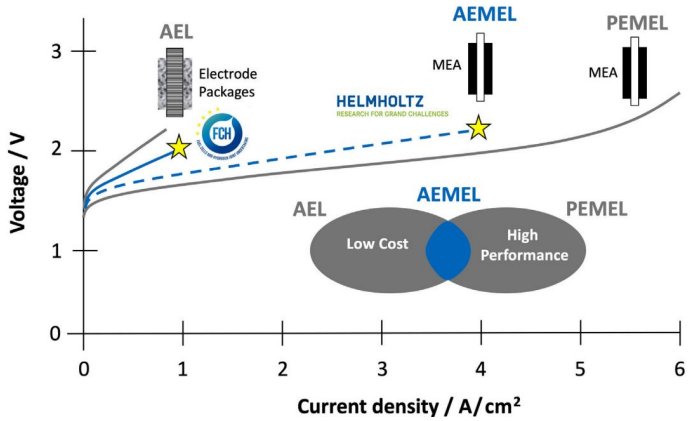

Figure 4.5: Comparison of the operating characteristic curves (cell voltage, current density) of the target in 2023-2027 for AEMEL with alkaline electrolysers (AEL) and PEM electrolysers (PEMEL),[2].

Advantages

- reduced concentration of KOH compared to alkaline electrolysers;
- does not require noble metals as catalysts nor titanium components (unlike PEMs);
- the HER side allows work at high pressures making the system more efficient without using external compressors;
- low costs;
- compact design.

Disadvantages

- degradation of the anion exchange membrane;
- new technology not yet mature.

4.1.4 SOE Electrolyzers

SOE (Solid Oxide Elecrolyzer) uses solid or ceramic oxide as electrolyte, in this case water is not used in liquid form but in the form of vapor, at high temperatures $(500 - 850°C)$ and pressures. The vapor is forced against a porous cathode, where the reduction reaction (4.18) takes place producing hydrogen H_2 (which is collected at the top) and the anion O^{2-} which diffuses through the electrolyte going towards the anode where the oxidation reaction (4.19) takes place obtaining gaseous oxygen which is collected at the top.

$$\text{Cathode} \quad H_2O + 2e^- \longrightarrow H_2 + O^{2-} \tag{4.18}$$

$$\text{Anode} \quad O^{2-} \longrightarrow \frac{1}{2}O_2 + 2e^- \tag{4.19}$$

$$\text{Global} \quad H_2O \longrightarrow H_2 + \frac{1}{2}O_2 \tag{4.20}$$

The main electrolytes used to conduct the anions O^{2-} are zirconia (ZrO_2) stabi-

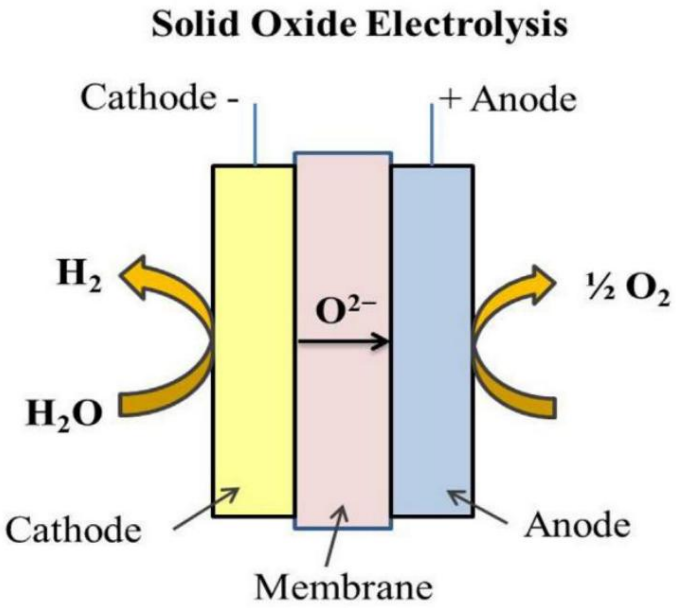

Figure 4.6: Pattern of operation of a SOE, taken from [36].

lized with Ni/Y (nickel/yttrium) or ceramic materials in general. Unlike other types

of studied electrolysis, this process occurs at high temperatures, which is advantageous for achieving higher yields. However, it also poses challenges related to system stability and significant electrode degradation, which currently hinder large-scale commercialization.

Advantages

- high operating pressures;
- high efficiency $(90 - 100\%)$;
- they do not use noble metals.

Disadvantages

- still low durability;
- large dimensions;
- still under development.

4.1.5 Performance indicators for PEM and ALK

We can consider various parameters when selecting the most suitable type of electrolyzer for a given system. These parameters include the following:

1. Availability of materials;
2. Investment cost;
3. Operating costs;
4. Useful life of the plant and efficiency.

Let us now analyze these parameters by comparing the PEM and ALK [2] electrolysers.

1) Availability of materials:

Currently, ALK (alkaline) electrolyzers can be readily sold on a megawatt (MW) scale without concerns regarding material scarcity for their construction. Nickel, the primary material used, is abundantly available at a low cost, around $14-15\ €/kg$ [2]. Additionally, potassium hydroxide, another crucial component, and also potassium hydroxide is already being produced on a large scale at low cost. In contrast, for PEM electrolysers the availability of materials is much lower and the related costs

are very high, around 50 $k€/kg$, in agreement with [2], for the extraction of Pt and costs equally high are the results for Ir and Ru. As a consequence, if substitute materials are not found for the construction of PEM electrolysers, market volatility resulting from material scarcity could lead to significant price fluctuations.

2) Investment cost (CAPEX):

According to [2], today the investment cost for the construction and commissioning of an electrolysis plant is around 1000 $€/kW$ for ALK electrolysers and around 2000 $€/kW$ for PEM electrolysers. According to future forecasts, by 2030 a price of around 600 $€/kW$ will be reached for both technologies, obviously these prospects will only be achievable if the sales volumes of the electrolysers increase significantly and consequently the production chain will be readapted for scale production. From the point of view of the investment to be made, ALK technology is already mature today and consequently the price depends less on technological development than on scale production.

3) Operating and maintenance costs (OPEX):

The operating costs excluding the cost of energy are those planned and unplanned costs to keep the installed system operating even in the event of a failure. These costs are taken into account as a percentage of the CAPEX (CApital EXpediture). In the case of ALK and PEM electrolysers between $2-5\%$ of the associated initial investment may be considered for the cost of materials. Labor costs vary according to the size of the system, in fact the greater the size of the system, the lower the labor costs for each kW installed. Annual labor costs for a 1 MW plant are estimated at approximately 5% of the investment, while for a 10 MW plant they are estimated at approximately 2% of the investment.

4) Useful life of the plant and efficiency:

For electrolysers, the useful life depends on the degradation of the electrodes, catalysts, membrane or separator over time and therefore on the increase in overall resistance. The degradation of these components leads to a degradation of the voltage, i.e. the voltage to be supplied to continue producing hydrogen increases and consequently efficiency is reduced over time. From [2], voltage degradation values between $0.4-5$ $\mu V/h$ for PEM and ALK electrolysers and 15 $\mu V/h$ for some PEM electrolysers have been reported. Furthermore, for alkaline electrolyzers, an estimated lifespan of approximately 90000 hours is projected, during which an acceptable level of efficiency can still be maintained. After this time, there are no component failures, but rather the efficiency gradually decreases below a critical threshold.

4.1.6 Choice between electrolysers on the market

In order to select the most suitable commercially available electrolyzer for the project at hand, a comparison was made among the different alternatives available in the market for various types of electrolyzers. Today, PEM electrolysers of the MW size can also be found on the market. The AEMELs are already on the market, in fact, even if the research field is very young for these electrolysers, studies have advanced faster thanks to past discoveries on parallel technologies. SOE electrolysers have not been considered in this analysis as they are not suitable for high temperatures and the overall dimensions due to the complexity of the plant.

PEMEL

Three models of PEM electrolysers have been identified and compared, the values summarized in the technical sheets have been reported in the Table4.1. HCS will be available from 2024, with promising features, and a small footprint as we can see in Table4.1. These electrolysers have small dimensions, plant simplicity as we can see in Figure4.7 and high yields at the beginning of their life (with a reduction of 1% every 8500 hours of operation). Furthermore, when the efficiency is reduced too much, the electrodes and membranes can be replaced and therefore the efficiency of the system restored. The installation is practical because turnkey solutions are offered. Furthermore, some of these self-produce demineralised water via reverse osmosis. The hydrogen produced is very pure, and pressurized without the use of a compressor. $\hat{e}_{system}$ is the overall specific energy consumed by the overall system, this can vary with respect to the data based on how the plant is built. WD_{H_2O/H_2} corresponds to the demineralised water used for each Nm^3 of H_2 produced, while W_{H_2O/H_2} corresponds to the water from the aqueduct used for each Nm^3 of H_2 produced. These plants are very well suited to renewables due to their simplicity and large operating ranges.

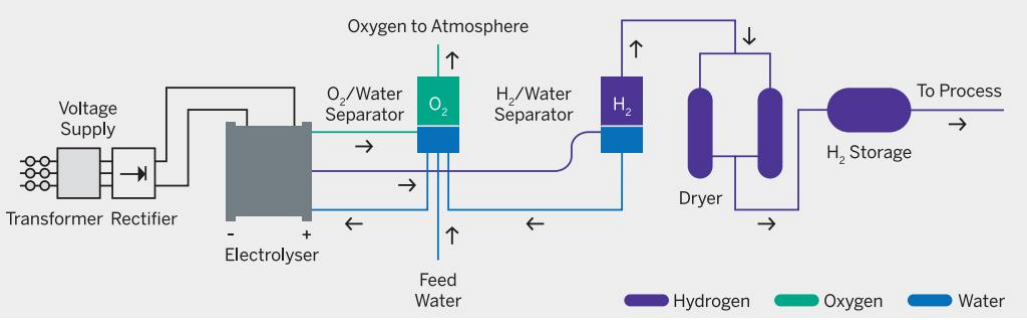

Figure 4.7: System diagram of a PEM electrolyser, taken from [30].

Type (PEM)	HyLYZER 500-30	MC 500	HCS	dim.
$\dot{V}_{H_2}$	500	492	420	Nm^3/h
$\dot{m}_{H_2}$	1080	1061	900	kg/day
P_{H_2} delivery pressure	30	30	$20-30$	bar
H_2 Purity	99.998%	99.9995%	99.999%	-
Operating range	$5\%-100\%$	$10\%-100\%$	$10\%-100\%$	-
$\hat{e}_{system}$ (average)	54	61	53	kWh/kg
$P_{tot,n}$	2530	2716	2000	kW
W_{H_2O/H_2}	1.35	-	-	L/Nm^3
WD_{H_2O/H_2}	0.8	0.9	1.43	L/Nm^3
T_{env}	$-20 \div 40$	$-20 \div 40$	$-20 \div 40$	-
dim.	61	61	18.2	m^2
η_{HHV}	0.73	0.64	0.74	-
η_{LHV}	0.62	0.54	0.63	-

Table 4.1: Comparison between PEM electrolysers on the market, taken from [30], [7] ,[22], NB: some data have been averaged or obtained from available data for the purpose of having a direct comparison.

AEL

Three models of alkaline electrolyzers were identified and compared to each other, and the findings are summarized in Table4.2. As mentioned earlier, these electrolyzers have more complex systems, as shown in Figure4.8. In fact, as we can see from the Table4.2, the overall dimensions are greater than the PEMs. Again with respect to PEMs, the yields are lower or equal, but alkaline electrolysers still have lower costs and do not use noble materials. Some of these alkaline electrolysers use water directly from the mains as the demineralization is done internally via reverse osmosis. Even these systems, after the life time established by the manufacturers, can renew their performance by replacing the deteriorated parts (cell stacks).

Type (AEL)	HySTAT 100-10	A485	Gateway-400	dim.
$\dot{V}_{H_2}$	100	485	400	Nm^3/h
$\dot{m}_{H_2}$	216	1046	864	kg/day
P_{H_2} delivery pressure	10 no compr.	$1-200$ with compr.	30 no spec.	bar
H_2 Purity	99.998%	99.998%	99.999%	-
Operating range	$40\%-100\%$	$15\%-100\%$	$10\%-100\%$	-
$\hat{e}_{system}$ (average)	57.5	56	58.4	kWh/kg
$P_{tot,n}$	517	2440	1920	kW
W_{H_2O/H_2}	1.6	-	-	L/Nm^3
WD_{H_2O/H_2}	0.8	1	0.82	L/Nm^3
Electrolyte	KOH	KOH 25%	KOH	-
T_{env}	$-20 \div 40$	$2 \div 40$	-	-
$dim.$	89	225	-	m^2
η_{HHV}	0.68	0.70	0.74	-
η_{LHV}	0.58	0.60	0.63	-

Table 4.2: Comparison between AEL electrolysers on the market, taken from [37], [8] ,[29], NB: some data have been averaged or obtained from available data for the purpose of having a direct comparison.

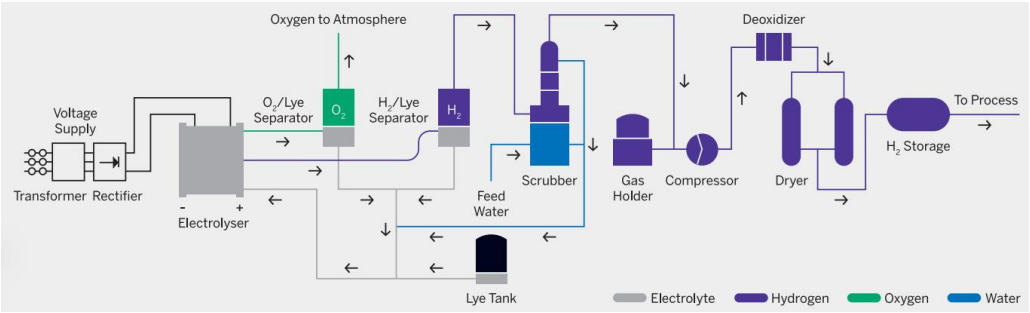

Figure 4.8: System diagram of a ALK electrolyser, taken from [30].

AEM

In this case, two AEM models were analyzed and compared, data reported in Table4.3. This technology has high yields, but it is still very young and consequently there is less data to support it. From the available data it can be seen that it works in high operating ranges, even smaller dimensions than PEMEL and high pressures without the use of compressors. This technology has great potential and will definitely expand its market in the future.

Type (AEM)	AEMWE	AEM Multicore	dim.
$\dot{V}_{H_2}$	60	210	Nm^3/h
$\dot{m}_{H_2}$	5.394	18.879	kg/day
P_{H_2} delivery pressure	25	35	bar
H_2 Purity	99.95%	99.90%	-
Operating range	-	$3\% - 105\%$	-
$\hat{e}_{system}$ (average)	56.9	65.5	kWh/kg
$P_{tot,n}$	250	1008	kW
W_{H_2O/H_2}	-	-	L/Nm^3
WD_{H_2O/H_2}	-	9	L/Nm^3
Electrolyte KOH	$3\% - 5\%$	-	-
T_{env}	-	-	-
dim.	-	29.7	m^2
η_{HHV}	0.85	0.74	-
η_{LHV}	0.72	0.625	-

Table 4.3: Comparison between AEM electrolysers on the market, taken from [24], [16], NB: some data have been averaged or obtained from available data for the purpose of having a direct comparison.

4.2 Investment analysis for systems

In this part the investment to be made is analyzed at an economic level. Three 2.5 MW PEM HyLYZER 500-30 electrolyzers were selected for this analysis.

4.2.1 Levelized cost of hydrogen (LCOH)

We can analyze the discounted hydrogen generation cost, understood as the industrial costs of the hydrogen produced by the electrolysers through the electricity generated by the photovoltaic and hydroelectric plant. This is based on the cost per kg discounted according to the following formula:

$$LCOH = \frac{\sum_{j=-t}^{j=0} I_j(1+k)^{-j} + \sum_{i=1}^{n} C_{opex,i}(1+k)^{-i} + \sum_{i=1}^{n} C_{en,i}(1+k)^{-i} - R_v(1+k)^{-n}}{\sum_{i=1}^{n} q_i(1+k)^{-i}} \tag{4.21}$$

Where:

- I_j is the investment made in the j-th year;
- t are the years that elapsed between the start of disbursements and plant entry into service;

- k is the discount rate, WACC (weighted average cost of capital);

- n useful life of the plant;

- $C_{opex,i}$ are all $O\&M$ operating, management and maintenance expenses incurred in the i-th year (excluding fuel costs, which in this case is the cost of electricity);

- $C_{en,i}$ is the cost of electricity (market value at which I could have sold the electricity);

- q_i is the hydrogen production in the i-th year;

- R_v residual value of the plant at the end of its life.

	$M€$	with financing 50% $M€$
I_0 (total)	22.6	11.3
I_{pv}	4.1	2.05
electrolysers	16.5	8.25
storage	0.2	0.1
other	1.8	0.9

Table 4.4: Estimated values of the investment, overall value I_0 and redivided into the various cost items, in the event that there is no or there is state funding;

The total investment cost amounts to $I_0 = 22.6$ $M€$, for which state funding of 50% was requested in the expression of interest presented in the PNRR tender. The investment ($I = 0.5\ I_0 = 11.3$ $M€$) was valued for a discount rate of 5%, $k = 0.05$ and an estimated useful life of $n = 30$ years for the electrolysis system and $n = 20$ years for the photovoltaic system. The investment was divided between the construction of the photovoltaic park I_{pv} and the electrolysis system including storage and other expenses I_{el}, data shown in Table4.4. For the photovoltaic system, the recoverability of the investment was verified for various energy values, while for the electrolysis plant, the leveled cost of hydrogen was evaluated and the recoverability of the investment based on the operating hours and the value of the energy. To produce green hydrogen, electricity must be drawn from renewable plants, in this case from the photovoltaic plant and the hydroelectric watercourse system, but even if the energy is not fed into the grid, it is necessary to understand what value to attribute to the latter in order to recover costs. For this first calculation of the

levelized cost of hydrogen, an energy cost of $C_{en} = 60$ €$/MWh$ has been chosen and $I_{el} = 9.25$ M€.

For an $P_n = 7.5$ MW electrolysis plant powered all year round, the annual electricity consumption E_{Cons} was calculated as:

$$E_{Cons} = P_n * h_y = 7.5 * 8760 = 65700 \ MWh/y; \tag{4.22}$$

and therefore a total annual cost of energy $C_{en,i}$:

$$C_{en,i} = E_{Cons} * C_{en} = 65700 * 60 = 3.94 \ M€/y \tag{4.23}$$

The operating and maintenance costs of the plant have been estimated for a value equal to 10% of the initial value of the investment I_{el} and other operating costs equal to 3% of I_{el}, for a total of $C_{opex,i} = 0.013$ I_{el}.

$$C_{opex,i} = 0.013 \ I_{el} = 80167 \ €/y \tag{4.24}$$

These costs were broken down as follows:

- for $i = 1$ to $i = 10$, $C_{opex,i=1,..,10} = 80167 - 50000 = 30167$ €$/y$;
- for $i = 11$ to $i = 20$, $C_{opex,i=11,..,20} = 80167$ €$/y$;
- for $i = 21$ to $i = 30$, $C_{opex,i=21,..,30} = 80167 + 50000 = 130167$ €$/y$;

in this way it is also possible to better estimate the higher operating and maintenance costs due to the aging of the system and the lower initial maintenance costs due to the guarantee given by the manufacturers.

In this calculation, a value of the plant at the end of the useful life of the investment was also taken into consideration, for a residual value equal to:

$$R_v = 0.15 \ I_{el} = 2.775 \ M€. \tag{4.25}$$

To estimate the quantity q_i of hydrogen produced by an electrolysis plant, the technical data sheet of a unit reported in [7], which can be used for the production of hydrogen and oxygen from renewable sources, was taken into consideration. To obtain an overall power of 7.5 MW, using units with nominal power of $P_{n,u} = 2.5$ MW would need a number N_{el} equal to:

$$N_{el} = int\left(\frac{P_n}{P_{n,u}}\right) = int\left(\frac{7.5}{2.5}\right) = 3 \tag{4.26}$$

Each unit produces a quantity q of hydrogen with a percentage purity of 99.998% equal to:

$$q = 500\ \frac{Nm^3}{h} = (500 * 0.0899)\ \frac{Nm^3}{h}\ \frac{kg}{Nm^3} = 44.95\ \frac{kg}{h} \tag{4.27}$$

$$q_i = q * N_{el} * h_y = 44.95 * 3 * 8760 = 1181286\ \frac{kg}{y} \tag{4.28}$$

for these values the levelized cost of hydrogen was calculated using the formula (4.21) and the following value was obtained:

$$LCOH = 3.8\ \frac{€}{kg} \tag{4.29}$$

The LCOH was then calculated for different electricity price values, without changing the other parameters, the results of this calculation are shown in the graph in Figure4.9. Consequently, if we value hydrogen with respect to the energy price on the market, we will have that its price will become highly variable during the day. But if instead we produce and accumulate hydrogen at an agreed sale price, we could fix the market value of the associated energy, below which it is convenient to produce hydrogen and above which it is instead convenient to sell on the network. Obviously in this way the quantity that can be produced during the day is limited to only some time slots in which the price of electricity is lower than or equal to the associated LCOH value established, moreover we will see that the investment is also influenced by the operating hours of the plant. The LCOH was also calculated by changing the number of operating hours of the plant as a parameter (initially assumed $h_y = 8760\ h/y$). In the graph in Figure4.10 we can observe that, in fact, as the number of hours increases, the LCOH decreases. On the other hand, the cost of electricity from the photovoltaic C_{pv} and hydroelectric C_{hy} plants are different thanks to the financing that would be obtained for the construction of the photovoltaic plant. So if we evaluate an energy cost weighted with respect to the equivalent operating hours of the two plants we will have a slightly increasing trend due to the fixed value of the annual operating hours of the photovoltaic plant $h_{e,pv}$ while the hydroelectric watercourse system will cover the remaining operating hours $h_{e,hy}$.

$$h_y = h_{e,pv} + h_{e,hy};\ \ \rightarrow\ \ C_{en} = C_{pv}\frac{h_{e,pv}}{h_y} + C_{hy}\frac{h_{e,hy}}{h_y}. \tag{4.30}$$

In subsequent analyses, the levelized cost of hydrogen (LCOH) was considered for 7000 hours per year, and it follows the linear equation $LCOH = 0.056\ C_{en} + 0.70$.

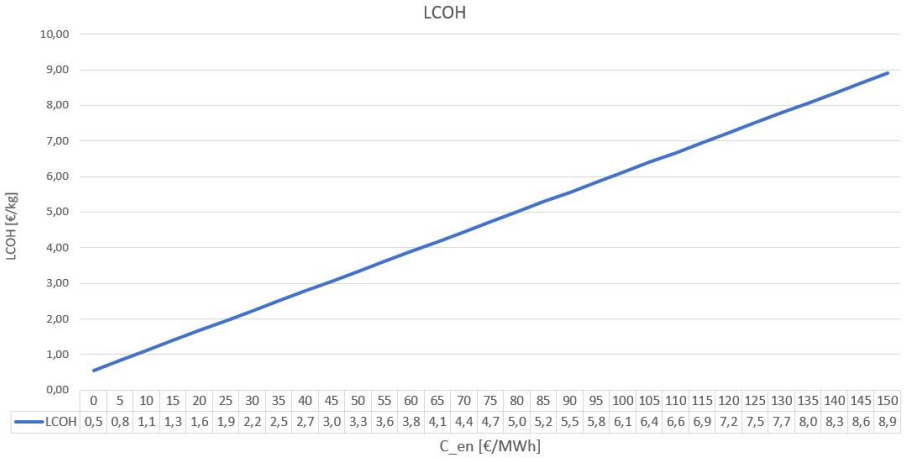

Figure 4.9: LCOH values for different electricity price values, $LCOH = 0,056\ C_{en} + 0,56\ \frac{€}{kg}$;

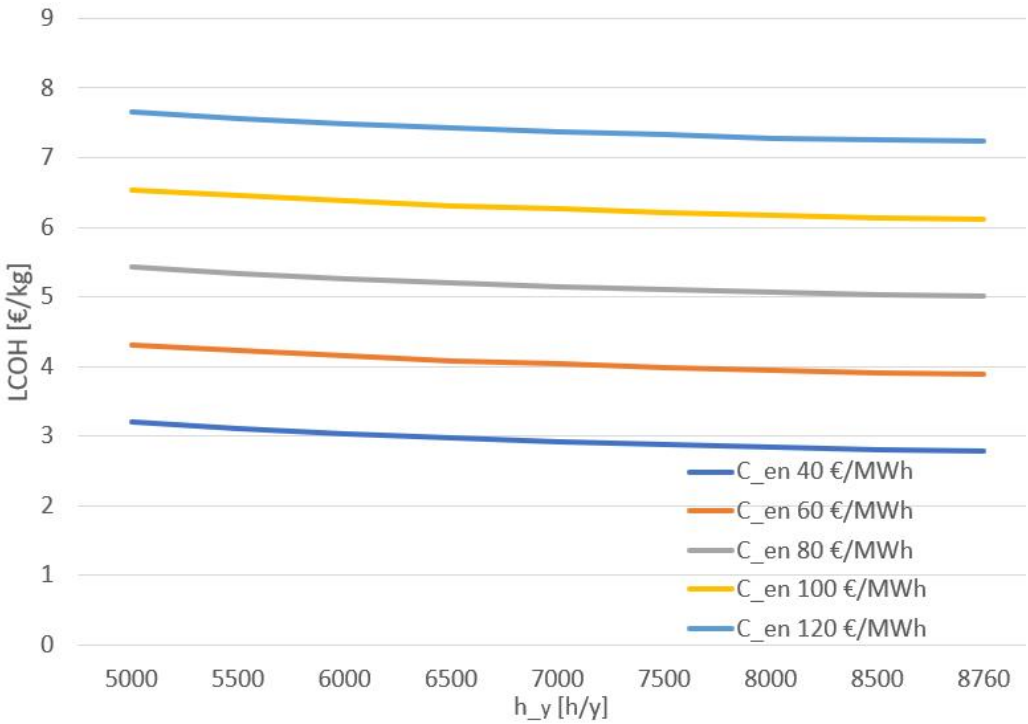

Figure 4.10: LCOH values for different electricity price values and different operating hours h_y;

4.2.2 Photovoltaic system investment analysis

An initial investment cost of $I_{pv} = 4.1\ M€$ was estimated for the $P_n = 6\ MW_p$ plant. As described in the previous chapter, the plant has an equivalent number of operating hours equal to $h_e = 1252.7\ h/y$ and an overall efficiency equal to $\eta = 19\%$. For this calculation, the operating and maintenance costs of the photovoltaic system equal to 3% of the capex ($C_{O\&M,tot} = 0.03\ I_{pv}$) were estimated. A discount rate of $k = 0.05$ was taken into consideration and a useful life of the investment of about $n = 20$ years has been estimated.

Let us now calculate the value of the operating and maintenance costs of the plant attributed to each MWh of energy produced by this $C_{O\&M}$:

$$C_{O\&M} = \frac{C_{O\&M}}{n * P_n * h_e} = 0.818\ \frac{€}{MWh}; \tag{4.31}$$

Let's analyze the investment cost for each MW installed i_0 and the discount coefficient α to then calculate the investment cost for each MWh produced C_{inv}:

$$i_0 = \frac{I_0}{P_n} = 0.683 \times 10^6\ \frac{€}{MW}; \quad \alpha = \frac{k}{1-(1+k)^{-n}} = 0.080243; \tag{4.32}$$

$$C_{inv} = \frac{i_0 * \alpha}{h_y} = 43.77\ \frac{€}{MWh}; \tag{4.33}$$

$$C_{tot} = C_{inv} + C_{O\&M} = 44.59\ \frac{€}{MWh}. \tag{4.34}$$

We can now calculate the net present value (NPV) of the investment on the photovoltaic system alone, which corresponds to the sum of all the initial payments ($CF_0 = I_0$ included) and all the cash flows in future years $CF_{i=1,..,n}$ discounted. This index gives us an idea of the value generated by a certain investment initiative. For this calculation, if the cash flows are constant from one year to the next, we can extract them from the sum and rewrite the sum as $\frac{1}{\alpha}$.

$$NPV = \sum_{i=0}^{n} \frac{CF_i}{(1+k)^i} = \frac{1}{\alpha}\ P_n\ h_e(P_{en} - C_{tot}) = 1.44\ M€; \tag{4.35}$$

for this calculation we have considered the energy price of $P_{en} = 60\ €/MWh$. The state-provided subsidy (of 50%) was not taken into account for this calculation, in order to compare the two cases.

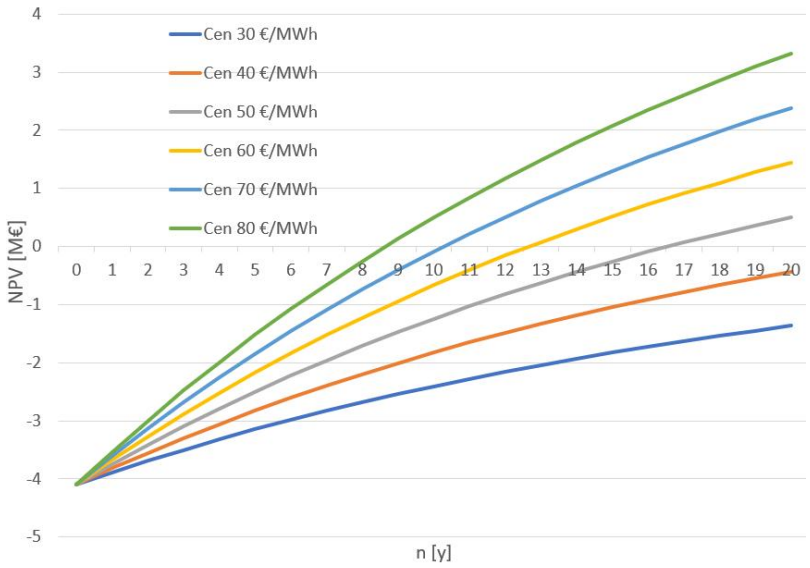

Figure 4.11: NPV $[M€]$, calculated for different energy prices versus time.

The same calculation was performed for different electricity prices, the NPV values obtained are shown in the graph in Figure4.11 with respect to time. As we can observe, the NPV is greater than zero if the average energy sale price is greater than the costs associated with the generation activity, therefore from $P_{en} \geq 45$ €$/MWh$. For prices around 60 €$/MWh$, the discounted payback period is around 13 years. The economic indices of the investment are shown in the Table4.5, such as NPV (Net Present Value), PB (Simple Payback Time), ROI (Return On Investment), PI (Profitability Index), Av (Availability Av = Revenue-Costs), Am (Amortization).

The simple payback time PB is the time it takes to recover the investment, without however taking into account the discount factor. It can be calculated by dividing the investment by annual availability $Av_i = R_i - C_i$ (considered constant Av):

$$\sum_{i=1}^{PB} Av_i = I_0; \quad \rightarrow \quad PB = \frac{I_0}{Av}. \tag{4.36}$$

The return on investment (ROI) tells us in percentage terms what is the average annual profit we get compared to the invested capital:

$$ROI = \frac{\sum_{i=1}^{n} \frac{Av_i - Am_i}{n}}{I_0} * 100 = \frac{Av - Am}{I_0} * 100 \tag{4.37}$$

P_{en}	NPV	PB	ROI	PI	Av	Am
€/MWh	M€	y	%	%	€/y	€/y
30	−1.37	18.69	0.3%	−33%	219336	205000
35	−0.90	15.96	1.3%	−22%	256917	205000
40	−0.43	13.92	2.2%	−10%	294498	205000
45	0.04	12.35	3.1%	1%	332079	205000
50	0.51	11.09	4.0%	12%	369660	205000
55	0.98	10.07	4.9%	24%	407241	205000
60	1.44	9.22	5.8%	35%	444822	205000
65	1.91	8.50	6.8%	47%	482403	205000
70	2.38	7.88	7.7%	58%	519984	205000
75	2.85	7.35	8.6%	69%	557565	205000
80	3.32	6.89	9.5%	81%	595146	205000
85	3.79	6.48	10.4%	92%	632727	205000
90	4.25	6.12	11.3%	104%	670308	205000
95	4.72	5.79	12.3%	115%	707889	205000
100	5.19	5.50	13.2%	127%	745470	205000

Table 4.5: Economic investment indices for different average electricity sales prices.

The profitability index PI compares the investment with the value created, this index allows us to compare different investments:

$$PI = \frac{NPV}{I_0} * 100 \tag{4.38}$$

The plot in Figure4.12 shows the NPV for different discount rates, in order to understand which rate is acceptable for such an initiative. This means looking for the internal rate of return IRR, i.e. the discount rate that equals the NPV to zero. As we can observe, as k increases, future revenues are worth less and less and consequently the NPV decreases.

$$\sum_{i=0}^{n} \frac{CF_i}{(1+k)^i} = 0 \quad \rightarrow \quad k = IRR; \tag{4.39}$$

Consequently, based on the average price at which we intend to sell energy, there will be a value of the interest rate above which the investment will not be recovered. For instance, if we were to sell energy at an average price of 60 €/MWh the initial investment must be made with an interest rate k not higher than 9%.

Let us now analyze the same investment initiative for the construction of the photovoltaic system but with an incentive of 50% from state funds from the PNRR. In

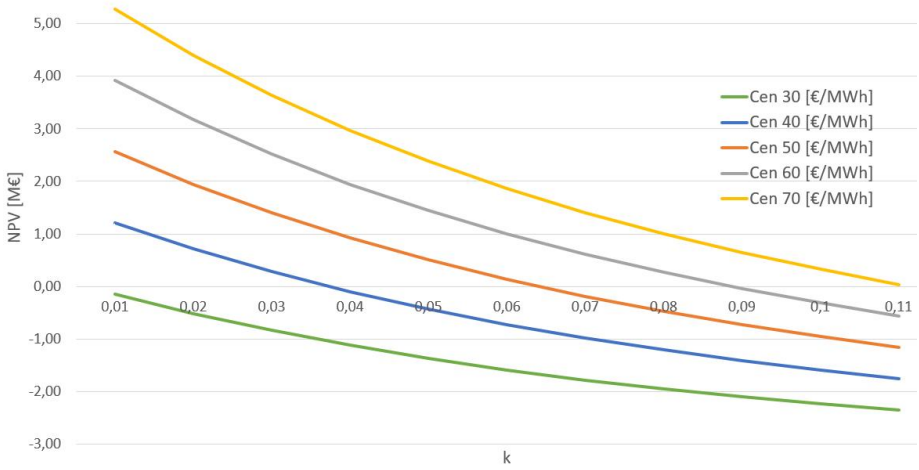

Figure 4.12: NPV calculated for different energy prices versus k.

this case the electricity is not sold on the grid but used directly by the electrolysers to produce hydrogen. We will therefore have a halved initial investment $I_0 = 2.05$ $M€$ to deal with, the operating and maintenance costs instead will remain unchanged compared to the previous case $C_{O\&M}$.

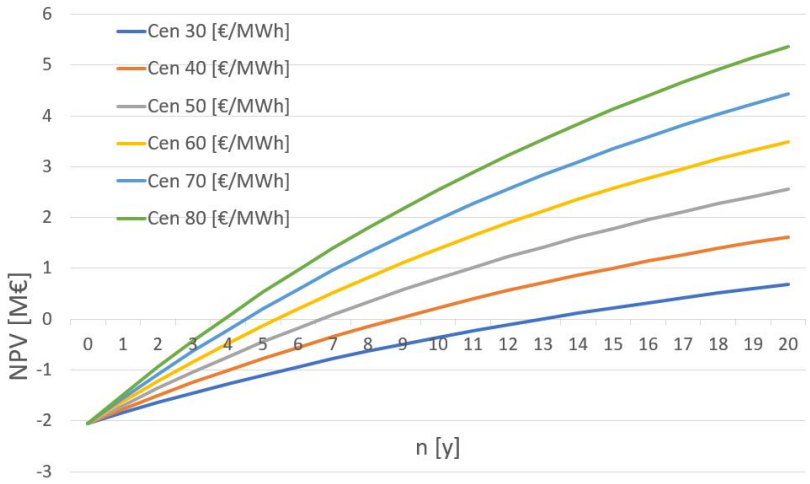

Figure 4.13: NPV[$M€$], calculated for different energy prices over time, in the event that 50% of the initiative is financed by the state through the PNRR.

As we can see from the graph in Figure4.13 the discounted payback time is now much reduced compared to the previous case Figure4.11. For instance, if we

consider the payback time discounted at 60 €/MWh in the previous case it was around 13 years, while in this case at that price we have a discounted payback time of around 5 years. Consequently, if in the previous case it was not possible to recover the investment over 20 years for low energy sales prices, now a recovery is possible even at these values. In this way it is possible to produce hydrogen considering an acceptable value of the electric energy used to produce it. The same calculation was then performed for different values of the discount rate k, where the results obtained are shown in the plot in Figure 4.14. In this case, a value of k not exceeding 9% can be accepted even for electrical energy values of 30 €/MWh. Instead, in the previous case this limit was for an average electricity price of 60 €/MWh. The new values of

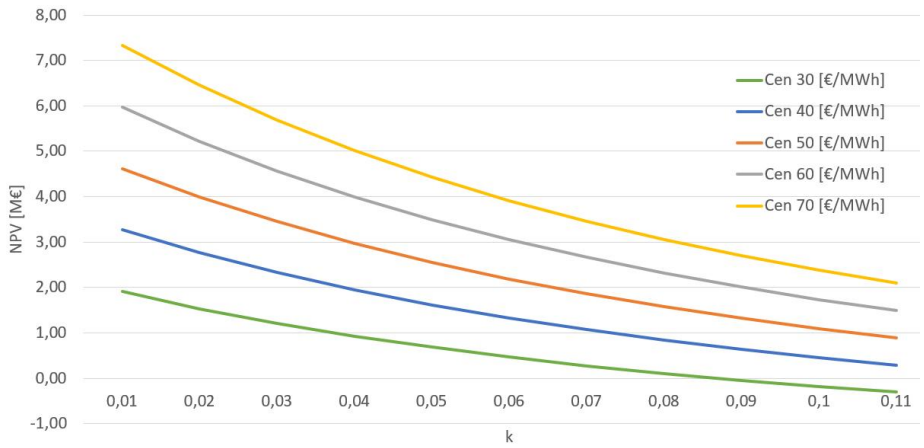

Figure 4.14: NPV calculated for different energy prices versus k, in the event that 50% of the initiative is financed by the state through the PNRR.

the economic indexes on investment in the event that there is state funding have been reported in the Table 4.6. In particular, we can observe a large increase in the PI profitability index compared to the previous case, this makes the investment much more convenient even considering lower electricity price values in order to encourage the production of hydrogen.

P_{en}	NPV	PB	ROI	IP	Av	Am
€/MWh	M€	y	%	%	€/y	€/y
30	0.683	9.346	5.7%	33.3%	219336	102500
35	1.152	7.979	7.5%	56.2%	256917	102500
40	1.620	6.961	9.4%	79.0%	294498	102500
45	2.088	6.173	11.2%	101.9%	332079	102500
50	2.557	5.546	13.0%	124.7%	369660	102500
55	3.025	5.034	14.9%	147.6%	407241	102500
60	3.493	4.609	16.7%	170.4%	444822	102500
65	3.962	4.250	18.5%	193.3%	482403	102500
70	4.430	3.942	20.4%	216.1%	519984	102500
75	4.898	3.677	22.2%	239.0%	557565	102500
80	5.367	3.445	24.0%	261.8%	595146	102500
85	5.835	3.240	25.9%	284.6%	632727	102500
90	6.304	3.058	27.7%	307.5%	670308	102500
95	6.772	2.896	29.5%	330.3%	707889	102500
100	7.240	2.750	31.4%	353.2%	745470	102500

Table 4.6: Economic investment indices for different average electricity sales prices, in case the financing takes place.

4.2.3 Electrolysis system investment analysis

Let us now analyze the investment dedicated to the electrolysis plant. An initial investment for PEM electrolysers of $i = 2200$ €/kW has been estimated for this plant. It was decided to use three 2.5 MW PEM HyLYZER 500-30 electrolysers, [7]. In addition, storage costs and other costs listed in Table4.4 were estimated for a total of $I'_{el} = 18.5$ M€ ($i_0 = 2466.7$ €/kW). As previously mentioned, this investment is encouraged by state funds at 50%, consequently the actual expenditure becomes $I_{el} = 9.25$ M€. These electrolysers provide a hydrogen outlet pressure of 30 bar without the use of a compressor which consequently has not been considered. For this evaluation we have remained consistent with the LCOH evaluation, therefore the discount rate was taken as 5% and $n = 30$ years and a number of operating hours $h_y = 7000$ h/y estimated by subtracting 5 hours per day at peak times when working at low load. We calculate the operating and maintenance costs C_{opex}, $C_{O\&M}$ as:

$$C_{opex} = 0.13 * 18.5 = 2.4M€; \quad C_{O\&M} = \frac{C_{O\&M}}{n * P_n * h_y} = 1.64 \ \frac{€}{MWh}; \tag{4.40}$$

Let's analyze the investment cost for each MW installed i_0 and the discount coefficient α to then calculate the investment cost for each MWh produced C_{inv}:

$$i_0 = \frac{I_{el}}{P_n} = \frac{9.25}{7.5} = 1.23 \times 10^6 \frac{€}{MW}; \quad \alpha = \frac{k}{1-(1+k)^{-n}} = 0.06505; \tag{4.41}$$

$$C_{inv} = \frac{i_0 * \alpha}{h_y} = 11.46 \ \frac{€}{MWh}; \tag{4.42}$$

In this case, electricity is considered a cost, so let's calculate the cost sustained by the electrolysis plant for each MWh of energy in the form of hydrogen produced. In this case, electricity is considered a cost, so let's calculate the cost sustained by the electrolysis plant for each MWh of energy in the form of hydrogen produced. For this calculation, an energy purchase price of $C_{en'} = 60 \ €/MWh$ was initially assumed, a yield at the beginning of life (BOL) $\eta_{HHV} = 0.73$ computed by [7].

$$C_{en} = \frac{C_{en'}}{\eta_{HHV}} = \frac{60}{0.73} = 85.7 \frac{€}{MWh}; \tag{4.43}$$

$$C_{tot} = C_{inv} + C_{O\&M} + C_{en} = 98.7 \ \frac{€}{MWh}. \tag{4.44}$$

To associate an adequate selling price P_{H_2}, the LCOH valued in the previous paragraph was considered, which corresponds to the discounted cost to be incurred to remunerate the plant itself. To this was added a margin $M = 0.3 \ €/kg$.

$$\hat{P}_{H_2} = LCOH + M = 4.03 + 0.3 = 4.33 \ €/kg; \quad P_{H_2} = \frac{\hat{P}_{H_2}}{HHV} = 110 \ €/MWh \tag{4.45}$$

We can now calculate the net present value (NPV) of the investment, which corresponds to the sum of all the initial payments ($CF_0 = I_{el}$ included) and all the cash flows in future years $CF_{i=1,..,n}$ discounted. This index gives us an idea of the value generated by a certain investment initiative. For this calculation, if the cash flows are constant from one year to the next, we can extract them from the sum and rewrite the sum as $\frac{1}{\alpha}$.

$$NPV = \sum_{i=0}^{n} \frac{CF_i}{(1+k)^i} = \frac{1}{\alpha} \ P_n \ h_y (P_{en} - C_{tot}) = 9.1 M€; \tag{4.46}$$

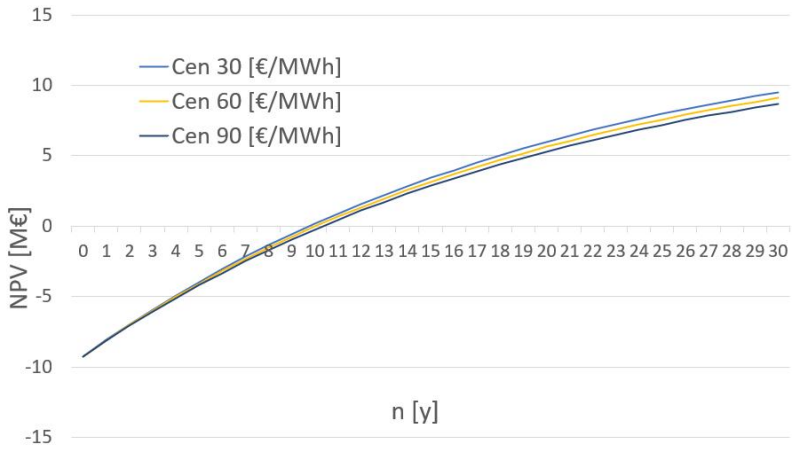

Figure 4.15: NPV $[M€]$ calculated for different energy prices versus k, in the event that 50% of the initiative is financed by the state through the PNRR.

The NPV calculation was repeated for different electricity sales prices. The results obtained are reported in the graph in Figure4.15. As we can see from the plot in Figure4.15, if the investment is evaluated using the LCOH as the price base and adding a constant margin, the net present value decreases less as the energy purchase price varies as this is part of the cost items considered by the LCOH, we also have a discounted return period of around ten years. We can therefore say that the investment is not affected so much by the energy purchase price as it is recovered. The final sale price will obviously depend on the market and the agreements made. The economic indexes evaluated are shown in Table4.7. We can see that as the energy purchase price increases, the margin is reduced by a little $\Delta M = 0.0866\ €/MWh$.

We can see a NPV between 8.5 and 9.5 $M€$, therefore, in addition to recovering the investment of 9.25 $M€$, value is generated. The profitability index with respect to the private amount invested is between $92 - 103\%$. A simple return time between 14 and 16 years is also estimated. From the results obtained, we can therefore say that this investment is worthwhile and guarantees good recoverability and profitability. To evaluate the purchase price of electricity from the two types of plants, photovoltaic and hydroelectric, we can think of associating an acceptable price for photovoltaics, i.e. one that allows the recovery of the investment, for example $P_{pv} = 40\ €/MWh$ and to buy energy to produce hydrogen at $P_{en} = 75\ €/MWh$. In this way, at $h_y = 7000h/y$ operating hours of the electrolysis plant we can associate the utilization factors of the two plants that cover its hydrogen production and find the energy sale

$C_{en'}$	$LCOH$	$\hat{P}_{H2}$	P_{H2}	C_{tot}	NPV	PB	ROI	IP
$€/MWh_{el}$	$€/kg$	$€/kg$	$€/MWh_{H_2}$	$€/MWh_{H_2}$	$M€$	y	%	%
30	2.37	2.67	67.6	55.8	9.5	14.9	3.4%	103%
35	2.64	2.94	74.7	63.0	9.5	15.0	3.3%	102%
40	2.92	3.22	81.8	70.1	9.4	15.2	3.3%	101%
45	3.20	3.50	88.8	77.3	9.3	15.3	3.2%	101%
50	3.48	3.78	95.9	84.4	9.2	15.4	3.2%	100%
55	3.76	4.06	102.9	91.6	9.2	15.5	3.1%	99%
60	4.03	4.33	110.0	98.7	9.1	15.6	3.1%	98%
65	4.31	4.61	117.0	105.8	9.0	15.7	3.0%	98%
70	4.59	4.89	124.1	113.0	9.0	15.9	3.0%	97%
75	4.87	5.17	131.2	120.1	8.9	16.0	2.9%	96%
80	5.15	5.45	138.2	127.3	8.8	16.1	2.9%	95%
85	5.42	5.72	145.3	134.4	8.8	16.2	2.8%	95%
90	5.70	6.00	152.3	141.6	8.7	16.4	2.8%	94%
95	5.98	6.28	159.4	148.7	8.6	16.5	2.7%	93%
100	6.26	6.56	166.4	155.8	8.5	16.6	2.7%	92%

Table 4.7: Economic investment indices for different average electricity sales prices, in case the financing takes place.

price for the unfunded plant (hydroelectric) P_{hy} as:

$$P_{hy} = \left[P_{en} - \left(P_{pv} * \frac{h_{e,pv}}{h_y} \right) \right] \frac{h_y}{h_{e,hy}} = 82.6 \, €/MWh \tag{4.47}$$

For $P_{en} = 60 \, €/MWh$ and $P_{pv} = 40 \, €/MWh$ we have $P_{hy} = 64.4 \, €/MWh$.

Also in this case the net present value was evaluated for different values of the discount rate k. From the graph in Figure4.16 we can see that a rate lower than or equal to 11% can be accepted.

Based on these analyses, a hydrogen sales price of 5.17 $€/kg$ (0.44 $€/Sm^3$) was chosen, corresponding to an energy value of 75 $€/MWh$. This value will be utilized for the usage study in the subsequent analyses.

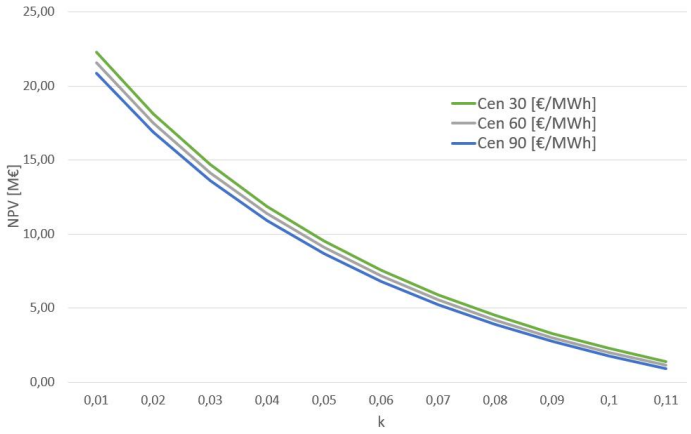

Figure 4.16: NPV calculated for different energy prices versus k, in the event that 50% of the initiative is financed by the state through the PNRR.

Chapter 5

Hydrogen end-users

5.1 Industry sector

Within industries, hydrogen can be used as a fuel. The heat produced by combustion makes it possible to heat the raw materials or semi-finished products so that they are transformed by industrial processes into finished products. This section analyzes the direct combustion processes in a burner in a billet preheating furnace for up to 20% hydrogen mixture. Furthermore, the heating of process water through a new boiler that can operate with mixtures up to 100% by volume of H_2 was also investigated for a company neighboring the hydrogen production site.

5.1.1 Conversion with energy-equivalent mixtures

In some circumstances, hydrogen may be suitable to be burned using hydrogen-natural gas mixtures; it is therefore possible to readapt pre-existing burners without further investment. These two gases have different characteristics, such as different density under standard conditions (STD) and different lower and upper heating value (LHV, HHV):

- $LHV_{ng} = 13.99\ \frac{kWh}{kg}$, $LHV_{H_2} = 33.33\ \frac{kWh}{kg}$;
- $\rho_{ng} = 0.74\ \frac{kg}{Sm^3}$, $\rho_{H_2} = 0.085\ \frac{kg}{Sm^3}$;

where subscript ng indicates natural gas and H_2 indicates hydrogen. So replacing a certain percentage by volume of natural gas with hydrogen, does not return the same percentage in the final mixture if we want it to also continue to contain the same thermal energy. In fact, to do this we must also consider the energy to be supplied ($E_t = V_{ng} * LHV_{ng}$) which is known to us since the pre-existing thermal

process to be supplied is known. This same energy will now have to be supplied by the contributions, natural gas ($LHV_{ng} * (V_{ng} - x_g)$) and hydrogen ($LHV_{ng} * (x_g + y_{gh})$). Here x_g represents the volume of natural gas replaced, while y_{gh} represents the volume adjustment of hydrogen, the sum of which $(x_g + y_{gh})$ represents the volume of hydrogen in the required volume percentage. We then impose that the final substituted hydrogen volume $(x_g + y_{gh})$, relative to the new total volume $(V_{ng} + y_{gh})$ is equal to the required percentage $H_{H_2\%}$ ($h = \frac{H_{H_2\%}}{100}$).
We then write the following system of two equations in the two unknowns x_g and y_{gh}:

$$\begin{cases} E_t = LHV_{ng}(V_{ng} - x_g) + LHV_{H_2}(x_g + y_{gh}) \\ \\ \frac{(x_g + y_{gh})}{V_{ng} + y_{gh}} = h \end{cases} \tag{5.1}$$

whose solution is

$$y_{gh} = \frac{E_t - [LHV_{ng}\ V_{ng}(1-h) + LHV_{H_2}\ h\ V_{ng}]}{LHV_{ng}(1-h) + h\ LHV_{H_2}} \tag{5.2}$$

$$x_g = h\ V_{ng} + y_{gh}(h-1) \tag{5.3}$$

$$V_{H_2} = x_g + y_{gh} = h\left[V_{ng} + \frac{LHV_{ng}V_{ng} - LHV_{H_2}V_{ng}}{(\frac{1}{h} - 1)LHV_{ng} + LHV_{H_2}}\right]; \tag{5.4}$$

In Figure5.1 we find the plot of an example of calculation for different percentages of blending of H_2 and natural gas. This was achieved by implementing the described computation using the Python programming language.

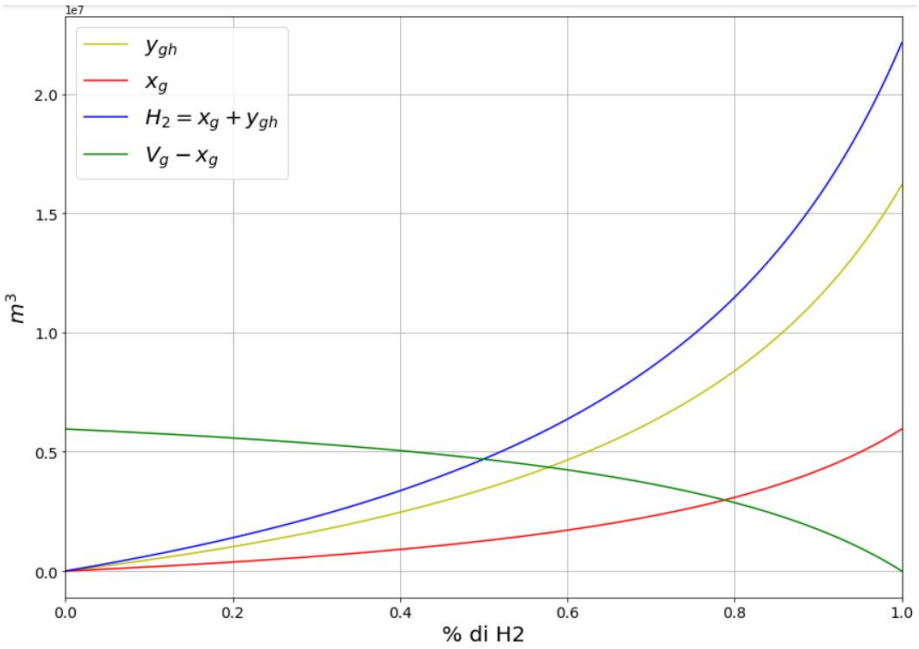

Figure 5.1: Plot volume of mix, natural gas, and H_2 versus H_2 percent change in final volume.

5.1.2 Steel mill burners for billet preheating furnace

The steelmaking process can be summarized in four main stages:

1. Scrap yard: at this stage the scrap is transported by rail or heavy truck to the scrap yard. A hydraulic spider picks up the scrap and loads the basket, this moves on rails to the steel mill. At this stage of production, the emissions generated are indirect, as they are generated by the transportation of the scrap.

2. Steel melting: an overhead crane picks up the basket from the scrap yard, the top of the furnace is opened and the scrap is loaded into the electric arc furnace (EAF), then it is closed and the melting process can begin. During melting, lime, coal, and ferroalloys are added to reach the right composition, also the slagging process is carried out, in fact by density difference the nonmetallic parts contained in the mineral aggregate to form a foamy and homogeneous floating compound. The ladle containing liquid steel is picked up by overhead crane and taken to where continuous casting takes place. The molten steel is poured from the ladle into a vessel lined with refractory material (called a tundish), which is responsible for maintaining a smooth outflow of the steel

and giving it an initial stable shape at the outlet. At the exit of the casting machine we have the billets (semi-product), which are cut to the proper length by means of an oxyfuel lance. Via rollers, the billets are transported to the reheating furnace or billet storage (semi-product stock). Emissions occur at this stage due to the use of natural gas and coal, and there are also indirect emissions during the smelting stage due to the use of electricity in the arc furnace.

3. Rolling mill: The rolling mill consists of several machines in series which by means of rotating parts slide the billet (or slab) through them giving it an increasingly similar profile to the finished product. Billets coming from the steel mill or semi-product stock are heated by the preheating furnace to a temperature of about $1050°C$ and then rolled in the first deformation sequence, in which the metal roughing process also takes place, and then move on to the intermediate in which the standard, rectangular or round shape is given. The billets are cut every 80 meters and brought to the cooling plate. The bars are cooled to a temperature of $80°C$, as a result the material undergoes considerable thermal deformation. The bars are then straightened and cut by automatic machines. The bars can have a length between 5 and 15 m, these through a machine are weighed, cataloged with a card containing production specifications, and tied and then transferred to the warehouse. At this stage direct emissions are due to the use of natural gas in the preheating furnace of the billets, while indirect emissions come from the electricity used to set the rolling machinery and automatic machines in motion.

4. Storage and shipment: finished products are handled by magnetic overhead crane, these can be delivered to the warehouse by a special rail car or shipped directly to customers by road or rail. At this stage we have direct emissions from in-house handling and storage, while there are indirect emissions from third-party transport and storage.

Of these processes, we are interested in evaluating the convenience of introducing hydrogen into billet preheating gas furnaces. These furnaces house natural gas burners, for these are guaranteed to operate with a mixture up to 20% by volume of H_2.

Natural gas calculation:
An ELTI preheating oven is used whose specific natural gas consumption per ton of steel produced is $\hat{V}_{ng} = 43\ Sm^3/t$. For an annual production of $M_{steel,y} = 140000\ t/y$ there is a natural gas consumption of $V_{ng,y} = M_{steel,y} * \hat{V}_{ng} = 6020000\ Sm^3/y$, for a corresponding energy consumption of $E_{ng,y} = V_{ng,y} * LHV_{ng} = 62288\ MWh/y$

where $LHV_{ng} = 10.347\ MWh/Sm^3$. Given the specific heat of steel, which is $c_{p,steel} = 0.703\ kJ/kgK$, the inlet temperatures $T_{in} = 20°C$ and outlet temperatures $T_{out} = 1100°C$ of the billets from the preheating furnace, we can calculate the ideal heat to be supplied to one ton of steel as:

$$\hat{H}_{id} = c_{p,steel} * (T_{out} - T_{in}) = 759.24\ MJ/t. \tag{5.5}$$

In reality, due to the losses, in order to guarantee a $\Delta T = 1080°C$, a quantity of heat equal to $\hat{H}_{re}$ must be provided:

$$\hat{H}_{re} = \hat{V}_{ng} * LHV_{ng} = 1601.70\ MJ/t; \tag{5.6}$$

We can now calculate the thermal efficiency of the process as the ratio between the ideal specific energy to be supplied in the form of heat with respect to the specific energy that the billet heating process really requires, η_{th}:

$$\eta_{th} = \frac{\hat{H}_{id}}{\hat{H}_{re}} \times 100 = 47\%. \tag{5.7}$$

This plant works for a number of hours per year equal to $h_y = 3200\ h/y$ with a productivity of:

$$\dot{M}_{steel} = M_{steel,y}/h_y = 44\ t/h. \tag{5.8}$$

The emissions of CO_2 produced by the plant through the combustion of natural gas are equal to $M_{CO_2} = 0,2017\ tCO_2/MWh$, to which we can associate an ETS market value of around $C_{CO_2} = 90\ €/tCO_2$.

In this analysis, we assume a natural gas cost $C_{ng} = 0.87\ €/Sm^3$, consistent with the average cost for the energy material from 2021 to 2023,[3]. Next, additional cost components were evaluated in the following percentages relative to the electricity price,[4]:

- system charges: 25%;
- transportation: 25%;
- taxes: 14%.

The cost for Sm^3 was then recalculated taking into account the additional cost components, as $C_{ng,t} = 1.43\ €/Sm^3$. We can now calculate the total annual cost as $C_{ng,t,y} = C_{ng,t} * V_{ng,y} = 8.59\ M€/y$, to this cost we must add the cost of CO_2 emissions, thus we get a total cost of:

$$C_{ng,tot} = C_{ng,t,y} + C_{CO_2} * M_{CO_2} * E_{ng,y} = 9.72\ M€/y; \tag{5.9}$$

$$C_{CO_2,tot} = 1.13\ M€/y; \tag{5.10}$$

Hydrogen calculus:
We now perform the same calculation but substituting for natural gas a gas mixture of final composition at 20% ($h = 0.2$) by volume of hydrogen and 80% of natural gas. In this case the burners inserted in the ELTI preheating oven also guarantee operation for this mixture, consequently we can assume that the efficiency and energy requirements reported above remain unchanged. We calculate the required volume $V_{H2,20\%}$ of hydrogen to ensure the thermal demand, this is the volume percentage required according to the following formula:

$$V_{H2,20\%} = h\left[V_{ng} + \frac{LHV_{ng}V_{ng} - LHV_{H_2}V_{ng}}{(\frac{1}{h}-1)LHV_{ng} + LHV_{H_2}}\right] = 1408236\ \frac{Sm^3}{y}; \tag{5.11}$$

the introduction of 20% in volume of H_2 corresponds to replacing $e_{H_2\%} = 6.43\%$ of the required energy, so $E_{H_2,20\%} = 4004\ MWh/y$. The remaining volume of natural gas corresponds to:

$$V_{ng,80\%} = V_{H2,20\%} * \frac{0.8}{0.2} = 5632943\ \frac{Sm^3}{y}; \tag{5.12}$$

This volume corresponds to a percentage of the supplied energy of $e_{ng,\%} = 93.57\%$, for a thermal energy of $E_{ng,80\%} = 58283\ MWh$. We now calculate the thermal equivalent cost in $€/MWh$ of natural gas.

$$C_{ng,e} = \frac{C_{ng} * (1 + 0.64)}{LHV_{ng}} = \frac{0.87 * (1 + 0.64) \times 10^3}{10.35} = 137.9\ €/MWh. \tag{5.13}$$

Assuming initially that this cost is equivalent to the cost of energy in the form of hydrogen $C_{ng,e} = C_{H_2,e}$, we derive the equivalent cost per kg and per Sm^3 in the case of hydrogen. The final cost of hydrogen takes into account truck transportation, assumed to be $0.47\ €/kg$ or $0.04\ €/Sm^3$, from [9], following the formula given here:

$$C_{transp} = \frac{(549 * t + 6.93 * d + 11 * w \times 10^{-3} + 136) * 2 * 0.085}{w} = 0.47\ €/\text{kg} \tag{5.14}$$

with $t = 2\ h$, $d = 215\ km$, and $w = 1000\ kg$.

$$C_{H_2,v} = C_{H_2,e} * LHV_{H_2} \times 10^{-3} = 0.1379 * 2.84 = 0.39\ €/Sm^3; \tag{5.15}$$

$$C_{H_2} = C_{H_2,e} * LHV_{H_2} \times 10^{-3} = 0.1379 * 33.33 = 4.59 \text{€}/kg. \tag{5.16}$$

We now analyze the total annual costs as:

$$C_{ng,80\%} = C_{ng,t} * V_{ng,80\%} + C_{CO_2} * M_{CO_2} * E_{ng,80\%} = 9.095 \ M\text{€}/y; \tag{5.17}$$

$$C_{CO_2,tot} = 1.057 \ M\text{€}/y; \tag{5.18}$$

$$C_{H_2,20\%} = C_{H_2,v} * V_{H_2,20\%} = 0.552 \ M\text{€}/y; \tag{5.19}$$

$$C_{tot,y} = C_{ng,80\%} + C_{H_2,20\%} = 9.647 \ M\text{€}/y. \tag{5.20}$$

As we can see, the total cost just calculated is lower than in the previous case. This is because introducing hydrogen decreases the CO_2 produced and thus reduces the total cost of CO_2. We can perform the same calculation by varying the volume percentage of hydrogen and obtain the graph in Figure5.2. As we can see from the graph in Figure5.2 as the percentage of H_2 increases, costs decrease due to the reduction of CO_2.

As we can see the graph does not have a linear trend, this is because the change in total volume is not linear with the percentage change in volume of hydrogen. Consequently, the non-linearity is also reflected in the graph of cost versus volume percentage of H_2. If we increase the cost of hydrogen to $C_{H_2,v} = 0.44$ €$/Sm^3$ and then to $C_{H_2,v} = 0.54$ €$/Sm^3$ we can see that the trend of the total cost curve goes from decreasing to constant in Figure5.3 and then becomes increasing as can be seen in the graph in Figure5.5.

Thus, in the situation shown in Figure5.2 it is convenient to replace natural gas with hydrogen, and this is all the more convenient the higher the final volume percentage of hydrogen replaced. As the price of hydrogen increases relative to natural gas, we have a transition situation in which the reduction in CO_2 emitted offsets the increase in price and consequently there is a break-even situation between costs Figure5.3. Above the break-even price Figure5.5, on the other hand, the cost of hydrogen increases as the volume percentage of H_2 increases, exceeding the cost of natural gas, but we can see that for percentages up to 20% of H_2 the incremental change in cost is smaller than the incremental change for higher mixture percentages. Let us analyze the case in which hydrogen is purchased and transported at a price of $C_{H_2} = 5.64$ €$/kg$ ($C_{en} = 75$ €$/MWh$), the cost per unit of corresponding volume

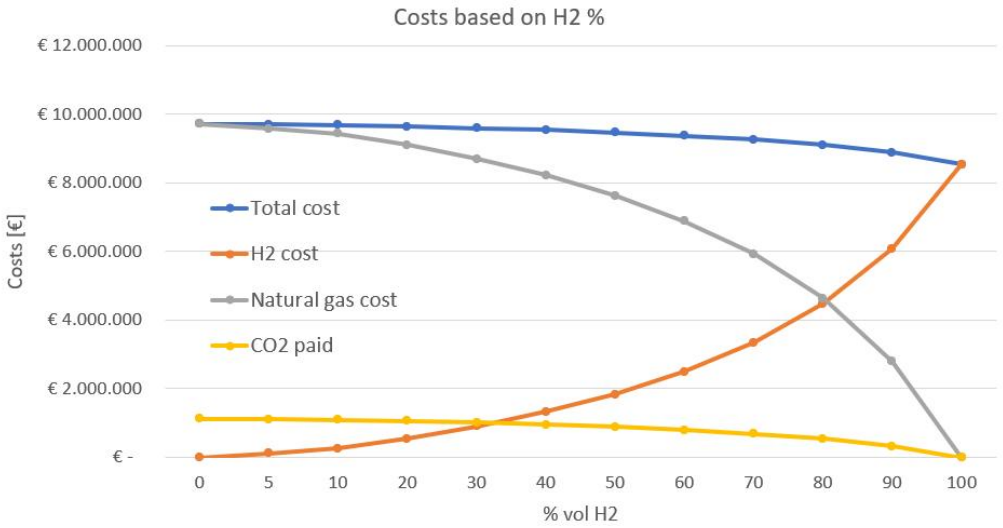

Figure 5.2: Costs associated with different volume percentages in the final mixture H_2 and natural gas; taken the cost of hydrogen equal to the thermal equivalent cost of natural gas ($C_{H_2,v} = 0.39\ €/Sm^3\ C_{H_2} = 4.59\ €/kg$).

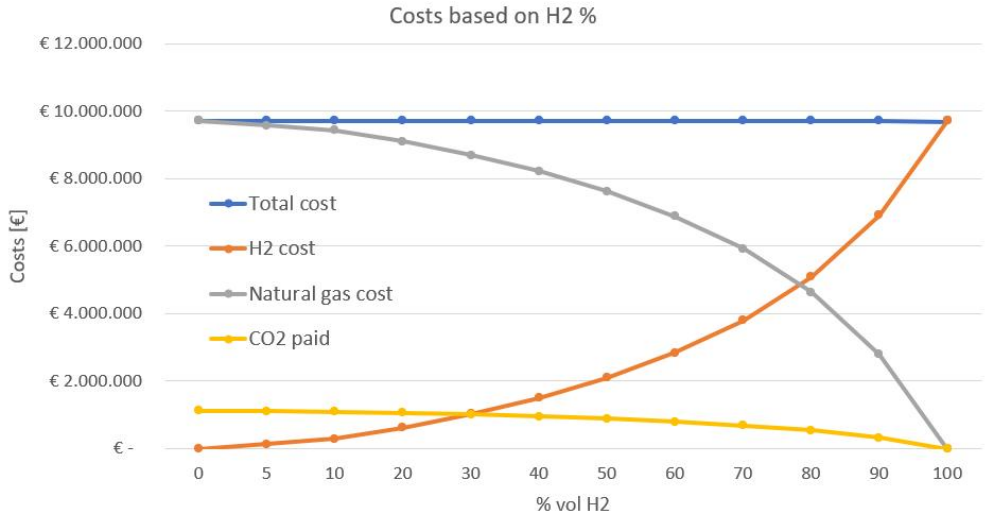

Figure 5.3: Costs associated with different volume percentages in the final mixture H_2 and natural gas; taken the cost of hydrogen greater than the thermal equivalent cost of natural gas, in order to even out the cost of CO_2 ($C_{H_2,v} = 0.443782\ €/Sm^3\ C_{H_2} = 5.17\ €/kg$).

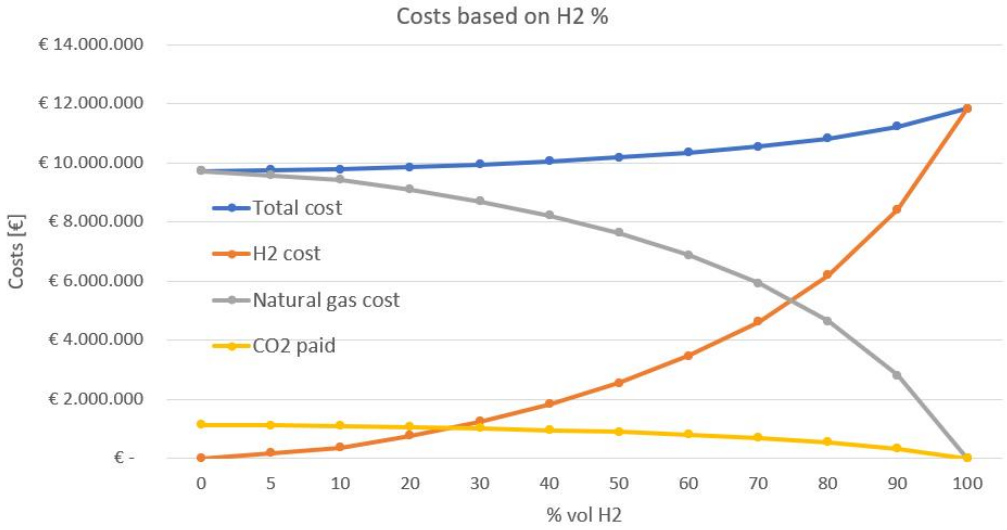

Figure 5.4: Costs associated with different volume percentages in the final mixture H_2 and natural gas; taken the cost of hydrogen greater than the thermal equivalent cost of natural gas ($C_{H_2,v} = 0.54\ €/Sm^3\ C_{H_2} = 5.69\ €/kg$).

would be $C_{H_2,v} = 0.48\ €/Sm^3$. In the case shown in Figure5.5 if we use a mixture of 20% by volume of H_2 and we would have an increase in cost compared to natural gas cost of:

$$\Delta C_{20\%} = C_{tot,y} - C_{ng,t} = 51\ k€ \tag{5.21}$$

In this case we have a cost increase over the natural gas alternative; however this increase is not excessive for hydrogen blends up to 20%. Thus, while suffering an increase in cost, we could expect to differentiate the final product due to the CO_2 reduction made in a hard to abate sector; but if the marginal abatement cost of CO_2 is higher than the market value there is more convenience in buying in the ETS market. Thus, for true substitution to occur, it would require a small government incentive or wait for the CO_2 market to increase until it exceeds the marginal abatement cost of $C_{CO_2} = 153.1\ €/tCO_2$, i.e. so that there is a real economic advantage in de-polluting. For a total hydrogen cost set at $C_{H_2} = 5.64\ €/kg$, a cost break-even with natural gas occurs if the CO_2 market reaches a price of $C_{CO_2} = 153.1\ €/tCO_2$. The marginal abatement cost was calculated as:

$$C_{CO_2} = \frac{C_{H_2,x\%} + C_{ng,(1-x)\%} - C_{ng,t,y}}{m_{CO_2,x\%}} = 153.1\ \frac{€}{tCO_2} \tag{5.22}$$

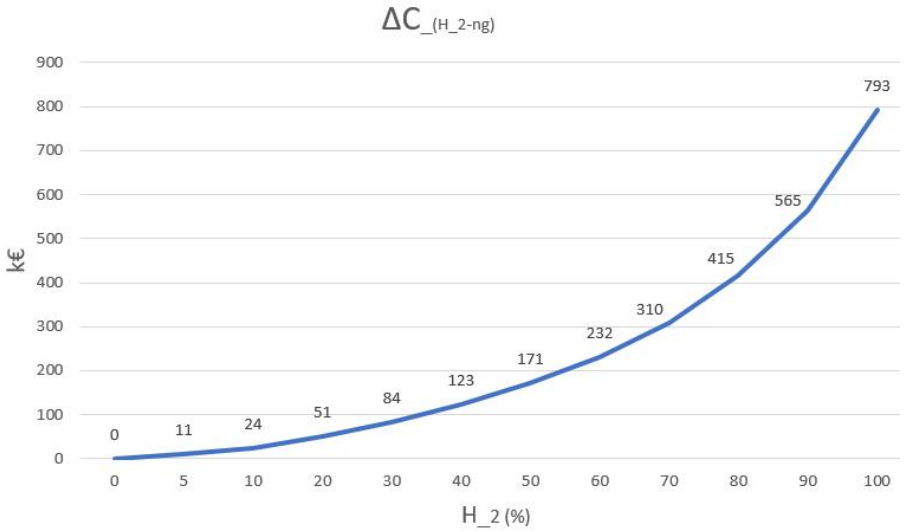

Figure 5.5: Incremental cost of hydrogen as the volume percentage increases relative to the cost of natural gas for ($C_{H_2} = 0.48\,€/Sm^3$ $C_{H_2} = 5.64\,€/kg$).

Where $m_{CO_2,x\%}$ represent the emission reduction in tons of CO_2, for a certain percentage x of H_2.

5.1.3 Hot process water

In this case, we analyze an industrial boiler that heats process water, located near the hydrogen production plant. For this problem, annual natural gas consumption of $V_{ng,y} = 2414856\ Sm^3/y$ is known, for a corresponding energy consumption of $E_{ng,y} = V_{ng,y} * LHV_{ng} = 24986\ MWh/y$. The industrial natural gas boiler currently in operation has a thermal efficiency of $\eta_{th} = 93.3\%$, so the annual energy useful for industrial processes corresponds to:

$$E_{th,y} = E_{ng,y} * \eta_{th} = 23312\ \frac{MWh}{y}. \tag{5.23}$$

Suppose we replace the current natural gas boiler with a new boiler with efficiency $\eta_{th'} = 95.5\%$ that can accommodate mixtures of natural gas and hydrogen up to 100% of H_2, [41]. We calculate the new natural gas consumption as:

$$E_{ng',y} = \frac{E_{th,y}}{\eta_{th'}} = 24410\ \frac{MWh}{y}; \tag{5.24}$$

needed to ensure the same annual energy useful for the process $E_{th,y}$. Now let's calculate the annual savings achieved, with the same cost of natural gas assumed previously, by replacing only the natural gas boilers without using hydrogen, we obtain:

$$C_{tot,y} - C_{tot,y'} = 89\ k€/y. \tag{5.25}$$

Using the same approach as in the previous subsection 5.1.2, we analyze annual costs against the different percentages of H_2 with the new boiler, for a market value of CO_2 equal to $C_{CO_2} = 90\ €/tCO_2$. In this case there is a balancing of the total costs between natural gas and hydrogen mixture at a cost of $C_{H_2,v} = 0.440022\ €/Sm^3$. We assume zero transportation costs for hydrogen, since the hydrogen production site is adjacent to the use site, we therefore associate a total hydrogen cost of $C_{H_2} = 5.17\ €/kg$ ($C_{en} = 75\ €/MWh$), which corresponds to $C_{H_2,v} = 0.44\ €/Sm^3$, very close to the break-even cost threshold. In fact, at this price results in a small cost difference of about 200 € saved with 100% H_2 compared to natural gas. We can calculate the marginal cost of abatement as:

$$C_{CO_2} = \frac{C_{H_2,x\%} + C_{ng,x\%} - C_{ng,t,y}}{m_{CO_2,x\%}} = 89.96\ \frac{€}{tCO_2} \tag{5.26}$$

So fixed of cost of natural gas, we have that when the market of CO_2 exceeds the value the marginal abatement cost of $C_{CO_2} = 89.96\ €/tCO_2$ the company will have an interest to de-pollute. In fact, as we can see in Figure5.6, when the market exceeds this value, the convenience to clean up increases more and more, for instance at $C_{CO_2} = 100\ €/tCO_2$ we have additional savings over natural gas of up to 45.8 $k€/y$ for 100% H_2, which added to the savings due to substitution with higher efficiency boiler would provide an annual cost reduction of 134.9 $k€/y$.

As the market for CO_2 today is already above $90\ €/tCO_2$, the purchase of a boiler that has greater efficiency, and dynamism of use, is cost-effective. This is because it can operate both with natural gas alone already recovering costs but also with blends up to 100% H_2, allowing it to de-pollute at a marginal cost of de-pollution that is already lower than the market cost of CO_2.

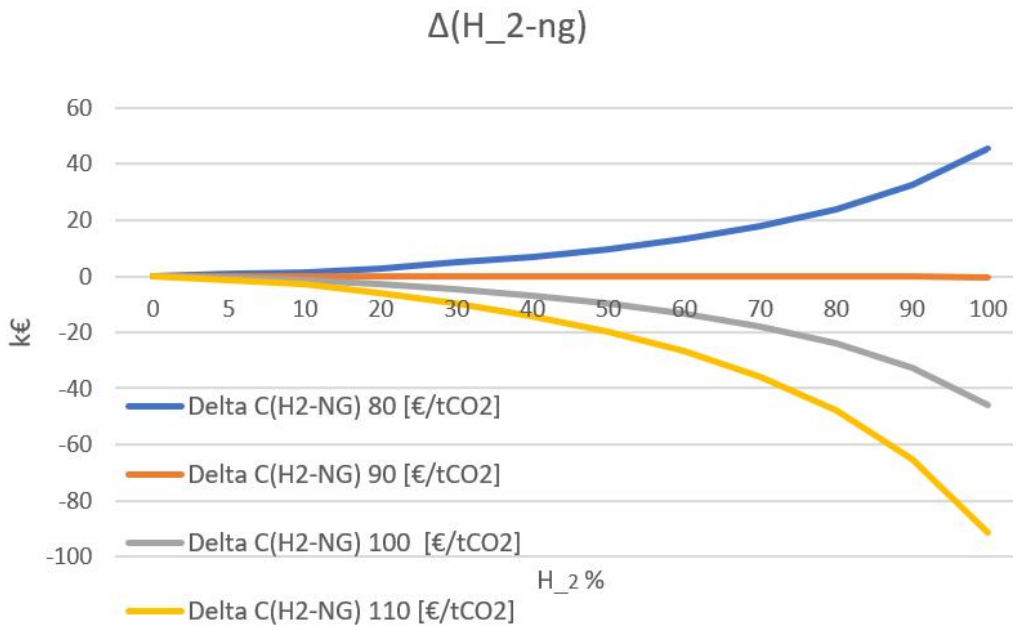

Figure 5.6: Change in cost/savings of hydrogen as the volume percentage increases relative to the cost of natural gas for $C_{H_2} = 0.44$ €$/Sm^3$ $C_{H_2} = 5.17$ €$/kg$, as the market value of CO_2 changes in €$/tCO_2$.

5.2 Transport sector

In this section, heavy transport is analyzed, specifically the total cost of ownership per kilometer of a diesel truck and a fuel cell truck is calculated under certain operational assumptions and based on data found in [1] for rigid transport.

5.2.1 Truck

In [1], the TCO (Total Cost of Ownership) of articulated and rigid trucks is analyzed in four distinct time phases:

- *R&D* phase (research and development) and implementation until 2025;
- industrial growth phase (first mass production) from 2025 to 2028;
- sustainable growth phase (price reduction for economies of scale) from 2028 to 2030;
- phase of full industrialization (high-volume production) from 2030.

In the different stages of growth of the fuel cell heavy transport sector, different ways have been identified, based on the level of industrialization of the sector, in which policies can act to make the purchase and maintenance of hydrogen vehicles affordable or at least equal to diesel vehicles.

The *R&D* phase, i.e., the current one results to be of interest to us. The support that could be provided at this stage is:

- capital cost discounting through project-based calls, where the cost of hydrogen trucks is equalized with that of diesel trucks;
- the addition of differentiated road tolls, which consist of a fixed rate per km traveled differentiated according to the emissions produced by the vehicles, 0.4 €$/km$ for diesel trucks and only 0.1 €$/km$ for hydrogen trucks (75% less than diesel);
- carbon tax, this is applied directly to the price of sale of diesel and veins calculated by multiplying the CO_2 content in the products of the combustion reaction (2.62×10^{-3} tCO_2/l) with the price of CO_2 under the emission trading scheme for road fuels (Fit for 55, 30 euro/$tCO2$ from 2022 to 2025).

We calculate the TCO per km traveled for rigid vehicles, assuming an annual distance traveled $d = 120000$ km/y, a lifetime $t = 5$ y, a government subsidy for vehicles hydrogen-powered rigid vehicles of $s = 300$ k€, and that both alternatives share the same personnel, insurance and maintenance costs. The component of the average investment TCO for hydrogen rigid vehicles $I_{0,H_2} = 534$ k€ and diesel $I_{0,D} = 93$ k€ are:

$$TCO_{inv,H_2} = \frac{I_{0,H_2} - s}{t * d} = 0.39 \ \frac{€}{km}; \quad TCO_{inv,D} = \frac{I_{0,D}}{t * d} = 0.155 \ \frac{€}{km}; \tag{5.27}$$

Road toll fees were taken as:

$$T_{toll,H_2} = 0.1 \ \frac{€}{km} \quad T_{toll,D} = 0.4 \ \frac{€}{km}. \tag{5.28}$$

The carbon tax T_{CO_2} was calculated by considering a cost of CO_2 equal to $C_{CO_2} = 30$ €$/tCO_2$, the amount of CO_2 given off by burning one liter of diesel 2.62×10^{-3} tCO_2/l, and using a consumption of $m_D = 0.3$ l/km found in [11] and [27]. For these values we obtain:

$$T_{CO_2} = C_{CO_2} * m_D * 2.62 \times 10^{-3} = 0.024 \ \frac{€}{km}. \tag{5.29}$$

For the rigid fuel cell vehicle reported in [25] we know the range $d_{max} = 400\ km$, and the tank capacity of $M_{H_2} = 32.09\ kg$, we can then calculate the consumption of H_2 per km as:

$$m_{H_2} = \frac{d_{max}}{M_{H_2}} = 0.08\ \frac{kg}{km}; \quad e_{H_2} = m_{H_2} * LHV_{H_2} = 2.67\ \frac{kWh}{km}; \tag{5.30}$$

While in the case of diesel we have:

$$m_D = 0.3 * 0.835 = 0.25\ \frac{kg}{km}; \quad e_D = m_d * LHV_D = 3.09\ \frac{kWh}{km}; \tag{5.31}$$

taken $LHV_D = 12.33\ kWh/kg$ and $\rho_D = 0.835\ kg/l$. As we can see there is lower energy consumption in the case of the fuel cell truck since it has higher efficiency and fewer moving parts than the diesel truck ($\Delta\% = 15.5\%$). Therefore, we consider a diesel cost of $C_D = 1.31\ €/l$ starting from a cost basis of $1.68\ €/l$ drawn from [33], deducting 22% vat. The equivalent cost of hydrogen with respect to energy and to the higher performance is $C_{H_2} = 4.89\ €/kg$ we get a cost per km of:

$$C_{F,D} = C_D * m_D = 0.393\ €/km; \quad C_{F,H_2} = C_{H_2} * m_{H_2} = 0.393\ €/km. \tag{5.32}$$

We now calculate the total TCO as the sum of investment, toll, carbon and fuel contributions per km:

$$TCO_D = 0.16 + 0.4 + 0.02 + 0.39 = 0.97\ €/km; \tag{5.33}$$

$$TCO_{H_2} = 0.39 + 0.1 + 0.39 = 0.88\ €/km. \tag{5.34}$$

For the value of $C_{H_2} = 5.17\ €/kg$ we get $C_{F,H_2} = 0.41\ €/km$ which returns a value of $TCO_{H_2} = 0.91\ €/km$ even lower than the TCO_D. A TCO break-even is achieved for $C_{F,H_2} = 0.48\ €/km$ corresponding to a price of approximately $C_{H_2} = 6\ €/kg$. We can therefore say that if fuel cell trucks were incentivized in this way they would be a better solution if the price of hydrogen is $C_{H_2} \leq 6\ €/kg$.

Considering the total production of hydrogen for 7000 h/y equal to $M_{tot} = 943950\ kg/y$ and subtracting the demand due to the industrial boiler equal to $M_{H_2,100\%} = 732394\ kg/y$ we get:

$$M_{tot'} = 943950 - 732394 = 211556\ \frac{kg}{y}. \tag{5.35}$$

A rigid fuel cell vehicle traveling $d = 120000\ km/y$ consumes:

$$M_{H_2,y} = \frac{d * M_{H_2}}{d_{max}} = 9627\ \frac{kg}{y}. \tag{5.36}$$

So with the remaining part the entire demand would be satisfied with a fleet of vehicles equal to:

$$N_v = int\left(\frac{M_{tot'}}{M_{H_2,y}}\right) = 21\ . \tag{5.37}$$

Since the annual demand due to the industrial boiler results in a large part of the production, the size of the storage can be reduced, around two or three tons of hydrogen under pressure, at 350 or 700 bars with compressor so that it is compatible with the pressure of the vehicles stocked up.

5.3 Process hydrogen for the chemical industry

The hydrogen that is used today as a raw material in the industrial chemistry sector is mainly made up of gray hydrogen, therefore hydrogen obtained from fossil fuels such as coal or natural gas by breaking the carbon bonds without special CO_2 removal systems.

Let us analyze the replacement of gray hydrogen with green hydrogenin a situation of self-production of gray hydrogen from natural gas in a chemical industry, useful as a feedstock for other processes. In this case, reforming data were taken from [43] without considering CO_2 capture systems in order to analyze the substitution from gray hydrogen to green hydrogen. Given the annual natural gas input quantity, for example $V_{ng,y} = 194751\ Sm^3/y$ (for a plant working eight hours a day for three hundred days), we can calculate the gray hydrogen production known the following production rate R in volume and r in kilograms, [43]:

$$R = \frac{\dot{V}_{ng}}{\dot{V}_{H_2,grey}} = \frac{81.1}{234.7} = 0.35; \quad r = \frac{\dot{m}_{ng}}{\dot{m}_{H_2,grey}} = 3. \tag{5.38}$$

We can also analyze the relationship between the thermal contents of input and output as η_{th}:

$$\eta_{th} = \frac{\dot{V}_{H_2,grey} * LHV_{H_2}}{\dot{V}_{ng} * LHV_{ng}} = 0.79; \tag{5.39}$$

to understand the cost of the process in energy terms.

We now calculate the annual production of gray hydrogen as:

$$V_{H_2,grey} = \frac{V_{ng,y}}{R} = 563239\ \frac{Sm^3}{y}. \tag{5.40}$$

Without the use of CO_2 capture systems, the production ratio of CO_2 for each kg of grey hydrogen is equal to:

$$r_{CO_2,H_2} = \frac{\dot{m}_{CO_2}}{\dot{m}_{H_2,grey}} = 8.86; \tag{5.41}$$

and the same with respect to natural gas:

$$r_{CO_2,ng} = \frac{r_{CO_2,H_2}}{r} = 2.95. \tag{5.42}$$

Let us take in this case a price of natural gas that is lower than the average of the last few months calculated in 5.1.2. We then start from a value of $C_{ng} = 0.656$ €$/Sm^3$ and assign the same transportation (25%), system (25%) and excise (14%) charges as in the 5.1.2 paragraph. We then obtain a total cost equal to $C_{ng,t} = 1.075$ €$/Sm^3$. Multiplying R by $C_{ng,t}$ we get a value of gray hydrogen equal to $C_{H_2,grey} = 0.37$ €$/Sm^3$. Let us now consider green hydrogen by assigning to it the previously considered value of $C_{H_2} = 0.44$ €$/Sm^3$ ($C_{H_2} = 5.17$ €$/kg$ considered a fair value for investment recovery). With a CO_2 market at $C_{CO_2} = 90$ €$/tCO_2$ we have a break-even cost

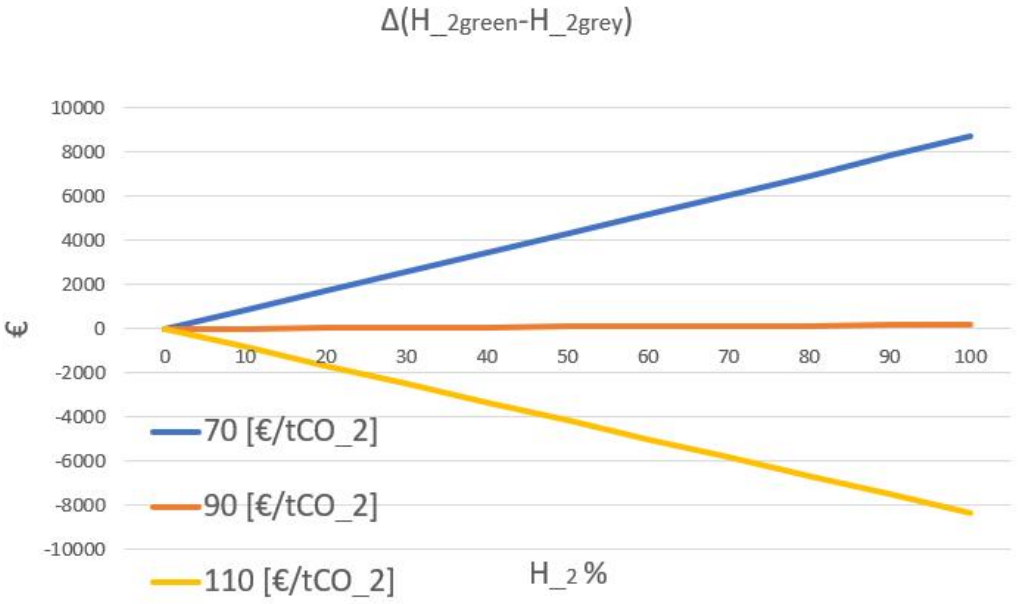

Figure 5.7: Change in cost/savings when increasing the percentage of green hydrogen substituted to gray hydrogen, $C_{H_2,grey} = 0.37$ €$/Sm^3$ for $C_{H_2} = 0.44$ €$/Sm^3$, as the market value of CO_2 changes in €$/tCO_2$.

situation, as we can see in Figure5.7 adding increasing percentages of green hydrogen and the remaining part constituted to be gray hydrogen. As we can observe, the curves shown in Figure5.7 that in 5.1.3 grew in a quadratic pattern as the volume percentage increased, now appear linear since we are substituting the same energy content into one Sm^3.

In this case we can see that already at a lower overall cost of natural gas than in the previous cases it is convenient to replace gray hydrogen with green hydrogen at the value of $C_{H_2} = 0.44$ €$/Sm^3$. This is because in this case hydrogen is useful as a raw material and therefore producing it implies an expenditure of energy and consequently an increase in its cost compared to natural gas, which makes it more comparable to green hydrogen.

We can then say that given the process described above, if the total cost of natural gas is above 1.075 €$/Sm^3$ with CO_2 market at 90 €$/tCO_2$ then it is convenient to completely replace gray hydrogen with green hydrogen. If the CO_2 market grows above the marginal abatement cost of 90 €$/tCO_2$ we will have that the convenience to substitution will also occur for lower total natural gas costs.

Conclusions

The choice of reference price for hydrogen at 0.44 €/Sm^3 is based on the recoverability of investments on electrolyzers and photovoltaics, and on the sales values of the baseload energy for already existing hydroelectric plants.

It is found that, using hydrogen in billet preheating ovens is still not economically convenient. In particular, a substitution with a blend of 20% of hydrogen in the steel mill preheating furnace has already a substantial cost, since the transportation costs are high, and despite an elevated price of the natural gas, due to recent geopolitical situations, has been taken into account. As a consequence, unless the CO_2 price becomes higher than the value of the marginal abatement cost (153 €/tCO_2), or a contribution from the State is put forward, the substitution is not convenient.

It would be interesting to study the recycling of the oxygen generated as a side product of the electrolysis process after the continuous casting, in order to perform oxylance cut on the billets. This could help reducing the expenses that are usually sustained for the purchase of oxygen from other companies.

For industries adjacent to the hydrogen valley we found that the replacement of the industrial boiler can lead to more savings in terms of efficiency and adaptability to the usage of hydrogen with zero cost transportation and blends of up to 100%. With the price of natural gas used for the analysis and the flexibility of the new industrial boiler we found that the substitution with hydrogen becomes convenient already at a CO_2 price of 90 €/tCO_2.

The analysis of the total cost of ownership gave positive results in the case of a State incentive for the investment and of differentiated road toll and carbon fees. The installment of a hydrogen fuel station for heavy trucks turns out to be strategic, since Villadossola is close to the border with Switzerland, with a direct highway connection (E62), where there has been a strong diffusion of hydrogen fueled vehicles, which could in turn lead to an expansion of demand also in Italy.

For chemical industry it is found that there is a great potential in the replacement of gray hydrogen with green hydrogen, already for a reduced price of natural gas with respect to current values and with the current price of CO_2. Finally, it would be

interesting to conduct an analysis also for train transportation, since the hydrogen valley would rise next to an existing railway.

In conclusion, this thesis argues that the employment of hydrogen is, for some applications, convenient even nowadays. In the hypothesis of increasing State incentives, CO_2 emission restrictions, and a growing price of CO_2, it is reasonable, and supported by the analysis in the thesis, that hydrogen will become more and more prominent in sectors as transportation, chemical industry and in industrial processes.

Thanks

Ringrazio di cuore la mia famiglia per avermi sostenuto e per aver sempre creduto in me. Desidero ringraziare mia madre Raffaella, che riesce sempre a tirarmi su il morale. Un ringraziamento speciale va a mio padre Maurizio, che mi ha costantemente spronato a non mollare e a perseguire i miei obiettivi. Voglio ringraziare mio nonno Giuseppe, che con il suo esempio mi ha guidato nel corso degli anni. Non posso dimenticare mia sorella Virginia, che è stata sempre al mio fianco e riesce a distrarmi quando serve.

Un ringraziamento particolare va a Francesco, che con la sua capacità di farmi concentrare e ispirarmi, è riuscito a tirare fuori il meglio di me anche quando ero giù di morale, rimanendo sempre al mio fianco.

Grazie Agnese per avermi fatto comprendere che molto spesso, quando le cose non vanno bene, il problema non siamo noi, ma è semplicemente il momento di apportare dei cambiamenti, anche se ciò ci spaventa.

Desidero ringraziare il mio gruppo di studio, senza il quale non avrei potuto confrontarmi e quindi comprendere le mie forze e soprattutto le mie mancanze. In particolare, desidero ringraziare la mia principale compagna di studi e amica Sara, che ha reso questo percorso più piacevole.

Ringrazio sinceramente l'ufficio Energy, in particolare l'ing. Gianmaria Zanni, il dott. ing. Giacomo Magoni e Alberto Beltrame, per la loro pazienza, gentilezza e per essermi stati vicini durante questi mesi. Un ringraziamento alla Professoressa Stoppato per il suo supporto e il suo auito.

Bibliography

[1] *Analysis of cost of ownership and the policy support required to enable industrialisation of fuel cell trucks*. 2023. URL: https://h2accelerate.eu/wp-content/uploads/2022/09/H2A-Truck-TCO-and-Policy-Support-Analysis-VFinal.pdf (visited on 2023).

[2] Asif S. Ansar, Aldo S. Gago, Fatemeh Razmjooei, Regine Reißner, Ziqi Xu, and Kaspar Andreas Friedrich. "Chapter 5 - Alkaline electrolysis—status and prospects". In: *Electrochemical Power Sources: Fundamentals, Systems, and Applications*. Ed. by Tom Smolinka and Jurgen Garche. Elsevier, 2022, pp. 165–198. ISBN: 978-0-12-819424-9. DOI: https://doi.org/10.1016/B978-0-12-819424-9.00004-5. URL: https://www.sciencedirect.com/science/article/pii/B9780128194249000045.

[3] *ARERA*. 2023. URL: https://www.arera.it/it/consumatori/placet.htm#econom (visited on 2023).

[4] *ARERA*. 2023. URL: https://www.arera.it/it/dati/ees5.htm (visited on 2023).

[5] BloombergNEF. "Hydrogen Economy Outlook". In: (2020).

[6] *CO2 emission standards for heavy-duty vehicles*. 2019. URL: https://www.europarl.europa.eu/RegData/etudes/BRIE/2018/628268/EPRS_BRI%282018%29628268_EN.pdf (visited on 2023).

[7] *Cummins, HyLYZER 500-30 (2.5MW)*. 2023. URL: https://www.cummins.com/sites/default/files/2021-08/cummins-hylyzer-500-specsheet.pdf (visited on 2023).

[8] *Cummins, HySTAT 100-10*. 2023. URL: https://www.cummins.com/sites/default/files/2021-08/cummins-hystat-100-specsheet.pdf (visited on 2023).

[9] Janis Danebergs. "Techno-economic Study of Hydrogen as a Heavy-duty Truck Fuel". In: *Department of Energy Technology Division of Heat and Power Technology SE-100 44 STOCKHOLM* (2019). URL: https://kth.diva-portal.org/smash/get/diva2:1372698/FULLTEXT01.pdf.

[10] APPENDIX A. CLIMATE DATA. *maximum and minimum temperatures in different parts of italy*. Tech. rep. 2022. URL: http://ideam.altervista.org/files_da_pubblicare/Temperature%20esterne%20di%20progetto.pdf.

[11] *dati emissioni veicolo trattore AS440S45TP*. 2023. URL: https://www.iveco.com/altra-en/collections/catalogues/Documents/tutti%20prodotti/ECOSTRALIS_CAT_ITA.pdf (visited on 2023).

[12] *DECRETO-LEGGE 30 aprile 2022, n. 36 Ulteriori misure urgenti per l'attuazione del Piano nazionale di ripresa e resilienza (PNRR). (22G00049) (GU Serie Generale n.100 del 30-04-2022)*. 2022. URL: https://www.gazzettaufficiale.it/eli/id/2022/04/30/22G00049/sg (visited on 2023).

[13] *DELIBERAZIONE 8 NOVEMBRE 2022, 557/2022/R/EEL*. 2022. URL: https://www.arera.it/allegati/docs/22/557-22.pdf (visited on 2023).

[14] Regione Piemonte Direzione Pianificazione Risorse Idriche. *Indagini e studi finalizzati alla predisposizione del piano di tutela delle acque (D.Lgs. 152/99), Allegato Tecnico PTA - Rev.01 Luglio 2004*.

[15] Ministero dello sviluppo economico. *Strategia Nazionale Idrogeno Linee Guida Preliminari*. 2020. URL: https://www.mise.gov.it/images/stories/documenti/Strategia_Nazionale_Idrogeno_Linee_guida_preliminari_nov20.pdf (visited on 2023).

[16] *Enaper, AEM Multicore*. 2023. URL: https://handbook.enapter.com/electrolyser/aem_multicore/downloads/Enapter_Datasheet_AEM-Multicore_EN_COM.pdf (visited on 2023).

[17] ENEA. *Atlante italiano della radiazione solare*. 2023. URL: http://www.solaritaly.enea.it/CalcComune/Calcola.php (visited on 2023).

[18] *EU Carbon Permits*. 2023. URL: https://tradingeconomics.com/commodity/carbon (visited on 2023).

[19] *Gli oneri generali del sistema elettrico*. 2018. URL: https://temi.camera.it/leg17/temi/gli_oneri_generali_del_sistema_elettrico (visited on 2023).

[20] GME. *Esiti mercato elettico*. Tech. rep. 2022. URL: https://www.mercatoelettrico.org/it/.

[21] *Guide on how develop a small hydropower plant*. 2004. URL: https://www.canyonhydro.com/images/Part_1_ESHA_Guide_on_how_to_develop_a_small_hydropower_plant.pdf (visited on 2023).

[22] *H-TEC,HCS*. 2023. URL: https://www.h-tec.com/en/products/detail/h-tec-pem-elektrolyseur-hcs/2-mw-hcs/ (visited on 2023).

[23] Michael Hirscher, Volodymyr A. Yartys, Marcello Baricco, Jose Bellosta von Colbe, Didier Blanchard, and Robert C. Bowman. "Materials for hydrogen-based energy storage – past, recent progress and future outlook". In: *Journal of Alloys and Compounds* 827 (2020), p. 153548. ISSN: 0925-8388. DOI: https://doi.org/10.1016/j.jallcom.2019.153548. URL: https://www.sciencedirect.com/science/article/pii/S0925838819347942.

[24] *HYTER, AEMWE*. 2023. URL: https://hyter.it/la-nostra-soluzione/ (visited on 2023).

[25] *Hyundai,4x2 XCIENT*. 2023. URL: https://hyundai-hm.com/wp-content/uploads/2020/10/XCIENT-Fuel-Cellcatalog_print.pdf (visited on 2023).

[26] *Impianti Piemonte Idroelettriche Riunite*. 2022. URL: https://idroelettricheriunite.it/impianti/ (visited on 2023).

[27] *IVECO,4x2 AS440S45TP*. 2023. URL: https://www.iveco.com/uk/collections/technical_sheets/Documents/stralis/Artic/AS/4x2/AS440S45TP_AS_3_EEV.pdf (visited on 2023).

[28] *MINISTERO DELLA TRANSIZIONE ECOLOGICADECRETO 21 settembre 2022, Condizioni per l'accesso alle agevolazioni sul consumo di energia rinnovabile in impianti di elettrolisi per la produzione di idrogeno verde. (22A05525) (GU Serie Generale n.223 del 23-09-2022)*. 2022. URL: https://www.gazzettaufficiale.it/eli/id/2022/09/23/22A05525/sg (visited on 2023).

[29] *nelhydrogen, A485*. 2023. URL: https://nelhydrogen.com/wp-content/uploads/2020/03/Electrolysers-Brochure-Rev-D.pdf (visited on 2023).

[30] *nelhydrogen, MC500*. 2023. URL: https://nelhydrogen.com/product/m-series-3/ (visited on 2023).

[31] Michel Noussan, Pier Paolo Raimondi, Rossana Scita, and Manfred Hafner. "The Role of Green and Blue Hydrogen in the Energy Transition—A Technological and Geopolitical Perspective". In: *Sustainability* 13 (2021).

[32] Autorità di bacino distrettuale del fiume Po. *Deliberazione n.4/2017*. URL: https://www.adbpo.it/PianoAcque2015/Direttiva_Deflusso/DelibCIP_4-2017_DeflEcol_14dic17.pdf (visited on 2023).

[33] *Prezzi medi settimanali dei carburanti*. 2023. URL: https://dgsaie.mise.gov.it/prezzi-settimanali-carburanti (visited on 2023).

[34] Inverter data sheet. *SUN2000-185KTL-H1 inverter*. Tech. rep. 2022. URL: https://solar.huawei.com/en-GB/download?p=%2F-%2Fmedia%2FSolar%2Fattachment%2Fpdf%2Feu%2Fdatasheet%2FSUN2000-185KTL-H1.pdf.

[35] PV data sheet. *JAM78S30 580-605 MR*. Tech. rep. 2022. URL: https://www.jasolar.com/uploadfile/2022/0513/20220513051007792.pdf.

[36] S. Shiva Kumar and V. Himabindu. "Hydrogen production by PEM water electrolysis – A review". In: *Materials Science for Energy Technologies* 2.3 (2019), pp. 442–454. ISSN: 2589-2991. DOI: https://doi.org/10.1016/j.mset.2019.03.002. URL: https://www.sciencedirect.com/science/article/pii/S2589299119300035.

[37] *Stargate Hydrogen, Gateway-400*. 2023. URL: https://stargatehydrogen.com/wp-content/uploads/2022/10/Stargate-Gateway-Specifications.pdf (visited on 2023).

[38] TERNA. *Carichi Pubblicazioni statistiche*. 2021. URL: https://www.terna.it/it/sistema-elettrico/statistiche/pubblicazioni-statistiche.

[39] *The European Hydrogen Backbone*. 2022. URL: https://ehb.eu/ (visited on 2023).

[40] pv tool. *PV location*. Tech. rep. 2022. URL: https://re.jrc.ec.europa.eu/pvg_tools/en/tools.html.

[41] *Viessman, VITOMAX HS*. 2023. URL: https://www.viessmann.it/it/prodotti/caldaie-industriali/vapore.html (visited on 2023).

[42] Immanuel Vincent and Dmitri Bessarabov. "Low cost hydrogen production by anion exchange membrane electrolysis: A review". In: *Renewable and Sustainable Energy Reviews* 81 (2018), pp. 1690–1704. ISSN: 1364-0321. DOI: https://doi.org/10.1016/j.rser.2017.05.258. URL: https://www.sciencedirect.com/science/article/pii/S1364032117309127.

[43] Yongliang Yan, Vasilije Manovic, Edward J. Anthony, and Peter T. Clough. "Techno-economic analysis of low-carbon hydrogen production by sorption enhanced steam methane reforming (SE-SMR) processes". In: *Energy Conversion and Management* 226 (2020), p. 113530. ISSN: 0196-8904. DOI: https://doi.org/10.1016/j.enconman.2020.113530. URL: https://www.sciencedirect.com/science/article/pii/S0196890420310608.